Data-Driven Constraint Learning and Screening for Operations of Sustainable Power Systems

Mohamed Awadalla

Department of Electrical & Computer Engineering
McGill University
Montréal, Québec, Canada

December 2023

A thesis submitted to McGill University in partial fulfillment of the requirements for the degree of Doctor of Philosophy.

©2023 Mohamed Awadalla

Abstract

The ongoing deepening penetration of renewable energy sources is posing significant challenges to electric power system operation and planning. High levels of renewable energy, particularly from wind and solar sources, introduce significant variability and uncertainties that system operators must integrate into operational planning problems to ensure secure and cost-effective operation. Solving NP-hard (Non Deterministic Polynomial-time) operational planning problems such as the unit commitment, security-constrained unit commitment, and ac optimal power flow (AC-OPF) repeatedly is essential for ensuring reliable and economical daily operations. However, their numerous constraints and the inclusion of uncertainties and variability can substantially prolong solution times and may render these problems intractable for large systems. Nevertheless, existing empirical evidence and prior research indicate that these problems often include numerous unnecessary constraints.

This thesis seeks to advance the state-of-the-art of optimization-based constraint screening approaches for power system operational planning problems. We leverage *constraint learning* to achieve efficient constraint screening outcomes. Constraint learning embeds trained machine learning models directly into constraint screening approaches. Constraint learning is primarily led by discovering insights from previously solved operations planning instances which inherit the economical aspect of their objective functions as well as the observed demand patterns.

In optimization-based constraint screening for operational planning problems, robust optimization is often employed to ensure the operator's ability to handle a broad range of possible *scenarios*, where scenarios refer to probable realizations of the system's sources of uncertainty. In this realm, we propose polyhedral uncertainty sets that are capable of capturing spatial correlations in the uncertainty space of variable renewable energy and demand, called *net load*. Polyhedral uncertainty sets offer coverage levels similar to those of convex hulls without the over conservatism of multidimensional bounding boxes. Afterward, we extend the optimization-based approach known as *umbrella constraint discovery* (UCD), in the context of polyhedral uncertainty sets integrated in unit commitment problems. The classical UCD approach identifies non-redundant constraints by enforcing a consistency logic on the set of constraints. Furthermore, we augment UCD with an upper bound cost-driven constraint derived by fitting an appropriate regression model using past solved instances of the unit commitment problem. This new formulation called *techno-economic UCD* screens out redundant *and* inactive constraints that are not necessary to achieve optimal solutions for unit commitment with significant computational enhancement. This is a key departure from UCD, which is only capable of screening out redundant constraints.

Furthermore, we extend the optimization-based bound tightening technique for constraint screening problem in the context of the AC-OPF problem using constraint learning. Due to the non-convexity of the AC-OPF problem, we investigate how different convex relaxations of the AC-OPF perform when performing line constraint screening.

Next, we propose an interpretable machine learning algorithm for real-time constraint generation for the security-constrained unit commitment problem. Our proposed approach is simplifying and accelerates the conventional constraint generation approach by leveraging machine learning approaches to learn the active set of pre- and post-contingency constraints. Those are then used to warm-start the constraint generation process used in the practical solution of security-constrained unit commitment problems to reveal the constraints set necessary and sufficient to guarantee the feasibility and optimality of the solution at a fraction of the computational cost needed by state-of-the-art approaches.

Finally, we develop a novel approach to determine the distance of an optimization problem solution to its non-redundant constraints defining its feasible region, or even its violated constraints in cases when problems are infeasible. Here, the notion of "distance" to a problem's constraints is associated with the ability of the power system to respond to uncertain events, i.e., how flexible it is. For this purpose, we propose novel system flexibility metrics which are calculated by solving an associated inverse optimization problem. We reveal that when applying this approach to the loadability set of a power system, it can accurately determine the feasibility of uncertain net load vector, and it is able to identify which constraints are closest to that uncertain net load vector.

Résumé

L'augmentation de la proportion des sources d'énergie renouvelable pose d'importants défis à l'exploitation et à la planification des grands réseaux électriques. Les niveaux élevés d'énergie renouvelable, en particulier à partir de sources éoliennes et solaires, introduisent des incertitudes et des niveaux de variation de la production significatives que les opérateurs doivent intégrer dans la planification opérationnelle pour garantir un fonctionnement sûr et économique. La résolution de manière répétée de problèmes de planification opérationnelle de difficulté NP (polynomiaux non déterministes) tels que l'engagement des unités, l'engagement des unités contraint par la sécurité et l'écoulement optimal de puissance en courant alternatif (AC-OPF) est essentiel pour les opérations quotidiennes. Cependant, leurs nombreuses contraintes et l'inclusion d'incertitudes peuvent considérablement prolonger les temps de résolution et rendre ces problèmes inextricables pour les grands systèmes. Néanmoins, des preuves empiriques et des recherches antérieures indiquent que ces problèmes incluent souvent de nombreuses contraintes inutiles.

Cette thèse vise à faire progresser l'état de l'art des approches de dépistage des contraintes basées sur l'optimisation pour les problèmes de planification opérationnelle des systèmes électriques. Nous utilisons *l'apprentissage de contraintes* pour obtenir des résultats efficaces de dépistage des contraintes. L'apprentissage de contraintes intègre directement des modèles d'apprentissage automatique formés dans les approches de dépistage des contraintes. L'apprentissage de contraintes est principalement dirigé par la découverte d'informations à partir d'instances de planification d'opérations résolues précédemment, qui héritent de l'aspect économique de leurs fonctions objectives ainsi que des schèmes de production et demande déjà observés.

Dans le dépistage des contraintes basé sur l'optimisation pour les problèmes de planification opérationnelle, l'optimisation robuste est souvent utilisée pour garantir la capacité de l'opérateur à gérer un large éventail de *scénarios* possibles, où un scénario correspond à une réalisation probable des sources d'incertitude d'un réseau. Dans ce domaine, nous proposons les ensembles d'incertitudes polyédriques capables de capturer les corrélations spatiales dans l'espace d'incertitude de l'énergie renouvelable variable et de la demande, appelée *charge nette*. L'ensemble d'incertitudes offre des niveaux de couverture similaires à ceux des enveloppes convexes, mais sans le conservatisme excessif des boîtes multidimensionnelles. Ensuite, nous étendons l'approche basée sur l'optimisation appelée *découverte de contraintes parapluie* (DCP), dans le contexte de l'ensemble d'incertitudes polyédriques intégré dans les problèmes d'engagement des unités de production. L'approche classique DCP identifie les contraintes non redondantes en imposant une logique de cohérence à l'ensemble des contraintes. De plus, nous augmentons DCP avec une contrainte axée sur les coûts de borne supérieure dérivée en ajustant un modèle de régression approprié à l'aide d'instances passées du problème d'engagement des unités. Cette nouvelle formulation appelée DCP *technico-économique* élimine les contraintes redondantes et inactives qui ne sont pas nécessaires pour obtenir des solutions optimales pour l'engagement des unités avec une amélioration significative des performances de calcul. On voit ici une avancée des plus utile, étant donné que le DCP technico-économique est en mesure d'identifier non-seulement les contraintes redondantes mais lesquelles devraient être actives.

De plus, nous étendons la technique de resserrement des bornes basée sur l'optimisation pour le problème de dépistage des contraintes dans le contexte de l'AC-OPF en utilisant l'apprentissage de contraintes. En raison de la non-convexité de l'AC-OPF, nous étudions comment différentes relaxations convexes du problème d'AC-OPF performent dans le dépistage des contraintes des contraintes de ligne.

Ensuite, nous proposons un algorithme d'apprentissage automatique interprétable pour la génération de contraintes en temps réel pour le problème d'engagement des unités contraint par la sécurité. Notre approche proposée simplifie et accélère l'approche conventionnelle de génération de contraintes en utilisant des approches d'apprentissage automatique pour apprendre l'ensemble actif de contraintes avant et après une contingence, puis pour amorcer l'approche de génération de contraintes afin de révéler l'ensemble critique de contraintes non contraignantes qui sont également nécessaires pour garantir la faisabilité et l'optimalité de la solution.

Enfin, nous développons une nouvelle approche pour déterminer la distance entre une solution de problème d'optimisation et ses contraintes formant l'intérieur de sa région de faisabilité, ou même ses contraintes violées dans les cas où les problèmes sont infaisables. Ici, la notion de « distance » par rapport aux contraintes d'un problème est associée à la capacité du système électrique à réagir à des événements incertains, c'est-à-dire à sa flexibilité. À cette fin, nous proposons des métriques de flexibilité du système qui sont calculées en résolvant un problème d'optimisation inverse associé. On révéle que lorsqu'on applique cette approche à l'ensemble de capacité de charge d'un système électrique, elle peut déterminer avec précision la faisabilité de vecteurs de charge nette incertaine, et elle est capable d'identifier quelles contraintes sont les plus proches de ce vecteur de charge nette.

Acknowledgements

First and foremost, I want to convey my thanks to the Almighty God, whose blessings made all of this possible. Also, I would like to express my thanks and gratitude to my Ph.D. supervisor Professor François Bouffard for his continuous support and guidance throughout my PhD studies. I want to extend my heartfelt appreciation to him for empowering me to exercise my academic independence while conducting my research. This thesis has been made possible with the financial support I received over the course of my Ph.D. studies. I thus would like to acknowledge McGill University for the McGill Engineering Doctoral Award. I also acknowledge the funding from the Natural Science and Engineering Research Council of Canada, Ottawa, ON, and IVADO, Montreal, QC, and from Trottier Institute for Sustainability in Engineering and Design, Montreal, QC, Montreal, QC. A very special appreciation also goes to all friends and colleagues at McGill power laboratories in particular Marzuq Ajani, Sanja Bajic, Fares Aljajeh, Navdeep Dhaliwal, Ehsan Dehghanpour, Asal Zabetian, Sony Varghese, Nino Ramos, Tayeb Meridji, Abdelrahman Ayad, and Karanvir Sidhu from ECE department for their company and support. Furthermore, I wish to express my gratitude to my Sudanese graduate student fellows in Montreal, with whom I have cherished wonderful moments throughout this remarkable journey.

To my parents, Ata Awadalla and Magda Ali, who made countless sacrifices for the well-being and prosperity of their children. You forever blessed me with unconditional love and support that I will spend the rest of my life trying to repay. Also, I am deeply indebted to my sisters for their unconditional love, encouragement, and support during my Ph.D. studies. Finally, I extend my heartfelt gratitude to my beloved wife, Azza, who stood by me during challenging times throughout my Ph.D. program. Her unwavering support and presence have been invaluable, and I am deeply thankful for her patience and encouragement. Lastly, this is dedicated to the Sudanese revolution and the courageous and noble young generation who selflessly gave their lives for the promise of a brighter future for our nation.

Preface

My Ph.D. work has resulted in three first-authored publications: two journal papers and one conference paper (as listed below). My main contributions include: identifying the problem definition, designing and developing the methodology, executing simulations and analyzing the results, and composing thesis articles. Prof. François Bouffard performed in-depth proofreading, refined the writing of the papers, assisted in addressing some of the gaps in the drafts of the original papers in terms of analysis, helped in addressing the reviewer's comments, and provided the necessary computing software.

Journal papers

- M. Awadalla, F. Bouffard "Tight and compact data-driven linear relaxations for constraint screening in unit commitment," in IEEE Transactions on Energy Markets, Policy, and Regulation, doi: 10.1109/TEMPR.2023.3327903.

  This research work is included in Chapter 2 of this thesis.

- M. Awadalla, F. Bouffard "Flexibility characterization of sustainable power systems in demand space: a data-driven inverse optimization approach," in IEEE Transactions on Power systems, Under review.

  This research work is included in Chapter 5 of this thesis.

  Conference papers

- M. Awadalla, F. Bouffard "Influence of stochastic dependence on constraint screening in unit commitment," in 11th Bulk Power Systems Dynamics and Control Symposium (IREP 2022), Banff, Canada.

Part of the research work in this conference paper is included in Chapter 2 of this thesis.

Finally, Chapters 3 and 4 are to be submitted as journal articles:

- M. Awadalla, F. Bouffard "Integrating learning and constraints generation for security-constrained unit commitment acceleration," To be submitted.
- M. Awadalla, F. Bouffard "Cost-aware bound tightening for constraints screening in ac OPF," To be submitted.

Contents

List of Figures

List of Tables

List of Acronyms

ACOPF	alternating current optimal power flow.
CG	constraint generation.
CO	constrained optimization.
DCOPF	direct current optimal power flow.
DER	distributed energy resources.
GSF	generation shift factor.
IEA	International Energy Agency.
IO	inverse optimization.
ISO	independent system operator.
KNN	K-nearest neighbor.
LP	linear programming.
MILP	mixed-integer linear program.
MIP	mixed integer program.
ML	machine learning.
NN	neural network.
OBBT	optimization-based bound tightening.
OPF	optimal power flow.
PMU	phasor measurement unit.
PTDF	power transfer distribution factor.
PV	photovoltaic.

QCR quadratic convex relaxation.

RES renewable energy sources.

RTO regional transmission organization.

SCOPF security constrained optimal power flow.

SCUC security-constrained unit commitment.

SDR semidefinite relaxation.

SFT simultaneous feasibility test.

SG smart grid.

SOCR second-order cone relaxation.

TCR tight-and-cheap relaxation.

UC unit commitment.

List of Symbols

The main symbols used in the thesis for problems with linear formulations, which are covered in chapters 2, 3, and 5, are defined here. Further symbols will be defined as required.

Indices and Sets

$\mathcal{C}$	Set of contingencies states, indexed by c and of size C.
$\mathcal{D}(\zeta)$	Minimal loadability set.
$\mathcal{J}$	Set of inequalities, indexed by j and of size J.
$\mathcal{L}$	Set of transmission lines, indexed by l and of size L.
$\mathcal{M}$	Set of generating units, indexed by m and of size M.
$\mathcal{M}_n$	Set of generating units connected to bus n.
$\mathcal{N}$	Set of buses, indexed by n and of size N.
$\mathcal{T}$	Set of time periods, indexed by t and of size T.
$\Xi_d(\zeta)$	Projection of the generation-demand space onto the demand space only.
$\Xi_{gd}(\zeta)$	Feasibility region of a power system in the generation-demand space.

Parameters

γ	Value of lost load and renewable generation curtailment.

c_m Incremental production cost of generating unit m.

d^0 Vector of nominal net load for inverse optimization.

d_n Net load at node n.

$f_l^{\max}$ Maximum flow capacity of transmission line l.

$g_m^{\max}$ Maximum power limit of generator m.

$g_m^{\min}$ Minimum power limit of generator m.

h_{ln}^c Power transfer distribution factor (PTDF) of line l for power injections at bus n for contingency state c.

h_{ln} Power transfer distribution factor of line l for power injections at bus n.

Variables

g_m Power output dispatch of generating unit m.

q_n Net injected power at node n.

u_m Commitment of generating unit m.

g_m^0 Scheduled base point of generating unit m.

$\hat{g}_n$ Total dispatchable generation output at bus n.

s Vector of slack variables associated with strong duality constraint in the inverse problem.

y Vector of dual variables associated with primary constraints in the forward problem.

ζ_m Schedules of generating unit m including commitment status, that is $\zeta_m = (u_m,\, g_m^0 + r_m^{\uparrow},\, g_m^0 - r_m^{\downarrow})$ in the operations planning horizon.

ζ	Collection of all ζ_m.
ρ	Flexibility (goodness of fit) metric for inverse optimization.
ϵ_n	Load shedding and renewable generation curtailment at bus n.

The main symbols used in the thesis for problems with non-linear formulations, which are covered in chapter 4, are defined next. Further symbols will be defined as required.

Sets and Indices

$\mathbb{H}^n$	Set of $n \times n$ Hermitian matrices.
$\mathbb{R}/\mathbb{C}$	Set of real/complex numbers.
$\mathcal{G}$	Set of generators.
$\mathcal{G}_k$	Set of generators connected to bus k.
$\mathcal{L}$	Set of branches, indexed by ℓ.
$\mathcal{N}$	Set of buses.

Operators

$(\cdot)^*$	Conjugate operator.
$\angle(\cdot)$	Phase operator.
$\mathrm{Re}(\cdot)/\mathrm{Im}(\cdot)$	Real/imaginary part operator.

Parameters

b'_k	Conductance of shunt element at bus k.
c_{g2}, c_{g1}, c_{g0}	Generation cost coefficients of generator g.

g_k'	Susceptance of shunt element at bus k.
p_{Dk}	Active power demand at bus k.
q_{Dk}	Reactive power demand at bus k.
$y_\ell^{-1} = r_\ell + jx_\ell$	Series impedance of branch ℓ.

Variables

$p_{f\ell}$	Active power flow injected along branch ℓ by its $from$ end.
p_{Gg}	Active power generation by generator g.
$p_{t\ell}$	Active power flow injected along branch ℓ by its *to* end.
$q_{f\ell}$	Reactive power flow injected along branch ℓ by its $from$ end.
q_{Gg}	Reactive power generation by generator g.
$q_{t\ell}$	Reactive power flow injected along branch ℓ by its *to* end.
v_k	Complex (phasor) voltage at bus k.

Chapter 1

Introduction

The integration of renewable energy sources (RES) is growing rapidly worldwide today. The International Energy Agency (IEA) predicts that between 2021 and 2026, renewable electricity capacity additions will increase approximately by 60% to almost 4800 GW globally by 2026. The percentage of renewable energy in total energy generation is forecasted to be 33%, surpassing coal-fired electricity generation by 2025 [1].

However, many issues can emerge from the massive penetration of renewable generation into the grid. The majority of RES production, such as wind generation and photovoltaic (PV) generation, is dependent on weather conditions, which makes it intermittent, variable, and uncertain in nature. These inherent characteristics of renewable generation lead to increased variability and uncertainty in the grid, and they undermine the security and reliability of power system operation [2]. Consequently, this has driven the emergence of techniques for power system operation and planning under uncertainty in academia and industry [3].

In fact, the unit commitment (UC) problem is one of the primary optimization problems for power systems operation and electricity market clearing [4], being solved daily multiple times by major Independent System Operators (ISOs) in the United States such as the New England ISO, California ISO, and PJM, and regional transmission organization (RTO) to schedule 3.8 trillion kilowatt-hours (kWh) of energy production and clear a $ 400 billion electricity market annually [5]. The problem seeks the most economically-efficient power generation schedule, while a large number of physical and engineering constraints are satisfied. However, solving this problem remains a challenge given the nature of UC and its large size.

1.1 Unit Commitment Problem Overview

ISOs established wholesale electricity markets to enable competition among generating resources which clear hourly and sub-hourly markets while determining corresponding clearing prices. Grid reliability must be maintained in all electricity markets besides balancing supply and demand. Reliability in the context of power systems can be seen as a combination of *security* and *adequacy* [6]. Security refers to the ability of the system to withstand and recover from disturbances such as equipment failures [7, 8], extreme weather events and natural disasters [9, 10], or cyber-physical attacks [11, 12]. In contrast, adequacy focuses on possessing appropriate generation and transmission infrastructure to meet the changes in the forecasted demand [2, 13].

Moreover, power system operators are now inclined to dispatch traditional generation in a sub-hourly manner to address the potentially rapid fluctuations induced by RES generation. Thus, to incorporate RES into UC, we define the *net load* to be the load from customers minus non-dispatchable renewable generation at a given time. Moreover, ISOs are responsible for maximizing the utilization of their regional generation resources and transmission network by running day-ahead and real-time markets. The heart of the electricity market clearing is the security-constrained unit commitment (SCUC) which on top of clearing the market, it is taking into account the need to make sure security and adequacy are satisfied with a high level of confidence [14].

The SCUC problem has been intensively studied in the literature over the years, and it is evidenced by several review papers and dedicated books [4, 15–18]. The SCUC determines which generators should be turned on and their output levels for each hour (or sub-hour period) of the next day. The objective of the SCUC is to minimize the global generation production and start-up and shut-down costs, while ensuring network and generating units' constraints are met [19]. Alternatively, the SCUC can be adapted to the maximization of social welfare as an objective function [20]. However, the demand side is fairly inelastic which makes the adoption of minimizing production cost more common in SCUC formulations. Mathematically, the SCUC problem is a non-convex, large-scale mixed integer program (MIP) with many binary and continuous variables, equality, and inequality constraints. SCUC is known to be NP-hard (Nondeterministic Polynomial-time hard) problem [21].

The North American Electric Reliability Corporation (NERC) develops and enforces reliability standards for bulk power systems, which include high-voltage transmission lines, power plants, and other equipment that make up the interconnected power grid in North America. Furthermore, the complexity of SCUC is even more stressed because of the standards set by NERC, whereby network outage scenarios (contingencies) have to be considered in the SCUC problem formulation [16]. Because of SCUC's inherent computational burden and for obvious economic reasons, system operators have typically considered the loss of one or two components at most as part of SCUC through the well-known $N-1$ and $N-2$ security criteria [22]. NERC standards can be fulfilled by following either preventive [23] or corrective [24] control approaches, where the values of decision variables when operating under contingencies are respectively forbidden or allowed to change with respect to those under the normal state. Actually, corrective paradigms, if not already automated like primary frequency control, often necessitate immediate operator actions, such as the rapid dispatch of multiple generating units within a tight time frame (typically between 10 to 20 minutes) to prevent further adverse situations such as component overloading and load shedding. In contrast, preventive actions, taken as part of SCUC solution, prevent overloading in the post-contingency steady states by maintaining the same decision variables values in the pre-and post-contingency states. As a result, a preventive approach for power system operation results in more costly optimal solutions [25] because operation decisions have to be consistent with pre- and all post-contingency conditions. Nevertheless, the implementation of a SCUC instance that implements preventive control is significantly simpler since it determines a single set of decision variables per time period. The efficiency of SCUC's computational performance is crucial in practice, as there are typically short time windows for clearing electricity markets. Therefore, a preventive SCUC can provide an effective compromise between cost optimization and computational burden.

This thesis primarily focuses on the deterministic SCUC problem that is being used in electricity market clearing in many jurisdictions in North America [16]. In the next subsection, we review SCUC: its mathematical formulation, state-of-art-solution techniques in solving electricity market clearing problems, and future emerging challenges of market clearing problems.

1.1.1 Unit Commitment Formulation and Solution Methods

In electricity markets, ISOs manage day-ahead and real-time markets. To solve the day-ahead market, a SCUC is solved for the 24 hours of the next operating day. The corresponding optimization problem considers several time periods.[1] This results in a large number of possible commitment decisions that need to be evaluated, which leads to a high computational complexity. Theoretically, all ac and dc load flow equations and possible contingencies can be imposed into one multi-period ac optimal power flow (AC-SCOPF) problem. Practically, the mainstream industry practice is to solve a SCUC which is formulated as a UC relaxation followed by an auxiliary security analysis called the simultaneous feasibility test (SFT) to iteratively add pre and post-contingency violated transmission constraints [6, 16, 26]. The overall SCUC solution process runs as follows:

1. The ISO clears the market by solving a unit commitment to optimize the generators' commitments by determining their on/off statuses and their active power schedules. Voltage controls and reactive power management are primarily handled outside of the market clearing and enforced as linear constraints on active power [27]. Impacts of

[1] As just mentioned, 24 in North American markets. Note, however, that some other markets, like that of England and Wales, have sub-hourly time steps (48 half-hourly steps in the British case).

losses are considered in the load forecast [16].

2. Next, a *security analysis* is run. It requires running dc load flows for each credible operating state and the generation schedules (found by the market clearing algorithm) and then identifying line flow violations.

3. The previously-identified violations are added in the next iteration in the unit commitment by introducing new constraint whose role is to make sure identified violations cannot take place. These added violations are formulated as linear inequality constraints using power transfer distribution factors (PTDFs) [26].

4. This process is repeated until all violations have been removed.

This pure optimization-based iterative method is also called a *constraint generation* algorithm [28].

At an abstract level, SCUC is minimizing the operating cost of the given set of resources, subject to the physical constraints of these resources and those of the entire system, a high level formulation of this problem can be cast as follows [16]:

$$\min f(u, g) = \sum_{m \in \mathcal{M}} C_m(g_m) \tag{1.1}$$

Subject to:

$$\sum_{m \in \mathcal{M}} (A_m g_m + B_m u_m) \leq D \tag{1.2}$$

$$(u_m, g_m, C_m) \in \Pi_m, \qquad \forall m \in \mathcal{M} \tag{1.3}$$

Decision variables include the commitment status of the generating units $u_m = \{0, 1\}$—0 if off, 1 if on—, and the power output schedules g_m. The objective function (1.1) minimizes the operating cost of the given set of generating units. The constraint (1.2) describes the physical operational constraints of the transmission network which include the power balance, transmission flow limits, and reserve requirements. The constraints

(1.3) abstractly represents the physical limits of generators' binary and continuous production variables.

Most studies have formulated SCUC as a MILP problem. Furthermore, the problem has been investigated in different ways to improve the MILP formulation performance considering two metrics: *tightness* and *compactness* [29]. The tightness of a MILP formulation measures the feasible region size that the solver has to search to find the optimal integer solution. If the search space of a formulation is smaller, then it can be considered a tighter formulation compared to others. Ideally, a tight MILP problem provides a linear programming (LP) relaxation feasible region which corresponds exactly to the convex hull of the feasible integer points [30]. Hence, the tightness can be determined using the distance between the LP and MILP solutions which is called the integrality gap [30, 31]. Measures of this type depend on how the solver approaches the problem. For instance, it may be possible to estimate the tightness by decoupling the problem performance from the solver's strategies (e.g., heuristics and pre-resolve). On the other hand, the compactness of an MILP problem corresponds to its size, which is primarily influenced by the number of binary and continuous variables, as well as constraints. A prominent approach for enhancing compactness is the elimination of redundant and non-binding constraints [32, 33]. In addition, another research stream has attempted to reduce the number of binary variables to improve MILP compactness [34, 35]. Also, spatial and temporal decomposition techniques [36–38] have been suggested to enhance the UC solution time. Typically, a more compact problem formulation will require less computer memory, and, therefore, will run faster and face a lower risk of memory overrun. Finally, for further reading on the subject, the reader invited to look at recent papers that assess and compare current state-of-the-art unit commitment formulations [19, 30].

1.1.2 Unit Commitment under Uncertainty

The ongoing surge in the deployment of RES—particularly wind and solar power generation—is causing increased disturbances when balancing supply and demand during real-time operations. In the formulation of the UC problem, system operators depend on different input data in determining certain parameters. Forecasts of load and renewable energy are examples of such parameters. Unfortunately, these parameters are uncertain, as RES output power depends on the weather, which is inherently stochastic in nature and is subject to high levels of variability and forecasting uncertainty. As a consequence of RES emerging in recent years, the conventional SCUC problem formulation has been shown to exhibit limitations in the presence of these uncertain parameters [39].

In day-ahead electricity market planning, utilities and system operators must select which generating units to commit to meet the expected demand for the following day before the exact renewable generation is known. Broadly speaking, the dilemma of how to achieve optimal decisions in the presence of uncertainty is directly linked to the field of *optimization under uncertainty* [3], which includes stochastic optimization [4], robust optimization [40], chance-constrained optimization [41], and distributionally-robust optimization [42]. As a matter of fact, the type of optimization formulation depends on the available information about the uncertain parameters and how we could model and represent these parameters on the specific problem.

Consequently, uncertain parameters in UC can be described broadly in three categories. The first family models uncertain parameters using probability distributions, resulting in stochastic programming or chance-constrained programming problems. In the second approach, a range of possible realizations including worst-case scenarios of the uncertain parameters are taken into account to optimize the objective function; this set is referred to as an uncertainty set and yields a robust optimization framework. Third, distributionally-robust optimization optimizes performance in worst-case distributions based on a family of inexact probability distributions restricted to an ambiguity set. A comprehensive review of stochastic, robust, chance-constrained, and distributionally-robust optimizations in power systems operation and planning can be found in [3].

In order to operate the system at the lowest expected cost and benefit from RES, the stochastic unit commitment problem aims to determine the optimal day-ahead commitment of generators and their planned generation output. This stochastic problem optimizes the fixed cost of committing generators and the variable dispatching cost based on a representative subset of possible realizations of uncertainty. The problem is primarily described as a two-stage stochastic program [43]. In the first stage, generating units are optimized and committed without perfect knowledge of uncertain parameters (based on the most-likely forecasted scenario), and then uncertainty is revealed in the form of realized forecast errors. To balance the system after uncertainty realization while respecting all constraints, the system is allowed to dispatch generators in the second stage. In the last decade, there has been a revival of interest in stochastic unit commitment as a way of assessing the effect of renewable resource integration on power system operating costs and reserve requirements [44, 45]. Nevertheless, stochastic optimization approaches do suffer from computational intractability due to the need to consider excessively large numbers of scenarios to achieve a realistic uncertainty characterization [46]. In light of the attractive tradeoff between tractability and accuracy, two-stage robust optimization has replaced stochastic methods to deal with uncertainty in day-ahead generation scheduling [47, 48]. Therefore, we mainly consider robust approaches for the generation scheduling and short-term characterization of operational flexibility in this thesis.

When optimizing day-ahead generation operations in the presence of power injection uncertainty (e.g., demand less non-dispatchable generation, also known as *net load*), one must characterize how this uncertainty propagates through the power system regarding quantities such as voltages and transmission line flows (to be kept within bounds). Based on this information, we can formulate optimization problems to limit the potentially negative impacts of uncertainty.

1.1.3 Operational Flexibility Characterization under Unit Commitment

The ongoing transformation of the conventional power systems paradigm leads to the study of the emerging concept of *power system flexibility* [2]. Power system flexibility is defined as the system's ability to accommodate any component outage or variation in its net load to keep the system secure [2,49,50]. The ultimate goal is to have enough flexibility to cope with the increasing RES levels so that economic and secure operation can still be maintained. In the literature, several definitions and metrics have been proposed to study the need for, and the provision of power system flexibility. Broadly, quantifying power system flexibility for bulk power system operation with RES can be classified into two main categories: implicit and explicit methods with respect to RES uncertainties [51].

The implicit approach addresses a pre-defined uncertainty and solves generation scheduling problems [50, 51]. Most contributions in this category use stochastic techniques and robust approaches which model uncertain parameters using probability distributions and worst-case scenarios, respectively [48], [52]. However, this category of approaches only focuses on how to optimally exploit existing generation assets to deal with a given amount of uncertainty. In short, research in the first family aims to address the question of how to manage a certain level of uncertainty using existing generation assets.

Conversely, the motivation for explicit approaches found in the literature is that future power systems are expected to operate near their conventional generators' flexible capacity limits due to the high shares of variable renewable energy [53]. Furthermore, they recognize that unit commitment problem solutions may be overly costly if worst-case realizations of uncertainty have to lead to feasible solutions by dispatching expensive generators. Moreover, they acknowledge that in extreme cases it may not even be possible find feasible UC solutions [54]. Thus, the practicality of classical robust UC, meant to support a wide range of operating conditions, could be severely limited under very deep penetrations of renewables. In order to address these shortfalls, the second class of approaches tackles the reverse question: how much uncertainty can be adopted using existing flexible resources? This necessitates the assessment of system flexibility for given operating conditions [51].

1.2 Optimal Power Flow

The optimal power flow (OPF) optimization problem seeks to find optimal operating conditions subject to physical and engineering constraints of electricity networks [33, 55]. The OPF incorporates physical constraints to model the power flow equations and engineering constraints such as voltage, generator output, angle difference, and line flow limits. The AC-OPF problem, when formulated with the ac power flow equations, is nonconvex and NP-hard [55]. Furthermore, the number of variables and constraints becomes large as the network size increases, posing more computational challenges for large realistic systems.

Numerous algorithms have been utilized to locate locally optimal AC-OPF solutions which tend, often, to coincide with globally optimal solutions [56]. In recent years, there have been various attempts to develop convex relaxation techniques for AC-OPF problems, which involve replacing the AC power flow constraints with a convex outer approximation of its feasible set [57, 58]. Convex relaxation is a technique that aims to convert a non-convex feasible region into a larger convex region using constraints that are less restrictive than the non-linear AC power flow equations. The constraints are designed to maintain convexity and carefully formulated to ensure the feasibility of the solutions within the convex region. The interested reader may refer to [59] for a comprehensive survey. Convex relaxations are useful as they provide a lower bound on the optimal objective value for the non-convex problem, they can determine whether the problem is infeasible, and, under certain conditions, can provide a globally optimal solution to the original non-convex problem [60].

The power flow equations dictate how uncertainties in power injections propagate into corresponding uncertainties in voltages and power flows. The choice of the power flow formulation, such as whether to use the full non-linear AC power flow equations (be its traditional version expressing voltage phasors in polar coordinates or the less common version expressing voltage phasors in rectangular coordinates), a linearized version, or a convex relaxation, can have a significant impact on the complexity of the problem [3]. In the rest of this chapter, we will discuss some of the challenges and solution approaches related to the use of different power flow formulations when dealing with power injection uncertainty.

1.3 The Challenges of Operational Planning Problems in Sustainable Power Systems

One aspect of UC/SCUC/OPF problems which has been understudied in previous research is that in many real-life situations, these problems are solved repeatedly with similar patterns in input data, often multiple times per day. Variability in operating conditions show up in problem input data. These are a consequence of renewable energy integration in power systems, uncertain demand-side behavior and asset failures. The majority of power systems parameters, such as generator characteristics and the topology of the transmission network, remain nearly unchanged from one solution instance to another. Moreover, the computational complexity of operational planning problems could be exacerbated if a significant number of uncertainties, sub-hourly operation features, and distributed energy resources are taken into account. Finding optimal solutions may become a daunting task in light of these additional challenges. Hence, machine learning is a promising alternative in support of these optimization problems. The purpose of this thesis is to present methodologies for using ML to efficiently extract information from previously-solved instances and leverage that information to increase the speed at which similar instances can be solved in the future. ML is a field that involves the development of algorithms and statistical models that can automatically learn from data and make predictions or decisions quickly and accurately without being explicitly programmed to do so.

1.4 Synergy Between Operational Cost Optimization in Power Systems and Machine Learning

Despite the extensive body of academic literature on machine learning approaches for power systems over the past 30 years, the practical applications have been limited in practice. The primary practical application is load forecasting, such as Artificial Neural Network Short

Term Load Forecaster tool [61], and few approaches have been associated with decision trees for security assessment [62]. In academia, numerous ML classification and prediction approaches, including artificial neural networks and, more recently, deep learning, have been employed for system stability assessment and frequency control [63, 64]. These methods encompass both supervised and unsupervised learning techniques. However, a breakdown of machine learning approaches in a recent review publication [65] reveals that, in reliability and energy management and security assessment applications, supervised learning is the predominant approach compared to unsupervised and reinforcement learning. We refer the interested reader to more general textbooks for further information about machine learning [66, 67].

Notably, there has been a recent research interest in employing machine learning for enhancing computations in operational planning problems, which constitutes the main focus of this thesis and will be discussed in detail in this section. Substituting ML predictions for optimizations is not the appropriate strategy in critical decision-making problems in power systems, as it does not ensure the provision of optimal operating points that will not violate any line limits [68]. In other words, machine learning methods do not offer assurances regarding potential constraint violations in their output. This is a significant drawback, especially when replacing operational planning problems [69]. Moreover, power system operators struggle to trust methods they don't comprehend, especially when these methods haven't offered any performance guarantees regarding the feasibility and optimality of their solutions [62].

1.4.1 Fusing Optimization and Machine Learning: Operation Research Background

The synergy between mathematical optimization and machine learning (ML) has gained prominence in recent years. In the operations research community, the use of machine learning is becoming increasingly widespread to facilitate the formulation and the solution of optimization problems [70–73]. For instance, ML has been used to direct branching in

MIP solution algorithms [74], aid in heuristic selection [75], and in data-driven scheduling heuristics approaches in exact MIP solvers [76]. An article published recently by Bengio *et al.* [72] discusses recent attempts to solve combinatorial optimization problems using machine learning methods. Moreover, another prominent paper [73] has highlighted two main directions in the current research on the nexus of constrained optimization and machine learning. The first direction is known as ML-augmented constrained optimization (CO), which emphasizes the use of machine learning to enhance the performance of CO problem solvers [72, 77]. The references [74–76] are examples of the former family. The second venue is end-to-end learning, which encompasses a broad range of work, including efforts to create machine learning architectures that can quickly and approximately solve predefined CO problems without relying on optimization solvers [71]. These architectures are typically trained using sets of solved instances or execution traces, with the goal of predicting solutions that are both fast and accurate. There is another emerging research venue that hybridizes learning and optimization by embedding learning inside a complex optimization problem. From a power systems operational planning perspective, we can summarize these emerging research venues in two main categories as follows:

- Optimization proxies: The concept of optimization proxies involves replacing a resource-intensive optimization model with a machine-learning proxy that can be used in real-time or in computationally demanding scenarios such as the unit commitment problem [78, 79]. However, a significant challenge in developing such proxies is to train them for large-scale optimization problems that incorporate physical, engineering, and operational constraints. This is also referred to as end-to-end learning.

- Learning to optimize: The notion involves substituting certain parts of optimization models with machine learning models.

The research areas mentioned in this section demonstrate how ML can be used to learn or solve optimization problems more efficiently. This goal was achieved by either enhancing the performance of MIP solvers or using optimization proxies. However, these ML-based methods have a major disadvantage in addressing engineering problems. In fact, all models are not adequate in enforcing constraints. This is due to the fact that the methods do not take advantage of prior knowledge about the mathematical optimization problem in the first place [80]. Therefore, our focus on this research falls within the last class which is mainly on how to fuse machine learning to learn constraints to speed up the solution of operational planning problems such as security-constrained unit commitment and optimal power flow.

1.4.2 Applications in Power Systems Operational Planning

In recent years, there has been considerable interest in using machine learning to speed up the solution of the UC/SCUC/OPF problems. This body of research is divided into two primary clusters which reconcile with the previously-discussed research directions regarding the intersection of artificial intelligence and operation research. The first direction focuses on end-to-end learning techniques that directly learn then predict the optimization decisions, effectively replicating the LP and MIP solvers. The second direction involves developing methods to identify a simplified version of the UC/OPF problem which, in turn, is easier to solve.

The majority of research on optimization proxies for UC focuses on utilizing different types of machine learning techniques such as K-nearest neighbors [79], neural network (NN) models [78, 81] to map uncertain load profiles to optimal problem decisions. Similarly, different neural networks have been utilized to obtain optimization proxies. These includes deep-NN in economic dispatch [82] and dc-OPF [83], as well as conventional NN for dc-OPF [84]. Nevertheless, power systems are considered critical infrastructures whose service is vital to society; therefore, systems operators tend to be risk-averse, which creates challenges for the adoption of optimization proxies (ML-based tools) for decision making [62]. This is because ML-based approaches do not provide any guarantees in terms of feasibility nor optimality. In other words, the publications [78, 79, 81–83] detail significant computational speed improvements and empirically analyze the accuracy and feasibility of the obtained solutions. Assessing the worst-case performance of ML-based methods based on discrete samples from the entire training and test datasets provides only an empirical lower bound for the worst-case guarantee [84]. Furthermore, recent research indicates that neural networks achieving high accuracy on unseen test data can be vulnerable to adversarial examples, resulting in significantly reduced accuracy on inputs crafted adversarially [85, 86]. The presence of adversarial examples in power system applications has also been demonstrated [87].

Furthermore, for the practical application of machine learning models to problems like the UC and OPF, it is essential to have transparency, interpretability, and most importantly performance guarantees. On the other hand, identifying the set of problem constraints that are binding at the optimal solution is typically less complex than predicting the optimal decisions. Consequently, this second category of approaches, which fuses machine learning and optimization, is much more attractive for practical applications, as it focuses on identifying the most likely active sets of constraints. With this information on hand, locating optimal solutions for UC [88, 89] and OPF [80, 90–92] is expected to be significantly faster and require fewer computing resources.

However, we believe that there is even more value in using ML for optimization: ML can be used to learn constraints [93–95]. ML enables learning functions that map decisions to the outcome of interest by leveraging data. Through ML, we can create predictive models for a certain outcome we seek to constrain, and subsequently embeds these models in optimization problems, a notion known as *constraint learning* [93]. These learned models can then be integrated into optimization problems as function approximations, by exploiting MILP reformulation capabilities inherent in numerous ML models [95]. In real-life engineering optimization problems, there are often constraints or objectives for which no explicit formulas exist. Nevertheless, in the presence of data, it is possible to utilize the data to mathematically formulate constraints that lack explicit formulas. Our objective is to close this gap by leveraging *constraint learning*.

The selection of the ML model relies on whether the constraint to be learned produces a discrete set of values (classification) or a continuous range of values (regression) [93]. If a classification model is used, it learns a feasible set or constraints, whereas a regression model learns an explicit function. The recent big data boom in smart grid (SG), where vast amount of data generated from different sources such as smart meters, phasor measurement unit (PMU), power market pricing and bidding data, and power system monitoring and control equipment historians provides vast possibilities to extract useful insights about the operation, planning and economics of power systems. As long as there is data available, which is the case in modern power systems [96], constraint learning is expected to be feasible.

1.5 Problem Identification

The computational performance of UC/SCUC is an extremely critical practical issue given the small time window mandated in most electricity markets to produce feasible and optimal schedules. Therefore, it is vital for system operators to solve SCUC problems quickly and robustly to secure the system's operation. On the other hand, the unit commitment problem has proven to be very difficult to solve. The size of these problems is enormous, and the existence of many integer variables renders it prone to difficult convergence [16, 33, 97].

The improvement of computational performance has the potential to enable electricity markets to implement several enhancements which could provide substantial economic benefits and boost market efficiency [16, 89], such as more accurate modeling of massive distributed energy resources (DER) [98], modeling the interdependency between electricity and gas networks [99], sub-hourly unit commitment and dispatch [100], among others.

To better illustrate our underlying motivation for this work with respect to the state-of-the-art, we present the following illustrative MILP example:

$$\min_{x \in \mathbb{N},\, y \in \mathbb{R}} x + y \tag{1.4}$$

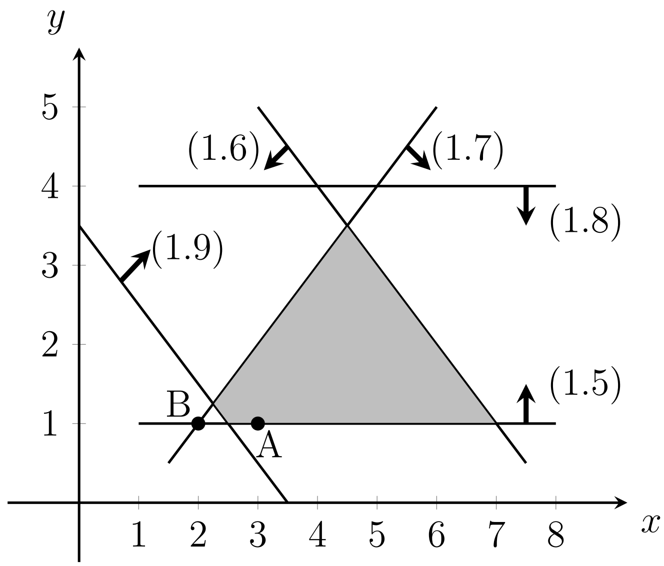

Figure 1.1: Types of constraints in MILP

Subject to:

$$y \geq 1 \tag{1.5}$$

$$x + y \leq 8 \tag{1.6}$$

$$y - x \leq -1 \tag{1.7}$$

$$y \leq 4 \tag{1.8}$$

$$x + y \geq 3.5 \tag{1.9}$$

The five constraints of problem (1.4)–(1.9) are depicted in Fig. 1.1. By inspection, it is clear that the solution of this problem is point A $= (3, 1)$. Let us now discuss the nature of the five constraints with respect to the objective function and the corresponding feasibility region:

- *Binding constraint*: Constraint (1.5) is an *active* or *binding constraint* that holds with equality at the optimum. If this constraint is removed both the feasible region and, therefore, the problem's solution would both change.

- *Non-binding constraint*: Constraint (1.6) does not hold with equality at the optimal point. If this constraint is removed, the feasible region changes but the optimal solution remains the same (for this particular objective function). This type of constraint can also be referred to as an *inactive* or a *non-binding constraint*.

- *Redundant constraint*: Constraint (1.8) does not hold with equality at the optimal point either. Note, however, that this is a very particular inactive constraint since, if removed, the feasible region is unaffected. This means that the optimal solution for any given objective function remains the same even when this constraint is eliminated from the problem.

- *Critical non-binding constraint*: Constraint (1.9) is not binding at the optimum either. However, the optimal solution would change from A to B $= (2, 1)$ if removed. This is a non-binding constraint that cannot be eliminated without affecting the optimal solution. Moreover, if (1.9) is removed (1.7) will become a critical binding constraint of the problem.

As a means of simplifying an optimization problem to obtain an instance with lower computational complexity than the original one, it is generally advisable to remove the inactive (1.6) and redundant (1.8) constraints. The reduction in complexity—the problem is made more *compact*—results primarily in less pressure on computer random access memory resources, a critical asset in the solution of large MIP problems.

In this context, we make a distinction between the two notions: that of binding constraints, and that of potentially binding or so-called *umbrella constraints*. Umbrella constraints are constraints that shape the feasibility region of an optimization problem [33, 97]. These constraints might not be active or binding for a particular solution obtained to minimize/maximize a certain objective function, but they have the "potential" to be binding for another objective function.

Most of the research in power systems which tackles UC/SCUC problem compactness is focused on identifying umbrella constraints. This approach is acceptable for power systems,

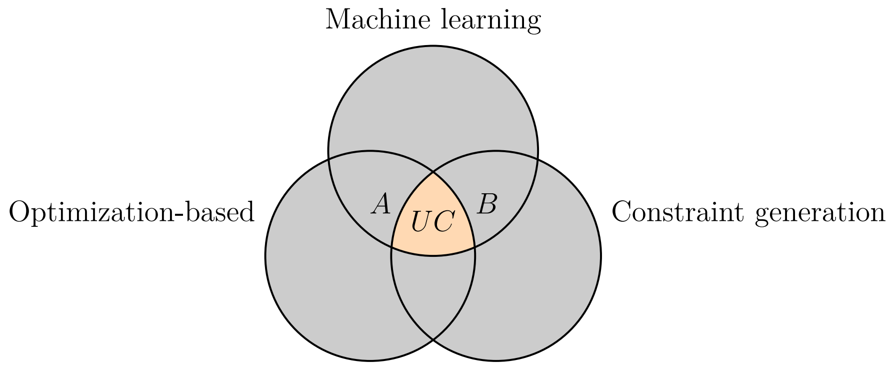

Figure 1.2: Types of constraints screening approaches

albeit it yields inadequate identification of the active and critical non-binding constraints. Hence, the elimination procedure may lead to sub-economical time savings as a result of eliminating only redundant constraints. On the other hand, if the potential binding and critical non-binding constraints are known ahead of solution time, UC/SCUC could be run subject to those constraints only, one expects further computational gains over solutions obtained with the full set of umbrella constraints. In fact, even further could be possible if the identified potential binding and critical non-binding set remains constant when a power system is facing similar net load patterns. Hence, system operators would save significant time, which can be used to make better decisions and plan for more sophisticated and, in turn, more economical control actions. Broadly speaking, constraints screening in generation scheduling problems in the power systems literature have been investigated using three main approaches: optimization-based methods, constraint generation approaches, and machine learning techniques. This thesis is devoted to enhance constraints screening capabilities in power systems. The work reported in the second and third chapters of this thesis respectively lie where labels A and B sit in Fig. 1.2.

1.6 State-of-the-Art on Constraint Screening in Power Systems

1.6.1 Optimization-Based Constraint Screening Approaches

Various optimization-based approaches have been proposed for constraint screening for the UC/SCUC problem. Leveraging the fact that a candidate unit commitment solution can easily be checked for feasibility, standard state-of-the-art approaches add constraints in an iterative way to a reduced base problem [101], which is a unit commitment problem with no transmission constraints [8]. This *constraint generation* approach is a well-known iterative technique where violated constraints from the original UC are gradually added to the reduced one until the solution to the latter is feasible in the former [102]. This method is applied to SCUC in [23, 103] to filter out post-contingency constraints. The drawback of the constraint generation method is that it is computationally expensive if the required number of iterations to guarantee a feasible solution is large. To alleviate the computational burden, decomposition techniques based on Bender's decomposition [104] and column-and-constraint-generation algorithms [105] have been proposed for the direct current optimal power flow (DCOPF) problem only.

Alternatively, the notion of *umbrella constraint* was introduced when identifying redundant constraints which do not alter the feasibility region of the original UC problem when they are removed from the original problem [33, 97]. Similarly, references [32, 106–108] use a *bound tightening* technique [109] and solve two optimization problems for each transmission line in the power system over LP relaxations of the feasible region to remove as many redundant constraints as possible from the full UC formulation. Also, the authors of [110] used *Clarkson's redundancy removal* algorithm that is based on LP and requires solving multiple maximization problems [111] for each possible line flow contingency constraint in a security constrained optimal power flow (SCOPF). The pricipal drawback of [110] is the ignorance of correlated patterns in historical samples of the load and renewable generation. Recently, an analytical approach was proposed by [112] based on an iterative heuristic approach to eliminate nonbinding constraints from UC problems on top of redundant constraints. Initially, the authors propose solving the UC problem without network constraints. After that, they modify this initial generator's schedule by transferring a percentage of total generation output to the nodes with either the highest or the lowest power transfer distribution factors for a given line. Then, they examine whether this modified solution creates congestion on the line. If it does not, the corresponding line constraint is deemed inactive.

In addition, the variability and uncertainty of renewable power generation have introduced new challenges to the operational planning problems [2]. The representation of uncertainty can take the form of scenarios or uncertainty sets for stochastic and robust optimization approaches, respectively. The computational burden of stochastic programming prompts to migrate towards tractable approaches for optimization under uncertainty, namely robust and chance-constrained optimization [68, 113]. Moreover, RES manifest cross-correlation over space and time. Predicting spatial and temporal scenarios has been of interest of power systems operation and planning community for a while now [50, 114–116]. When modeling multivariate correlated scenarios, uncertainty sets take the form of boxes, polyhedral [114], and ellipsoidal sets [115]. An "uncertainty budget" is utilized to control the size and conservativeness of renewables' uncertainty sets in the form of polyhedra in [54, 116] and in the form of ellipsoids in [117]. Conversely, references [48, 50] take a distinct approach by defining prediction regions for wind power as the convex hulls of spatial and temporal scenarios. However, decision-making problems in power systems which include network constraints need different forms of uncertainty sets. For instance, integrating polyhedral uncertainty envelopes with a linear programming problem results in a linear programming problem, whereas the same problem with the ellipsoidal uncertainty sets is a second-order cone programming (SOCP) problem. Even though SOCP is convex, its nonlinearity is deemed a practical pitfall [114].

In fact, the dominant technique in the literature that is optimization-based bound tightening (OBBT) [118, 119] was primarily proposed to enhance the quality of convex relaxations solutions by tightening convex relaxation formulations [120]. The general procedure of OBBT is to perform successive minimization/maximization of a desired variable while considering the constraints of the relaxation. The current research on screening AC-based constraints originates from the literature on bound tightening, which aims to enhance the quality of convex relaxations by tightening the voltage magnitude and angle difference limits. As a result, this leads to distinct variations in the methodology and substantial differences in the rationale and understanding compared to basic constraint screening. However, the bound tightening method has been extended to screen out line flow constraints in ACOPF [121]. Using OBBT, the authors of [121] identify line flow limits that never become active by solving one minimization and one maximization optimization problem associated with each line flow limit. In a broader sense, several constraints are satisfied indirectly through other constraints in the problem, allowing them to be eliminated confidently before requesting the solver's assistance.

1.6.2 Machine Learning and Constraint Generation Approaches

ML-based approaches are beginning to emerge as promising tools for reducing the computational complexity of traditional optimization algorithms. Several ML techniques have been proposed to predict the set of redundant constraints for the optimal power flow [80, 90, 122, 123] and unit commitment problems [88, 89]. In the same vein, some papers have suggested the use of statistical learning algorithms to provide a proxy for the unit commitment status [79, 124]. Particularly, replacing the MIP unit commitment problem with a machine learning algorithm can achieve the most computational time savings, but it is incapable of guaranteeing optimality and/or feasibility. From a power system operator perspective, these approaches are still considered as black boxes and lack transparency and interpretability to replace entirely the MIP decision-making problem [62]. As a matter of fact, these ML-based methods seek to learn from the information provided by the MIP optimal solution to build a simpler formulation of the original MIP that is faster to solve.

The main limitation of these ML-based methods when applied to physical and engineered

Table 1.1: Machine Learning approaches for constraint screening in power systems operation planning

Publications	Objective	Problem	Limitation
[88]	learn active line constraints	UC	infeasibility and suboptimality of UC solution
[28]	learn binding and critical non-binding line constraints	UC	contingencies are not considered
[89]	learn non redundant constraints	SCUC	constraints identification based on heuristics
[123]	learn active constraints	DCOPF	suboptimality of the DCOPF solution
[90]	learn active constraints	DCOPF	suboptimality of the DCOPF solution

systems is their failure to accurately enforce constraints [80]. This drawback can be linked to the fact that these algorithms cannot utilize pre-existing knowledge about the mathematical structure (which captures the physical and engineering limitations of the system) of the optimization problem. For best results, the learning methods should exploit any known structure of the optimization problem in consideration. Machine learning reduces the time spent on online solving by moving the selection of necessary constraints to an offline process, which is particularly beneficial when solving a similar problem multiple times.

The publications summarized in Table 1.1 are in the spirit of constraint learning using ML classification approaches in power systems operation problems which include OPF, UC, and SCUC.

1.7 Gaps in the State of the Art

1.7.1 Optimization-based Constraint Screening Approaches

Within the context of constraint screening for the UC problem with deep penetration of correlated uncertainties, advancement in three aspects is required to close the gap between computationally-tractable, robust, and optimal solutions to the UC constraint screening problem. First, it is necessary to design a computationally-tractable scalable optimization approach that can handle a high degree of uncertainty. Second, it is critical to define a robust and tractable uncertainty set that can capture stochastic dependence between different uncertainties—*i.e.*, loads and renewable generation—, and be used as an input to a robust optimization approach [114]. Third, to yield optimal solutions in constraint screening problems means screening out not only redundant constraints with respect to the feasibility region but also as guided by the UC problem's objective function. In other words, a UC's non-active constraints can be part of its minimal feasible region, but they are never active constraints as they do not oppose the minimization of the UC's objective function [88, 108].

From a methodological point of view, previous work [33, 97] developed MILP and LP formulations respectively, for umbrella constraint discovery (UCD) with a single residual demand parameter vector. The authors of [125] enhanced the original UCD notion from [33, 97] that has lighter computational demands and is better adapted when residual demand uncertainty is considered. The merit of the enhanced approach in [125] is the direct identification of umbrella constraints in lieu of the identification of non-umbrella constraints. This is so because in practical UC problems, the number of umbrella constraints is much smaller than that of non-umbrellas. References [106, 121] considered uncertain residual demand parameters for robust optimization problems. However, these studies built box-shaped uncertainty sets for the univariate system net load (*i.e.*, load less renewable generation) and ignored the inherent spatio-temporal couplings of renewable generation and demand. Although robust optimization techniques immunize the system according to very stringent potential events, it is easy to yield sub-economical outcomes as seen in [50]. The conservativeness of a robust solution is directly related to the *size* of the uncertainty set [114]. By *size* here, we mean the extent of possible random events which the UC will be able to provide a robust solution; larger uncertainty sets, which capture both very likely and very rare events, incur larger operating costs than smaller uncertainty sets because that do not capture all of the very rare events.

On the other hand, previous research on AC constraint screening has mainly been derived from the bound tightening literature [118, 119]. The primary goal of this literature is to enhance the quality of convex relaxations by tightening the limits on voltage magnitudes and angle differences. The bound tightening technique has been used in computing the feasible space of optimal power flow problems [126]. Nevertheless, the methodology used in AC constraint screening exhibits some dissimilarities compared to the primal objective of this technique, where there are key variations in motivation as well. The objective of bounding-based techniques is to eliminate a maximum number of redundant constraints from the complete ACOPF formulation [121]. However, even if all the redundant constraints are identified and screened out, some constraints may still be present in the reduced ACOPF problem that are superfluous because they do not hinder the ACOPF cost minimization, as explained already in Section 1.5.

1.7.2 Machine-Learning and Constraint Generation Approaches

The publications seen in Table 1.1 are in the spirit of constraint learning using ML in power systems operation problems which includes OPF, UC, and SCUC. Several ML techniques have been proposed to predict the set of active line constraints in optimal power flow [90, 123] and unit commitment problems [88]. Particularly, replacing the optimization-based constraints screening with machine learning algorithms can achieve the most computational time savings but it is incapable of guaranteeing optimality, or/and feasibility.

Our work in this thesis is closest related to the proposed approaches in [28, 89] which integrates ML and CG in SCUC and UC, respectively. Xavier *et al.* [89] suggested a heuristic refinement to the CG approach which goes as follows. Rather than including all of the violated post-contingency transmission constraints in the UC relaxation, as previous methods have done [23, 103], they devised a rapid heuristic procedure to narrow down this list by selecting the constraints that exhibit the most significant violation [8]. The drawback of this ad-hoc approach is that it relies on empirical evidence and does not provide a well-defined constraint set to be selected with certain performance guarantees. In other words, the most probable violated constraint set is ill-defined, and consequently, the constraint generation approach might necessitate a potentially significant number of iterations, leading to only minor computational savings. Furthermore, reference [28] enhanced the idea of Xavier *et al.* [89] by defining binding and critical non-binding constraints set for a UC problem. The downside of [28] is that its authors did not include contingencies as part of their developments. In fact, the work by [28] only addressed a simplified unit commitment problem and did not tackle the more intricate and demanding task of security-constrained unit commitment, which necessitates additional investigation.

1.8 Thesis Contributions

We first seek to reduce the conservativeness of the constraint screening for unit commitment problems by proposing *techno-economic umbrella constraint screening*. We extend the UCD formulation of Abiri-Jahromi and Bouffard [125], by comprehensively capturing the spatial correlation of historic net load prediction errors when identifying the umbrella line flow limits in the UC problem. Consequently, we focus on generating computationally-tractable and robust *data-driven polyhedral uncertainty sets*. Compared to previous work, our proposed uncertainty set is less conservative than a conventional box-shaped uncertainty sets as used by [106] and computationally cheaper to set up than the convex hull of compiled historic net load prediction error data [48]. We demonstrate how it provides more conservative uncertainty coverage while, at the same time, improving significantly the computational performance of the constraint screening while guaranteeing the same cost and technical outcomes. From the research gaps presented earlier, state-of-the-art uncertainty set determination methods considering spatial correlations suffer from either conservativeness or computational burden in high-dimensional cases, which is one of the problems to be solved in this thesis. Furthermore, we introduce a valid upper bound inequality constraint whose calculation is based on past UC solution runs as suggested by [108] to eliminate a subset of non-binding constraints on top of non-umbrella constraints. This allows the elimination of unrealistic generation schedules—with, for example, prohibitively high costs—as we run UCD. In contrast to the suggestion from [108], we include adjustment factors to mitigate model misspecification and potential UCD infeasibility, known weaknesses of "predict-then-optimize" and moving towards "smart predict-then-optimize" approach [127].

To this end, we tighten the LP relaxation of the UC by imposing the data-driven polyhedral uncertainty sets and cost-driven upper bound as inequality constraints in the problem formulation. In doing so, we substantially increase the number of line flow constraints that should be eliminated from the original UC without jeopardizing its feasibility nor its optimality. Furthermore, as the UCD algorithm can lend itself well to decomposition, we deploy the decomposition technique suggested (but never tested) by [125] to further expedite its solution. This considers a crucial feature compared to the state-of-the-art *Clarkson's redundancy removal* in [110], where the inherent sequential nature of the algorithm prevents parallel computation because every constraint is checked against both already identified non-redundant constraints and unchecked constraints.

We next explain the notion of *constraint learning* using a regression model for constraint screening in the UC problem. We introduce three cases for UCD and UC problems using an illustrative optimization problem in two variables with schematic diagrams as shown in Fig. 1.3, Fig. 1.4, and Fig. 1.5. By inspection, it is clear that the solution of the UC problems in Fig. 1.3(b), Fig. 1.4(b), and Fig. 1.5(b) is point A. The first case shows the UCD problem where a line flow constraint represented by the red line in Fig. 1.3(a) does not intersect the feasibility region of the UCD problem. Consequently, this constraint –represented by a red dotted line– will be flagged as redundant in the corresponding UC problem in Fig. 1.3(b). Case 2 shows that the line constraint contributes to shaping the minimal feasibility region in the UCD problem in Fig. 1.4(a) and is consequently flagged as a non-redundant (umbrella) constraint in the UC problem in Fig. 1.4(b). Lastly, we introduce a new constraint inferred from previous instances of the UC commitment represented by the blue line in Fig. 1.5(a) through *constraint learning* approach. The addition of this constraint which embodied the economical nature of the UC problem makes the line constraint in case 2 flagged as a non-umbrella constraint in the UCD problem as shown in Fig. 1.5(a). Although the line constraint represented by a red dotted line in Fig. 1.5(b) is necessary for shaping the minimal feasible region of the UC problem but does not affect the minimization of the UC problem. Hence, this constraint is a non-redundant constraint in the UC problem, but it's also an *inactive constraint* that can be eliminated from the UC problem without affecting the minimization of the objective function.

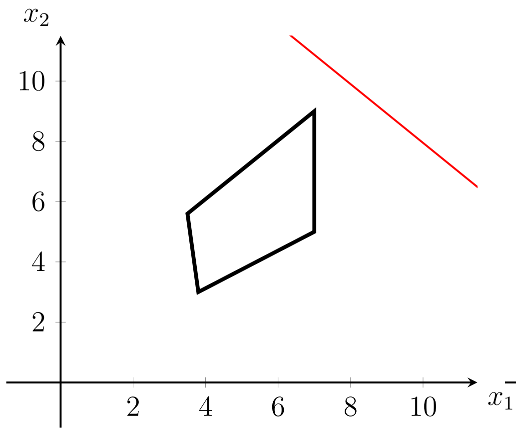

(a) UCD problem - case 1

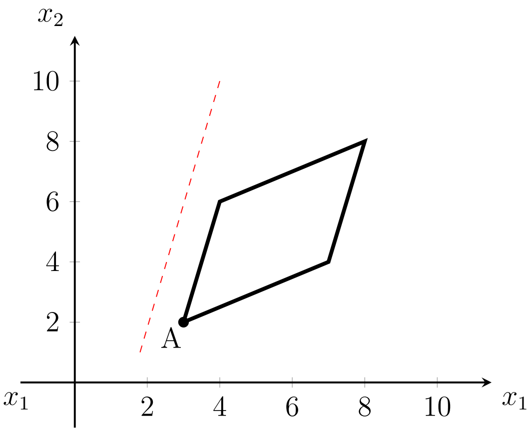

(b) UC problem - case 1

Figure 1.3: UCD and UC case 1

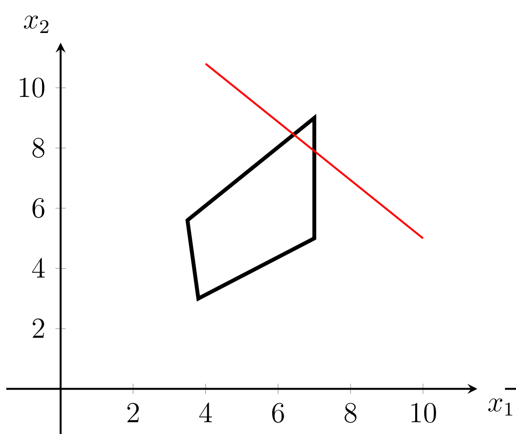

(a) UCD problem - case 2

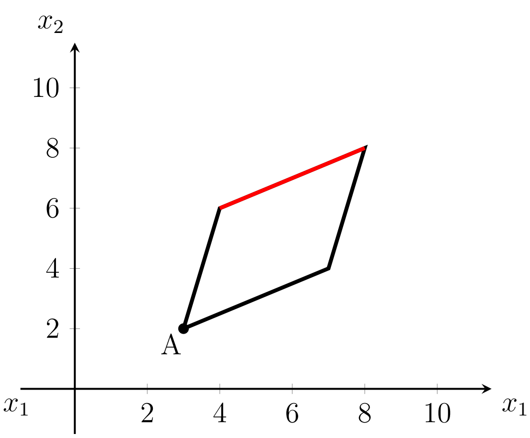

(b) UC problem - case 2

Figure 1.4: UCD and UC case 2

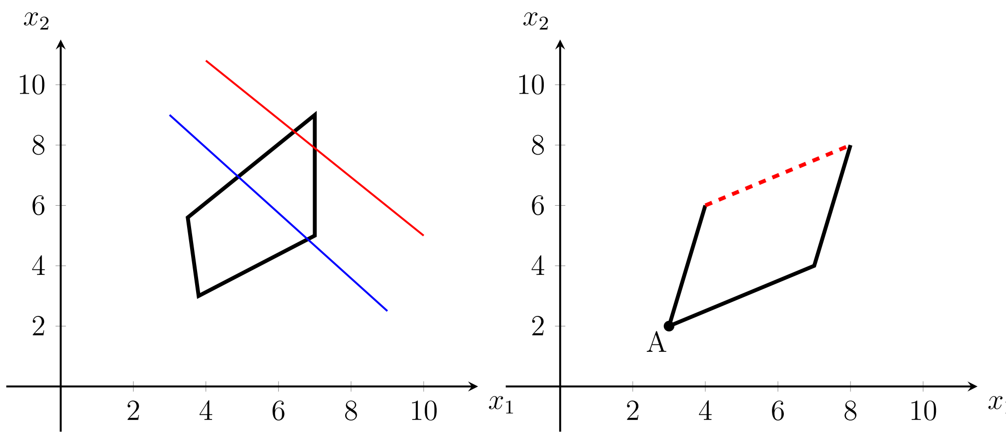

(a) UCD problem - case 3 **(b)** UC problem - case 3

Figure 1.5: UCD and UC case 3

In the context of a nonlinear problem such as ACOPF, we propose a refinement to the OBBT approach. First, instead of attempting to solve OBBT with the nonconvex ACOPF problem directly, we utilize convex relaxations to establish an upper limit on the global solution. Second, rather than identifying only redundant line constraints in the ACOPF, as suggested in [121], we propose a valid upper bound inequality constraint that embodied prior economical information to filter down these redundant constraints.

After discovering the optimal solution for operational planning problems through a more compact formulation, we present a novel method for assessing the distance associated with the obtained solution with respect to the umbrella constraints set, or even its violated constraints in cases when problems are infeasible. This assessment is meant to be quantitatively indicative of how much *flexibility* exists in the bulk power system to handle net load uncertainty for given unit commitment solutions and network topologies. We propose novel system flexibility metrics which are calculated by solving an associated inverse optimization problem. Finally, we enhance the loadability set characterization previously proposed in [125, 128] by incorporating data-driven polyhedral uncertainty set along with the proposed flexibility metrics results from the inverse optimization problem.

1.9 Claim of Originality

This thesis makes the following distinct original contributions to the field of power systems operation and planning, computation, and operational flexibility characterization in power systems.

1. We propose a reformulation of the umbrella constraint discovery problem, which was originally presented for identifying all the redundant constraints in the unit commitment problem. This new formulation, called *techno-economic umbrella constraint discovery*, tightens the linear relaxation of the original UC problem constraints in the UCD formulation by adding two data-driven distinct sets of inequality constraints:

   (a) We set forth a tractable and robust polyhedral uncertainty set induced by historical net load prediction errors. This set of inequality constraints is an uncertainty set that captures correlated net load prediction errors compared to the conventional UCD formulation that ignores them.

   (b) The second inequality constraint is a linear upper bound based on historical objective function values whose role is to predict which of the umbrella constraints have the potential of being active.

2. We propose a refinement to the constraint generation procedure in security-constrained unit commitment. The primary contribution of this approach is that it employs a machine learning technique to warm-start the constraint generation technique in SCUC. This narrows down the number of violated post-contingency transmission constraints, rather than including all of them in the iterative scheme. This goal has been achieved by defining binding and critical non-binding constraints.

3. This thesis addresses the constraint screening problem using the bound tightening technique in the context of the OPF problem formulated with a full ac power flow

characterization. Due to the non-convexity of the ACOPF, we investigate line constraint screening under different convex relaxations of the problem. To the best of our knowledge, this is the first comprehensive comparative analysis of constraint screening under state-of-the-art convex relaxation techniques. This allows us also to evaluate how the economics of the OPF impact screening outcomes.

4. Finally, a novel data-driven inverse optimization problem formulation is proposed which seeks to identify existing system flexibility for uncertainty mitigation. This accomplishes three objectives for flexibility characterization:

    (a) The notion of the *loadability set* is redefined in the context of data-driven polyhedral uncertainty sets.

    (b) We propose a unified framework to characterize power system flexibility explicitly and geometrically in the demand space using data-driven inverse optimization (DDIO).

    (c) We demonstrate how DDIO can be used to determine system flexibility deficits and how to mitigate them.

1.10 Thesis Outline

This thesis is organized as follows.

Chapter 2 presents the formulation of the umbrella constraint discovery approach for unit commitment, and it explains how it is able to incorporate net load uncertainty set details to capture spatial correlation. Furthermore, we show how UCD can be tightened using an economic-driven constraint inferred from previous UC instances. Also, the proposed updated UCD methodology is then validated on IEEE test cases by comparing with the bound tightening constraint screening technique that uses conventional box uncertainty sets.

In Chapter 3, we integrate learning and constraint generation to develop a computationally efficient and rigorous approach for implementing faster security-constrained unit commitment solution in online applications with the objective of preserving feasibility and optimality. Our proposed method is based on learning offline relevant sets of constraints, from which the optimal solution can be obtained efficiently. Then online, we predict these relevant constraints set and warm-start the constraint generation method. We conduct case studies on IEEE test cases to demonstrate the effectiveness of the proposed approach.

Chapter 4 addresses the constraint screening problem using the bound tightening technique in the context of the OPF problem formulated with a full ac power flow characterization. Due to the non-convexity of the ac OPF, we investigate line constraint screening under different convex relaxations of the problem. We propose a novel constraint learning approach that first learns from previous instances and then embodied that constraint which inherits the economical information from the objective function into the bound tightening technique. Finally, we evaluate the constraints screening approach on PgLib test cases.

The aim of Chapter 5 is to introduce a framework for defining the feasibility region of power systems within the demand space, referred to as loadability sets. These sets are projections of the generation-demand-network space onto the demand space. In the past, loadability sets were characterized for power systems without capturing spatial correlation. However, this chapter expands on this characterization by accurately capturing the net load uncertainty set. Additionally, we propose a novel data-driven inverse optimization framework for flexibility characterization of power systems using loadability sets along with its geometric intuition. The proposed inverse optimization scheme, recast as a linear optimization problem, is used to infer system flexibility adequacy from loadability sets.

Chapter 6 closes the thesis by summarizing its contributions and suggesting lines of future investigation.

Chapter 2

Tight Data-Driven Linear Relaxations for Constraint Screening in Unit Commitment

The daily operation of real-world power systems and their underlying markets relies on the timely solution of the unit commitment problem. However, given its computational complexity, several optimization-based methods have been proposed to lighten its problem formulation by removing redundant line flow constraints. These approaches often ignore the spatial couplings of renewable generation and demand, which have an inherent impact of market outcomes and corresponding transmission network use. Moreover, the elimination procedures primarily focus on the feasible region and exclude how the problem's objective function plays a role here.

In this chapter, we address these pitfalls, by ruling out *redundant* and *inactive* constraints over a tight linear programming relaxation of the original unit commitment feasibility region by adding valid inequality constraints. We extend the optimization-based approach called *umbrella constraint discovery* through the enforcement of a consistency logic on the set of constraints by adding the proposed inequality constraints to the formulation. Hence, we reduce the conservativeness of the screening approach using the available historical data and thus lead to a tighter unit commitment formulation. Numerical tests are performed on standard IEEE test networks to substantiate the effectiveness of the proposed approach.

2.1 Unit Commitment Model

2.1.1 Introduction and Assumptions

For expository purposes, we carry out our developments using a simplified single-period unit commitment [88, 106, 108] according to the following simplifying assumptions:

- Single-period: UC is usually formulated as a multi-period problem that incorporates inter-temporal constraints typically associated to generation, for example minimum up and down times. However, since this work focuses on investigating the impact of net load spatial correlation on network reduction, we prefer to investigate this solely by considering a single-period UC [88, 106].

- DC power flow: The power flows in the transmission lines are estimated via a dc approximation by using power transfer distribution factors (PTDF) to keep the model linear. The PTDF of line l with respect to node n is denoted as h_{ln}. Besides, $f_l^{\max}$ represents the maximum flow capacity of transmission line l. The number of buses and lines are denoted by N and L, respectively. The PTDF formulation compared to the $B\theta$ formulation leverages an important characteristic of the UC problem, where only a small percentage of line flow limits with the PTDF formulation is binding at the optimal solution [129].

- Generation portfolio: Each generating unit m is characterized by a minimum and a maximum power output which are denoted as $g_m^{\min}$ and $g_m^{\max}$, respectively.

- Net load: The net demand at bus n, d_n, is a net load (demand less non-dispatchable renewable generation). Without loss of generality, we assume that the forecast errors are multivariate normally distributed correlated random variables.

- No contingencies: We assume that all generators and lines are fully operational and therefore security constraints are neglected.

2.1.2 Problem Formulation

The optimization problem corresponding to this simplified UC is a MILP problem and formulated as in [88]:

$$\min_{u_m, g_m, q_n} \sum_{m \in \mathcal{M}} c_m g_m \tag{2.1}$$

Subject to:

$$q_n = \sum_{m \in \mathcal{M}_n} g_m - d_n, \qquad \forall n \in \mathcal{N} \tag{2.2}$$

$$\sum_{n=1}^{N} q_n = 0 \tag{2.3}$$

$$u_m g_m^{\min} \leq g_m \leq u_g g_m^{\max}, \qquad \forall m \in \mathcal{M} \tag{2.4}$$

$$-f_l^{\max} \leq \sum_{n=1}^{N} h_{ln} q_n \leq f_l^{\max}, \qquad \forall l \in \mathcal{L} \tag{2.5}$$

$$u_m \in \{0, 1\}, \qquad \forall m \in \mathcal{M} \tag{2.6}$$

Decision variables include the commitment status of the generating units u_m, the power output schedules g_m, the net power injections at each node q_n. The objective function (2.1) minimizes the total generation cost. Constraint (2.2) computes the net injected power at each node, while constraint (2.3) ensures power balance in the system. Constraints (2.4) and (2.5) respectively enforce limits on generator outputs and power flows on transmission lines using PTDFs. Finally, (2.6) requires that the on/off status of generators are binary ($u_m = 0$ if off, $u_m = 1$ if on). We note here that the problem (2.1)–(2.6) could be also formulated to include curtailment decision variables meant to reduce the input of wind or solar power. In that case, curtailment variables would need to be added to the nodal power balances (2.2) along with bounds on those variables and corresponding penalties in the objective function.

2.2 Umbrella Constraint Discovery

An *umbrella constraint* [33] of an optimization problem is a constraint that, if removed, changes the feasibility region of that problem. The *umbrella set* of an optimization problem is the set of constraints containing the fewest constraints preserving the original optimization problem feasibility region.

2.2.1 Identification of Umbrella Network Constraints in UC

The UC problem (2.1)–(2.6) can be made significantly easier to solve if constraints (2.5) with no impact on the optimal UC plan are removed [33]. In this chapter, we tailor the UCD problem with the objective of favoring the identification of potentially active transmission lines power flow constraints in the unit commitment problem rather than identifying the complete umbrella set.

In its original incarnation UCD, see for example [33], can identify the set of umbrella line flow limits constraints. That minimal set of constraints is necessary and sufficient to characterize the feasible region of the original UC problem. We utilize the enhanced UCD (E-UCD) formulation proposed by authors of [125] that has lighter computational demands and is better adapted when net load uncertainty is considered. In fact, E-UCD is an iterative algorithm which, at each iteration, solves the optimization problem (2.7)–(2.20) stated next. Each iteration finds the set of line constraints forming one of the vertices of the feasible region of the original UC problem. Once all vertices have been found, the algorithm terminates. Specifically at each iteration, we solve for the binary vectors $v_l^{\pm} \in \{0, 1\}^L$, and continuous vectors $g \in \mathbb{R}^M$, $q \in \mathbb{R}^N$, $d \in \mathbb{R}^N$ and $z^{\pm} \in \mathbb{R}_+^L$.

$$\min \sum_{l \in \mathcal{L}} (v_l^+ + v_l^-) \tag{2.7}$$

Subject to:

$$q_n = \sum_{m \in \mathcal{M}_n} g_m - d_n, \qquad \forall n \in \mathcal{N} \tag{2.8}$$

$$\sum_{n=1}^{N} q_n = 0 \tag{2.9}$$

$$u_m g_m^{\min} \leq g_m \leq u_g g_m^{\max}, \qquad \forall m \in \mathcal{M} \tag{2.10}$$

$$\sum_{n=1}^{N} h_{ln} q_n \leq f_l^{\max}, \qquad \forall l \in \mathcal{L} \tag{2.11}$$

$$-\sum_{n=1}^{N} h_{ln} q_n \leq f_l^{\max}, \qquad \forall l \in \mathcal{L} \tag{2.12}$$

$$\sum_{n=1}^{N} h_{ln} q_n + z_l^+ \geq f_l^{\max}, \qquad \forall l \in \mathcal{L} \tag{2.13}$$

$$-\sum_{n=1}^{N} h_{ln} q_n + z_l^- \geq f_l^{\max}, \qquad \forall l \in \mathcal{L} \tag{2.14}$$

$$v_l^+ - \frac{z_l^+}{\Omega} \geq 0, \qquad \forall l \in \mathcal{L} \tag{2.15}$$

$$v_l^- - \frac{z_l^-}{\Omega} \geq 0, \qquad \forall l \in \mathcal{L} \tag{2.16}$$

$$z_l^+, z_l^- \geq 0, \qquad \forall l \in \mathcal{L} \tag{2.17}$$

$$v_l^+, v_l^- \in \{0, 1\}, \qquad \forall l \in \mathcal{L} \tag{2.18}$$

$$0 \leq u_m \leq 1, \qquad \forall m \in \mathcal{M} \tag{2.19}$$

$$d_n^{\min} \leq d_n \leq d_n^{\max}, \qquad \forall n \in \mathcal{N} \tag{2.20}$$

where Ω is a large positive number. Here, the binary variables $v_l^\pm$ take the value of 0 if one of the flow limits associated with line l are umbrella ($v_l^+ = 0$ if the upper flow limit is umbrella or $v_l^- = 0$ if the lower flow limit is umbrella). Otherwise, $v_l^\pm$ are set to 1.

The objective function (2.7) aims to minimize the sum of the binary variables, $v_l^\pm$, by finding the maximum number of line flow constraints that can be hit as part of the UC problem solution.

The set of constraints (2.8)–(2.10) from the UC, controls the decision variables q_n and

g_m. Each line flow constraint in the blocks of constraints (2.11) and (2.12) is paired with a constraint in the block (2.13) and (2.14). By inspection, the auxiliary variables $z_l^{\pm}$ can be equal to zero only if there is $\sum_n q_n$ satisfying both (2.11) and (2.13) for the upper flow limits, or (2.12) and (2.14) for lower flow limits. As a result, the binary variable $v_l^{\pm} = 0$. Conversely, $z_l^{\pm}$ has to be positive and the binary variables $v_l^{\pm} = 1$ as required by (2.17). Furthermore, the constraints for which $v_l^{\pm} = 1$ have to intersect at the same value of $\sum_n q_n$. Since $\sum_n q_n$ is an intersection of line constraints over the LP-relaxation of the feasible set of the UC problem, it is therefore a vertex of this set. Additionally, the vector of net load at each bus n is turned into a vector of decision variables as in (2.20).

Following the first iteration, which revealed the vertex with the most intersecting constraints, the next step is to pinpoint the other vertices that have the same or fewer intersecting umbrella constraints. This is done while the previously discovered umbrella constraints are removed from the search by setting their respective binary variable $v_l^{\pm}$ equal to 1. We terminate the search when there are no more umbrella constraints to identify. The UCD [1] procedure is summarized in Algorithm 1.

Algorithm 1: Umbrella Constraint Discovery

Data: Network and generators data, historical net-load
Result: Non redundant constraints.

1 **while** $\sum_l v_l^+ + v_l^- \neq 2L$ **do**
2   Solve UCD (2.7)–(2.20);
3   **if** *($v_l^+ = 0$ OR $v_l^- = 0$)* **then**
4   Set $v_l^+ = 1$ OR $v_l^- = 1$;
5   go to step 2;
6   **else**
7   go to step 9;
8   **end if**
9 **end while**

The drawback of the UCD algorithm relates to the modeling of net load forecast errors in constraint (2.20). This result will be sub-optimal because it ignores the spatial correlation

[1] Note that there is some abuse of notation in UCD here. In order to be rigorous, we should write E-UCD. Nevertheless, in order to make the notation clearer, we remove the prefix E in E-UCD in this chapter.

among the net loads. Therefore, we propose next a data-driven UCD (D-UCD) where the net load vector is characterized using polyhedral uncertainty sets as described in Section 2.3, rather than a simple box in N-dimensional space. We will refer to the UCD framework described in (2.7)–(2.20) as the base UCD (B-UCD) approach. In addition, note that the UCD solution benefits from decomposition; the interested reader can view its details in Appendix A.

2.3 Tightening Umbrella Constraint Discovery

As argued in Chapter 1, our goal is to eliminate both redundant and inactive constraints with the aim of running a computationally-lighter unit commitment. At the same time, we have to target a formulation that is able to map adequately net load forecast uncertainty. As a first step to accomplish this, we compute uncertainty sets of net load forecast errors as a function of historical records of net load and their initial forecasts.

We are aiming to obtain a compact formulation of the UC problem by predicting its potential active constraints out of its umbrella set. Being able to do so leads to two main benefits: first, having obtained a compact formulation entails that the UC is formulated with much fewer "symbols", constraints here, which reduces memory requirements; and, second, with an accurate prediction of the UC's active set, solution times for the UC are expected to be reduced dramatically. From a practical perspective, the use of these techniques could allow for much faster market clearing which, in turn, could allow for UCs with finer time resolutions (*e.g.*, sub-hourly rather than hourly), a key feature for running efficient electricity markets in the presence deep penetrations of variable generation like wind and solar power.

2.3.1 Data-Driven Polyhedral Uncertainty Sets

Without loss of generality, we focus on capturing the spatially-correlated uncertain net load. Inspired by [114, 130], we develop two data-driven polyhedral uncertainty sets by leveraging principal component analysis (PCA) [50, 131]. PCA is applied to historical time series of net load. All the input time series have the same length of T, and they are synchronized and evenly spaced in time (*e.g.* one hour intervals).

We denote a matrix $W \in \mathbb{R}^{T\times N}$ whose elements w_{nt} are the time series of *observed* net load at bus $n \in \mathcal{N} = \{1, ..., N\}$ for each time instance $t \in \mathcal{T} = \{1, ..., T\}$. Similarly, we define the matrix $\mu \in \mathbb{R}^{T\times N}$ whose elements μ_{nt} are the time series of past *forecasted* net demand at bus $n \in \mathcal{N}$ for each past time instance $t \in \mathcal{T}$.

Using μ, we obtain the centered data matrix W_c [50, 131], whose contents are the net load forecast errors at all nodes $n \in \mathcal{N}$ and times $t \in \mathcal{T}$

$$W_c = W - \mu \tag{2.21}$$

Assuming net load forecast errors are unbiased[2], its spatial forecast error covariance matrix $\Sigma \in \mathbb{R}^{N\times N}$ is approximated by

$$\Sigma = \frac{1}{T-1} W_c^\top W_c \tag{2.22}$$

PCA is performed by conducting an eigenvalue decomposition of the covariance matrix. We let the columns of an $N \times N$ matrix V and the diagonal entries of another $N \times N$ matrix Λ represent, respectively, the orthonormal eigenvectors and the eigenvalues of Σ. Here, the diagonal elements of Λ are ordered such that $\lambda_{11} \geq \lambda_{22} \geq \cdots \geq \lambda_{NN}$, while the columns of V are arranged such that its nth column (eigenvector) is associated with the nth eigenvalue, λ_{nn}.

We underline that when net load forecast errors follow a multivariate Gaussian distribution the resulting principal components are independent. However, in possible cases when net load forecast errors are non-Gaussian and/or biased, there are techniques capable of transforming original net load forecast errors into are approximately unbiased and Gaussian ones [50, 131].

The spatial decorrelation process proposed by [131, 132] can transform detrended time series of observed net load forecast error in (2.21) into Gaussian time series onto which PCA is

[2] In the case where errors are unbiased, one would need to calculate the biases at each node and then remove them from W_c.

then performed. Once the spatial dependency is eliminated from non-Gaussian observations, the resulting principal components are, therefore, independent of each other.

Thus, we can project the data contained in W_c onto the eigenvectors $k = 1, \dots, N$ of the covariance matrix [131]

$$Z_k = W_c V_k \tag{2.23}$$

where Z_k is a $T \times 1$ vector of data which has been projected onto V_k, the kth principal component of Σ.

Next, let us find the coordinates of the extrema of each data projection Z_k

$$\bar{\mathcal{S}}_k = \arg\max_{t \in \mathcal{T}} \|Z_k\|^2 \tag{2.24}$$

that is $\bar{\mathcal{S}}_k$ is the data point projected along principal component V_k which is the furthest away from the origin. Keeping a conservative approach, we will assume data can range between $-\bar{\mathcal{S}}_k$ and $\bar{\mathcal{S}}_k$ along the principal component V_k. Moreover, we can argue that the extrema of the original data points can be reconstructed using the K principal components and their data projections Z_k [3] recentered on a net load forecast $d^0 \in \mathbb{R}^N$

$$\mathcal{S}_k^+ = d^0 + \bar{\mathcal{S}}_k V_k^T \tag{2.25}$$

$$\mathcal{S}_k^- = d^0 - \bar{\mathcal{S}}_k V_k^T \tag{2.26}$$

In the case where W_c was originally biased and/or non-Gaussian, the spatial biases would be re-incorporated in (2.25) and (2.26), and the transformed non-Gaussian data can be reverted into its original non-Gaussian form [131, 132]. The use of this technique enables one to handle diverse types of forecasting errors and thus enable the use of our proposal for realistic systems with wind and photovoltaic generation, whose forecast errors are themselves biased and/or non-Gaussian, as can be seen in details in [50], for example.

Considering that typically only the first few dominant principal components are sufficient

[3] In the case where W_c was biased, the forecast error biases found prior to applying PCA would also need to be added back.

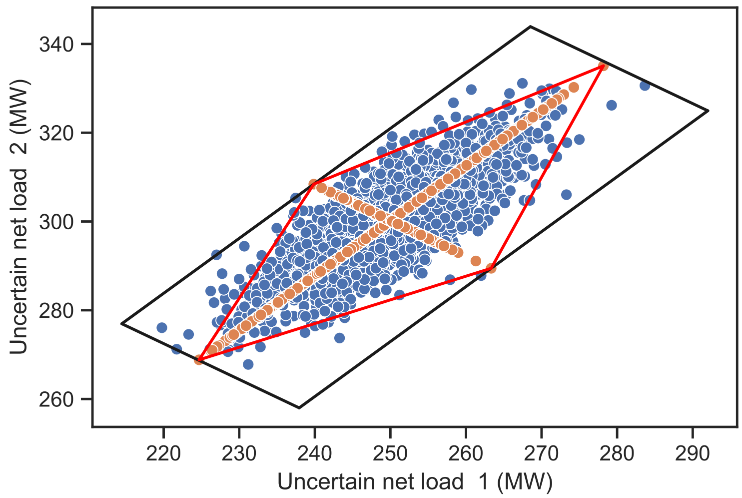

Figure 2.1: Schematic illustration of polyhedral uncertainty envelope with $d^0 = (250, 300)$ MW and $K = 2$.

to describe accurately the original data's uncertainty, it is common practice to limit the number of principal components to $K < N$. A first *data-driven polyhedral uncertainty set* (DPUS), as proposed in [133], is

$$\begin{aligned} P_1(\mathcal{S}, K) = \Bigg\{ &\mathbf{E} \in \mathbb{R}^N \mid \mathbf{E} = \sum_{k=1}^{K} \left(\omega_k \mathcal{S}_k^+ + (1-\omega_k)\mathcal{S}_k^-\right) \\ &0 \leq \omega_k \leq 1, k \in \{1, \dots, K\} \Bigg\} \end{aligned} \tag{2.27}$$

Fig. 2.1 illustrates the construction of a polyhedral uncertainty set in a two dimensional uncertainty space. Fig. 2.1 shows $P_1(\mathcal{S}, K)$ for $K = 2$ in black. The orange dots represent the original data as it is projected along the two principal components of historical forecast error data. By inspection, we see that this polyhedral set encloses all original data points.

Inspired by the data-driven convex hull uncertainty set concept proposed previously in [48, 114], we propose to define an alternative *data-driven polyhedral uncertainty set* (DPUS)

$$
\begin{aligned}
P_2(\mathcal{S}, K) = \Bigg\{ & \mathbf{E} \in \mathbb{R}^N \mid \mathbf{E} = \sum_{k=1}^{K} \left(\omega_k^+ \mathcal{S}_k^+ + \omega_k^- \mathcal{S}_k^- \right), \\
& \sum_{k=1}^{K} \left(\omega_k^+ + \omega_k^- \right) = 1, \\
& 0 \leq \omega_k^+ \leq 1, \; 0 \leq \omega_k^- \leq 1, \\
& k \in \{1, \ldots, K\} \Bigg\}
\end{aligned} \tag{2.28}
$$

where we notice that $P_2(\mathcal{S}, K) \subseteq P_1(\mathcal{S}, K)$.

The set $P_2(\mathcal{S}, K)$ represents the smallest convex set that contains every data point projected onto the K retained principal components. Moreover, that DPUS $P_2(\mathcal{S}, K)$ is a convex hull of the extrema of the retained Z_k data projections, where we define $\mathcal{S} = \cup_k (\mathcal{S}_k^+ \cup \mathcal{S}_k^-)$. In Fig. 2.1, we see the historical data, represented by blue dots, and the data projected onto two of its principal components (orange dots). By inspection, the rhombus-shaped red envelope, whose principal axes correspond to the principal components of the data, encapsulates the vast majority of the original data [4].

Later in Section 2.4, we will examine the pros and cons of these two net load uncertainty representations as applied to the UC problem and the reduction of its number of constraints.

2.3.2 Cost-Driven UCD (CD-UCD)

Another relevant limitation of conventional UCD as seen in (2.7)–(2.20) is that it solely seeks to establish the minimal set of constraints required to describe the feasible space of the UC. It is incapable of providing information regarding which of the umbrella constraints could

[4] We underline that the historical data used here may contain points corresponding to instances where renewable generation curtailment was applied. If many such points exist, we would expect that the portions closest to the origin of the net demand point clouds (like the one in Fig. 2.1) would display points congregated along the horizontal and/or the vertical. Such behavior would happen because past curtailment stopped the net demand from going further down. We argue that the approach presented here would still be valid; however, it is clear that in such cases the data would not be as Gaussian than if curtailment was not present, and the resulting DPUS might look more like a box.

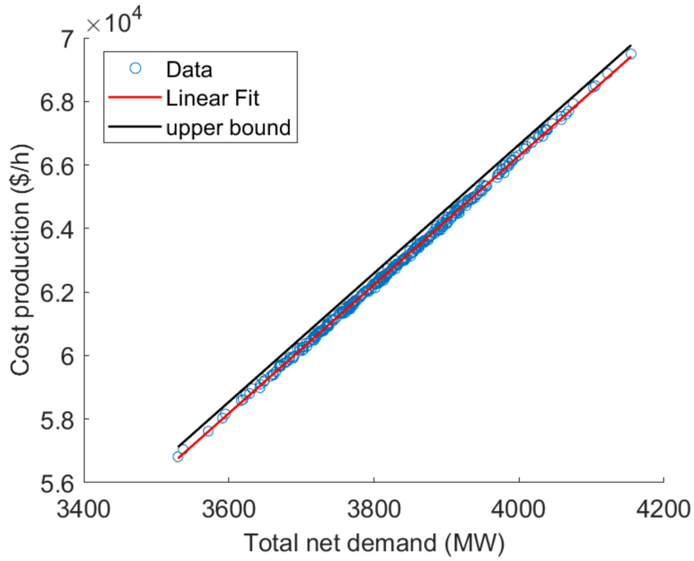

Figure 2.2: Observed production cost against system net load.

become active as we solve the UC. We argue that having such information ahead of UC solution would be a valuable asset in UC solution time reduction.

To illustrate this, consider Fig. 2.2 that shows how the total production cost of a UC problem formulation as a function of the total net load for 400 solution instances of a given UC problem. Clearly, the positive correlation between the operating cost and total net demand drives towards modeling this relationship using a linear regression technique.[5] In fact, if the range of total net load variation is small enough, you can approximate the cost with a linear function only. We argue that all UC outcomes in a given range of net demand would have their corresponding production costs bounded above by the dashed line shown in Fig. 2.2.

Therefore, we propose that if we are to add the following new constraints to the UC,

[5]We note that a family of such curves may be necessary to cover a wider range of net demands. One would expect that these taken together would form a piecewise linear convex function of the total net demand. In addition, knowing that in the case of multi-period UC (which we do not consider explicitly here), system-wide incremental costs are expected grow with net demand, one might have to employ piecewise linear cost approximations especially. This decision should be taken by the user in light of historical cost information.

which we cast as follows [108]:

$$\sum_{m \in \mathcal{M}} c_m g_m \leq (1 + \Delta\sigma) a_0 + (1 + \Gamma) b_0 D \tag{2.29}$$

$$D = \sum_{n=1}^{N} d_n \tag{2.30}$$

$$D^{\min} \leq D \leq D^{\max} \tag{2.31}$$

and perform UCD on the resulting problem, we would be able to identify which of the original problem's umbrella constraints are most likely to be active at the UC's own optimum. The premise here is that (2.29) should be intersecting the active umbrella constraints of the original UC. Obviously, here there is some tuning to be carried out in determining the parameters a_0 and b_0 of the proposed cost upper bound, while $\Delta\sigma$ and Γ are user-specified conservativeness parameters.

The upper bound uses a basic linear fitted model $a_0 + b_0 D$. The minimum and maximum aggregate net load for each is denoted by $D^{\min}$ and $D^{\max}$, respectively. The upper bound can impact the screening outcomes in terms of expected eliminated constraints.

Through the selection of the value of $\Delta \geq 0$, which multiplies the standard deviation σ of its underlying data with respect to the best fit line, it is possible to push up on the cost upper bound. This way it is possible to capture most if not all prior cost observations. For example, with 3σ one will typically capture production costs of almost (if not) all prior observed instances as shown by the dashed line in Fig. 2.2. On the other hand, if Δ is set too high, there will be a risk that the cost upper bound (2.29) is in fact found to be redundant when running UCD on the augmented UC constraint set and, thus, be of little value. Moreover, we note that if Δ is too small, we run the risk that (2.29) renders the augmented UCD infeasible. However, in this chapter, we adjust the Δ parameter to create a 100% prediction interval, ensuring that the cost upper bound encompasses all prior cost observations.

Second, we add the factor $\Gamma \geq 0$ to the linear model to further trade-off between the number of retained umbrella constraints and the risk of excluding an umbrella constraint which may become active in the UC. The consequence of excluding potentially active constraints will be that UC solutions may be infeasible since one or more UC constraints are not satisfied by virtue of having been excluded by the augmented UCD. In fact, by setting $\Gamma > 0$ one is lowering the risk of the augmented UCD weeding out constraints that need to be considered in the UC. The optimal choice appears to be $\Gamma = 0$. However, additional empirical analysis, in conjunction with the UCD algorithm, would recommend adjusting this value to mitigate the possibility of active constraint elimination.

Finally, we note that the cost-driven upper bound can be extended using a piecewise linear set of constraints to capture net load and cost data over different ranges of net demand as suggested by [108]. The interested reader may refer to Appendix B for detailed modeling of piecewise linear cost upper bound. Also, we will consider a modified cost-driven upper bound constraint by defining a subset of generators that were historically committed in given ranges of net demand, $\mathcal{M}_c$, and restricting the summation in the left-hand side of (2.29) to this subset. At the same time, the total running cost associated with the historically uncommitted generators (subset $\mathcal{M}_{nc}$) in that net demand range is forced to zero through a complementary equality constraint. This enhanced CD (ECD) replaces (2.29) with the following

$$\sum_{m \in \mathcal{M}_c} c_m g_m \leq (1 + \Delta\sigma) a_0 + (1 + \Gamma) b_0 D \tag{2.32}$$

$$\sum_{m \in \mathcal{M}_{nc}} c_m g_m = 0 \tag{2.33}$$

while (2.30) and (2.31) still apply [6].

Next, we will illustrate how the combination of data-driven polyhedral uncertainty sets and CD-UCD can reduce dramatically the computational effort required to solve robust UC problems. Table 2.1 summarizes the various tightened UCD problems which we will be comparing in the following section. Using this information, Fig. 2.3 presents a Venn diagram

[6] In the case where the UC is formulated with curtailment variables, the cost upper bounds ((2.29) or (2.32)) would need to include a second summation on their respective left-hand sides to account for the cost of wind and solar power curtailments.

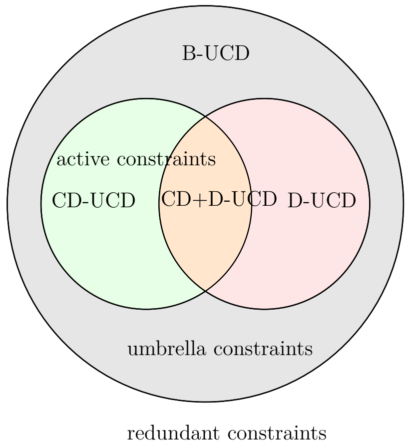

Figure 2.3: Venn diagram of the solutions sets for various UCD (set sizes in this illustration are not to scale)

Table 2.1: Constraints Screening Methods

Method	Screening optimization problem	Description
B-UCD	(2.7) s.t (2.8)–(2.20)	base approach
D1-UCD	(2.7) s.t (2.8)–(2.19), (2.27)	data-driven
D2-UCD	(2.7) s.t (2.8)–(2.19), (2.28)	data-driven
CD-UCD	(2.7) s.t (2.8)–(2.20), (2.29)–(2.31)	base cost-driven
CD+D1-UCD	(2.7) s.t (2.8)–(2.19), (2.27), (2.29)–(2.31)	data and cost-driven

of UCD tightening approaches to reflect the various strengthened relaxations considered here and the types of screened constraints.

2.4 Case Studies

2.4.1 Benchmark Approach (BA): Roald's Method

This method was proposed in [106]; it is based upon the solution of one maximization and one minimization for each transmission line $\hat{l}$, these two optimizations are jointly formulated as

$$\max / \min \sum_{n=1}^{N} h_{\hat{l}n} q_n \tag{2.34}$$

Subject to:

$$(2.8) - (2.12),\ (2.19) - (2.20) \tag{2.35}$$

In short, problem (2.34)–(2.35) seeks to maximize/minimize the power flow through each transmission line $\hat{l}$ over an LP-relaxation of the feasible region of the UC problem. If the maximum (minimum) limit for the flow of line $\hat{l}$ given by the objective function does not reach line capacity limit $f_l^{\max}$, then the upper (lower) line constraint is flagged as redundant. We note that for realistic systems containing thousands of lines, this method is very time consuming, while, at the same time, it is highly conservative due to its use of box uncertainty sets (2.20). Also, we introduce a cost-driven version of the BA by adding the extra constraints (2.29)–(2.31) to (2.34)–(2.35), as proposed in [108]. We will refer to this benchmark as CD-BA (cost-driven BA).

2.4.2 Benchmark Approach 2: Constraint Generation (CG)

As highlighted in the introduction, this approach begins by solving the UC without imposing any network flow constraints. Subsequently, by running a simultaneous feasibility test (SFT) line flow constraint violations are identified. The corresponding violated flow constraints are added iteratively into the UC, which is re-solved until all previously-violated constraints have been accounted for and satisfied [102]. We note that the solution of this iterative process leads to the same solution as that the of the UC with all its network flow constraints taken into account simultaneously. However, we note that CG works for a single vector of nodal net demands, not a set of net demands or net demands forecast errors as it is the case for Roald's method and our proposal. To offer a fair comparison between CG and our approach (as well as Roald's method), we utilize a vector of nodal net demands which corresponds to the peak net demand of the test system, as was suggested by the authors of [134]. The computational burden of this method is heavily influenced by the number of iterations needed since a UC problem needs to be solved at each iteration. In the end, the reason why CG is a relevant benchmark here is that it is implicitly a potentially-active constraint identification tool.

2.4.3 Procedure for Constructing Correlated Net Load Time Series

We generate N synthetic spatially-correlated net load time series of length T, which are then consigned to matrix W. They consist of historic net load forecasts $\mu \in \mathbb{R}^{T\times N}$, which correspond to the nominal demand values from the data sets in [135]. These are superimposed with zero-mean normally-distributed forecast errors with spatial correlation given by a covariance matrix Σ. Here, we take the approach outlined in [136], where errors are assumed to be proportional to forecasts and whose variance and correlation are adjusted with an uncertainty level parameter. Thus, this parameter controls the magnitude of net load forecast errors. We utilize the exact data generation approach proposed by [136] which includes a random process in modeling net loads' correlation. First, we generate a positive definite matrix $C = \widehat{C}\widehat{C}^\top$ where each element of the matrix $\widehat{C}$ is a sample randomly drawn from a uniform distribution with support in $[0, 1]$. Then, to obtain a positive definite covariance matrix in which the diagonal elements are $c_{nn} = (\eta d_n^0)^2$, and off-diagonals

$$\sigma_{nm} = \eta^2 \frac{c_{nm}}{\sqrt{c_{nn}c_{mm}}} d_n^0 d_m^0, \quad \forall n, m \in \mathcal{N}, n \neq m \tag{2.36}$$

where c_{nm} are the nmth elements of the matrix C, and d_n^0 is the net demand forecast at node n. Finally, we generate $T = 8760$ nodal net load vectors using the described approach. Of the 8640 values of net load generated, 7200 are randomly selected to obtain the data-driven cost upper bound (2.29) and uncertainty sets (2.27) and (2.28), and the remaining 1440 instances are used for testing and investigating UC performance. This division of datasets into training and testing subsets is approximately aligned with the commonly employed split ratio in machine learning applications, typically set at 80/20.

2.4.4 Performance Evaluation

The procedure to measure the performance of the method described in Section 2.2 and its coupling with Section 2.3 to remove redundant line flow constraints—with the overarching objective of reducing the UC solution computational effort—is run as suggested by [88]:

1. Given the historical data, set up net load uncertainty representations (as described in Section 2.3). Then, determine the transmission constraints that can be eliminated according to each approach described in Table. 2.1.

2. Record the computational time needed to screen out the redundant network constraints using each screening approach. We consider that the computational time of each approach is given as the sum of the time required to run each iteration for different versions of the UCD algorithm. On the other hand, the benchmark approach runs in a sequential manner for transmission line constraint screening.

3. Solve the reduced UC problem on the set of unseen time periods without the superfluous constraints identified in Step 1.

4. Use the binary commitment variables obtained in Step 3) as a warm start solution and solve the unit commitment problem including all constraints.

5. Assess the performance of the screening method in terms of (i) the percentage of retained network constraints from each screening approach in Step 1, (ii) the

Table 2.2: Description of test power systems

System	# Nodes	# Generators	# Lines
IEEE-RTS-73	73	96	120
IEEE-118	118	19	186
CASE500_pserc	500	49	733

computational time required to run each screening approach, (iii) the computational time required to solve the reduced UC problem in Step 3) with respect to the full UC formulation, and (iv) whether or not all necessary and sufficient constraints needed to solve the UC have been retained. The latter performance measure applies to CD-UCD and CD+D1-UCD since the application of the production cost upper bound may discard potentially active UC constraints out of the original umbrella set, as explained in Section 2.3. (v) the cost error (optimality loss) of the solution obtained in step 3 with respect to that of the full UC problem in Step 4.

2.4.5 Experimental Setup

The B-UCD, D1-UCD and D2-UCD screening approaches and the UC are formulated as MILP problems. We test our algorithm in two standard IEEE test networks, namely IEEE-RTS-73 and IEEE-118 test systems [137]. Also, another test case is adopted from the IEEE PES PGLib-OPF v17.08 benchmark library [135] which is called CASE500_pserc. All the technical data related to these systems are available in [137], and their main features are listed in Table. 2.2. For these medium size test networks, the solution optimality gap was set to 0%. For the benchmark approach, we run $2L$ optimizations in a sequential manner. The calculations have all been performed using GAMS and the CPLEX MILP solver. The computer used is equipped with an Intel Core i7 3.10 GHz processor and 16 GB of RAM.

Table 2.3: Solution time for redundant constraint screening for medium size networks

	Screening time (s)			
Method	BA	B-UCD (% change)	D1-UCD (% change)	D2-UCD (% change)
IEEE-RTS-73	45	10	14	15
	-	(−77.7%)	(−68.9%)	(−66.6%)
IEEE-118	62	17	35	38
	-	(−72.6%)	(−43.5%)	(−38.7%)

2.4.6 Redundant Constraints' Screening Results

Medium-Size Networks

In this subsection, we provide simulation results for the two medium-size test systems provided in Table 2.2 (IEEE-RTS-73 and IEEE-118), and we assess the computational complexity of each screening approach. We set the uncertainty parameter $\eta = 0.035$ for the two test systems [7]. For the umbrella constraint screening algorithm with polyhedral uncertainty sets, all principal components are utilized to determine the corresponding uncertainty sets.

First, one of the main advantages of the proposed approach is that in terms of run time, it is significantly faster than Roald's method (BA), as seen in Table 2.3. Note that we assess the computational time while we consider all $K = N^\star$ principal components, where $N^\star$ is the number of nodes with uncertain net demand such that $N^\star \leq N$. The conventional UCD algorithm has lower computational cost compared to the enhanced data-driven versions (D1-UCD and D2-UCD); however, with B-UCD a higher number of umbrella constraints are recorded. Table 2.3 clearly shows that the solution time of the BA is directly proportional to the number of lines in the power system. The performance of the UCD runtime is primarily

[7] Setting $\eta = 0.035$ yields load variations of approximately 10% to 12% around the nominal loading, a valid assumption for short-term operational planning studies. Moreover, for the IEEE-RTS-73 test system, setting η to a value greater than 0.035 results in the UC problem becoming infeasible. However, in Chapter 5 of this thesis, we evaluate higher variations, up to $\eta = 0.1$. Indeed, as the value of η increases, so does the likelihood of encountering additional umbrella constraints.

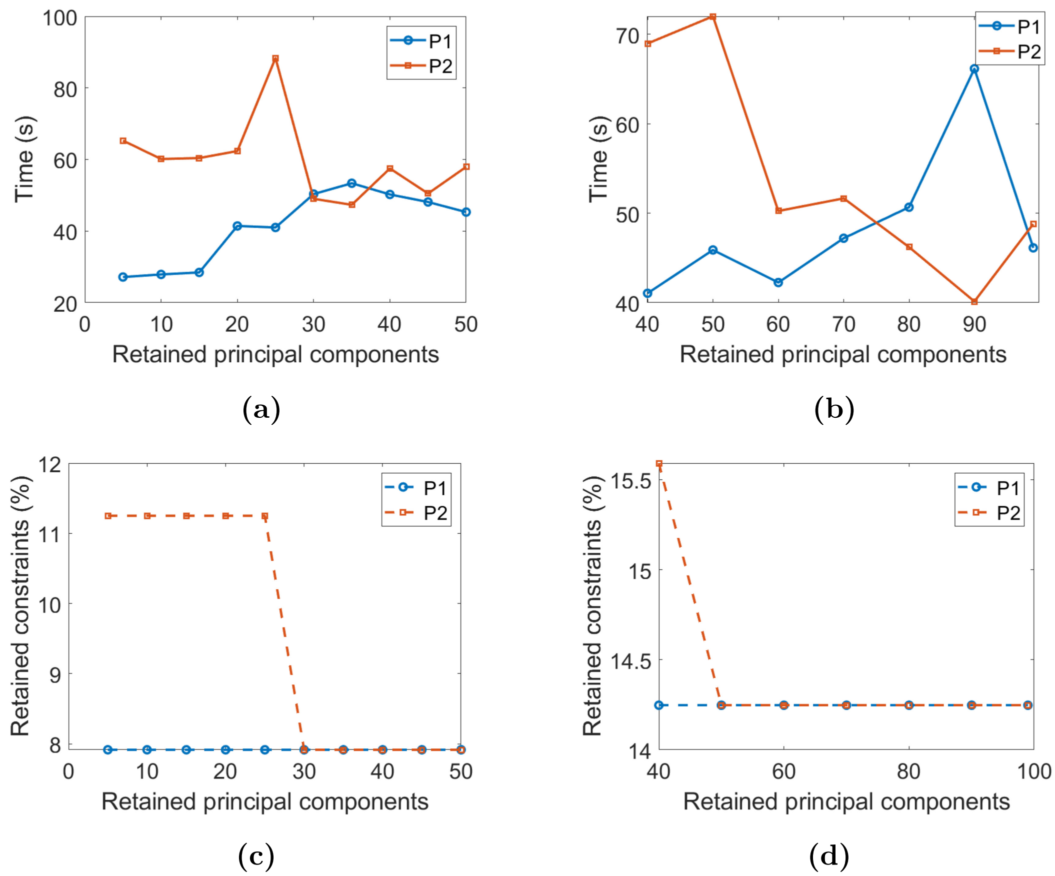

Figure 2.4: (a) The impact of K on screening time in IEEE-RTS-73; (b) The impact of K on screening time in IEEE-118. (c) The impact of K on retained constraints in IEEE-RTS-73; (d) The impact of K on retained constraints in IEEE-118.

Table 2.4: Number of Umbrella Constraints Identified by UCD Iteration for Medium-Size Networks

	Number of constraints found										Total
Iteration number	1	2	3	4	5	6	7	8	9	10	
					B-UCD						
RTS-73	10	5	2	2	2	1	1	1	–	–	24
IEEE-118	22	11	9	7	3	2	2	2	2	–	60
					D1-UCD						
RTS-73	8	5	2	2	1	1	–	–	–	–	19
IEEE-118	22	9	7	4	3	3	2	2	1	1	53

influenced by the system size, as well as the total number of identified umbrella constraints.

Fig. 2.4 illustrates the impact of the number of retained principal components on the constraint screening time and the proportion of retained constraints when running UCD without relaxing the generator's commitment variables. We see that through the use of DPUS $P_1(\mathcal{S}, K)$, while retaining only 10% (for IEEE-RTS-73) and 40% (for IEEE-118) of the most dominant principal components (Fig. 2.4c and Fig. 2.4d, respectively), it was possible to obtain the minimum number umbrella constraints for each system. On the other hand, $P_2(\mathcal{S}, K)$ needs respectively 60% and 50% of the principal components to match the umbrella constraint set counts found with $P_1(\mathcal{S}, K)$.

By inspection of Fig. 2.1, $P_1(\mathcal{S}, K)$ is much more robust to outliers than $P_2(\mathcal{S}, K)$. In fact, we argue that the use of $P_2(\mathcal{S}, K)$ could be risky in practice. In addition, its use leads to significantly improved constraint screening performance over $P_2(\mathcal{S}, K)$ without having to consider a large number of principal components. This behavior can be explained by the fact that the volume occupied in the net load forecast error space by $P_1(\mathcal{S}, K)$ is larger than that of $P_2(\mathcal{S}, K)$. In turn, the likelihood that several of the constraints defining $P_1(\mathcal{S}, K)$ intersect with other problem constraints is increased. As UCD seeks to find the largest number of intersecting constraints at every iteration, this is why $P_1(\mathcal{S}, K)$ is preferable to $P_2(\mathcal{S}, K)$.

The number of umbrella line flow constraints identified in each iteration of the UCD algorithm is provided in Table 2.4. The B-UCD flavor of the algorithm identifies the umbrella line flow constraints of the networks IEEE-RTS-73 and IEEE-118 in eight, and nine iterations, respectively. On the other hand, D1-UCD converges in six iterations for IEEE-RTS-73, and in 10 iterations for the IEEE-118 test system. The results further indicate that the maximum number of line flow limits which may become active simultaneously under D1-UCD is at most eight and 22 for IEEE-RTS-73 and IEEE-118, respectively. This is the case because in the first iteration UCD found the maximum number of intersecting constraints for each problem. We note also that D1-UCD retains fewer constraints in comparison to B-UCD. This is because the DPUS used here are tighter than the box sets defined by (2.20).

On the contrary, the first important observation to be made is that the UCD approaches yield for the 1440 time periods in the test set the same optimal UC solutions and costs as those obtained with BA constraint screening—since all necessary constraints are retained by UCD. Consequently, the performance of these methods, which is summarized in Table 2.5, is assessed and compared in terms of the percentage of umbrella constraints and the computational burden of the reduced UC running time relative to the computational time required to solve the full UC problem. Our proposed approach outperforms Roald's method in terms of network constraints removal for both IEEE-RTS-73 and IEEE-118. Therefore, the proposed approach provides UC solution time computational savings 21.7% and 14.8% lower than Roald's method for IEEE-RTS-73 and IEEE-118, respectively. Note that UC performance results using D1-UCD are identical to those for D2-UCD; this explains why the D2-UCD results have been omitted from Table 2.3. Also, CG retained only 5% of the line flow constraints; this is lower than the retained constraints for the BA and D1-UCD screening approaches for IEEE-RTS-73. Nevertheless, D1-UCD results in a reduced UC problem that is 699% faster than running UC with CG. While for the IEEE-118 test system, CG keeps 20.9% of the line flow constraints and reduces the UC computational time to 24.9% of the time required by the full UC. In fact, CG takes 47.3% longer to reach the optimal UC solution when compared to solving the reduced UC problem obtained from D1-UCD. This is due to the fact that CG retains more constraints and the fact that three iterations (*i.e.*, three UC solutions) are needed to converge to the global optimal solution.

Table 2.5: Redundant Constraint Screening for Medium-Size Networks

	D1-UCD	BA (% change)	CG (% change)
		IEEE RTS-73	
Retained constraints (%)	7.9	10.0 (+26.6%)	5 (−36.7%)
Reduced UC compute time (%)	11.5	14.0 (+21.7%)	91.9 (+699.13%)
		IEEE-118	
Retained constraints (%)	14.2	16.1 (+13.4%)	20.9 (+47.7%)
Reduced UC compute time (%)	16.9	19.4 (+14.8%)	24.9 (+47.3%)

Table 2.6: Redundant Constraint Screening Time for the Large-Size Network

Method	B-UCD	D1-UCD	D2-UCD
Total screening time (s)	122	355	380
Average screening time per block (s)	15.2	44.3	47.5

Finally, we also see the advantage procured by the use of DPUS over box-shaped uncertainty sets. D1-UCD and D2-UCD both yield constraint counts under those offered by Roald's method and B-UCD which both make use of box-shaped uncertainty sets whose principal axes are independent from each other. The reason why D1-UCD and D2-UCD offer improved screening performance is because their respective DPUS are much tighter and aligned with historical net demand forecast error observations.

Large-Size Network

To show the efficiency of the proposed approach for more realistic cases, this section compares the simulation results of the different methods for the CASE500_pserc test system which has 500 buses and 733 lines. All system data are available from the IEEE PES PGLib-OPF v17.08 benchmark library [138]. To keep computational times within reasonable limits, the optimality gap is set to 1% when solving UC problems. Line-based decomposition [97, 125] is used to partition all versions of UCD problems (B-UCD, D1-UCD, D2-UCD) into smaller sub-problems as explained in UCD decomposition in Appendix A. These sub-problems are independent from each other and have been considered in a sequential manner to allow

Table 2.7: Large-Size Network Computational Results

Method	D1-UCD	BA (% change)	CG (% change)
Retained constraints (%)	6.34	8.45 (+25.0%)	0 (−100%)
Screening time (s)	380	690 (+81.6%)	–
Reduced UC compute time (%)	3.0	3.7 (+23.3%)	0.9 (−70%)

for a fair comparison with Roald's benchmark approach. To this end, we have partitioned arbitrarily the full line constraint set which consists of 1466 line constraints into 8 blocks; each subgroup $\mathcal{L}_\kappa$ contains 183 line flow constraints to be considered by each sub-problem (A.1)–(A.8) in Appendix A except for the last block which has 2 extra line constraints to be examined.[8] The training set contains 7200 time periods instances while the test set was reduced to 480 time periods. Here, we consider keeping $K = 50$ principal components to formulate both P_1 and P_2. Results in Table 2.6 illustrate that B-UCD's screening time is lower than P_1's and P_2's by an average of 65%. This is a direct result of the fact that the number of constraints retained by DPUS is significantly larger than that of the box constraint set (2.20).

On the other hand, results found in Table 2.7 show that the proposed method involves reductions in the number of umbrella constraints and screening time compared to the benchmark, consequently, the reduced UC problem and computational time decrease. The screening time of our proposed method is 81.9% faster than the benchmark approach. Also, imposing a polyhedral uncertainty set reduces the number of retained UC umbrella constraints and computational time for solving the UC by 25% and 23.3%, respectively. Finally, CG does not add any line constraints. This is indicative of the fact that the network is lightly loaded, while its reduced UC computation time is just under 1% of the full UC compute time.

[8] This choice is purely arbitrary here. Other partitioning approaches are possible.

Table 2.8: Parameters of Production Cost Upper Bounds

Test system	a_0	b_0	Δ	Γ
IEEE-RTS-73	-6.03×10^4	24.64	5.0	0
	-8.80×10^4	27.79		
IEEE-118	-1.35×10^4	18.9	3.7	0
CASE500_pserc	-8.84×10^4	20.52	3.6	0
	-1.03×10^5	21.44		
	-2.63×10^5	30.00		

2.4.7 Inactive Constraints Screening

Finally, we experiment on evaluating the benefits of adding the production cost upper bound (2.29) (along with (2.30) and (2.31)) to the UC constraints prior to solving its corresponding UCD. Here, we test for the addition of the cost upper bound with (i) box uncertainty sets (CD-UCD), (ii) data-driven polyhedral uncertainty sets, namely P_1 (CD+D1-UCD). In this study, the same data sets used in prior sections are deployed for DPUS computation and cost upper bound characterization.

For the IEEE-RTS-73 system, there are two constraints set up to provide a piecewise cost upper bound, while we use a single linear constraint for the IEEE-118 test system—see Table 2.8 for the production cost upper bound parameters used. Here these choices were made upon visual inspection of the historical production cost data plotted against observed system-wide net load for each system. As a first observation, the two cost-driven approaches provide for the test set the same optimal costs as obtained by the benchmark approach except for two instances (out of 1440) of the IEEE-RTS-73 which provides infeasible UC results. This happened as a result of two outliers from the historical production cost data points in the cost-net load regressions which were not covered by the upper bound constraints. The total cost error for the test instances is 0.006%. The results in Table 2.9 show that CD+D1-UCD leads to considerable reductions in both the number of retained constraints and computational burden in comparison to CD-UCD. For the IEEE-RTS-73 test system, imposing a data-driven uncertainty set combined with the cost-driven constraints reduces retained constraints and computational time by 100% and 32%, respectively. For the IEEE-

Table 2.9: Inactive Constraints Screening

Method	CD+D1-UCD	CD-UCD (% change)	CD-BA (% change)
IEEE RTS-73			
Retained constraints (%)	4.6	9.2 (+100.0%)	9.2 (+100.0%)
Screening time (s)	19	25 (+31.5%)	175 (+821%)
Number of infeasibilities	2	2	2
Cost error (%)	0.006	0.006	0.006
Reduced UC compute time (%)	8.0	11.9 (+32.8%)	11.9 (+32.8%)
IEEE-118			
Retained constraints (%)	4.5	10.2 (+126.7%)	10.2 (+126.7%)
Screening time (s)	19.7	40.3 (+104.6%)	256 (+1200%)
Number of infeasibilities	0	0	0
Cost error (%)	0	0	0
Reduced UC compute time (%)	6.8	12.0 (+76.5%)	12.0 (+76.5%)
CASE500_pserc			
Retained constraints (%)	0.8	1.7 (+112.5%)	1.7 (+112.5%)
Screening time (s)	166	217 (+30.7%)	690 (+315.6%)
Number of infeasibilities	0	0	0
Cost error (%)	0	0	0
Reduced UC compute time (%)	1.0	1.1 (+10%)	1.1 (+10%)

118 test system, CD+D1-UCD obtains reduced UC problems with 126.7% fewer constraints than CD-UCD with a computational time lower by 7%. In that case none of the 1440 cases tested led to infeasible UC results. The CD-BA approach reveals the same result as the B-UCD method in terms of retained constraints. Hence, the cost error, the number of infeasibilities, and reduced compute time are similar to B-UCD as shown in Table 2.9. However, the screening time is slower than CD+D1-UCD by 821% and 1200% for IEEE-RTS-73 and IEEE-118 test systems, respectively.

For the CASE500_pserc case, the cost-driven approach has been applied by fitting three piecewise linear segments; see Table 2.8. The results reveal the percentage of retained constraint with CD+D1-UCD slightly below 1%, indicating that this network is not congested for the patterns of net load it has to handle. Also, the result reveals the reduced UC computation time from CD+D1-UCD is slightly faster than that obtained after running CD-UCD with a lower screening time. The screening time for CD-BA is slower than CD+D1-UCD by 315%.

2.4.8 Sensitivity Analysis – Effects of the Conservativeness Factor Γ

Since the conservativeness factor has the potential of influencing the retained constraints, this section provides an analysis of the sensitivity of the proposed CD-UCD approach to variation in the slope value. To that end, Fig. 2.5 shows how the conservativeness factor Γ influences the constraint screening performance in CD+D1-UCD for the IEEE-RTS-73 and IEEE-118 cases. The conservativeness factor increases the fitted slope values and yields higher numbers of retained umbrella constraints. For the IEEE-RTS-73 system, with conservativness factor values above 4%, constraint screening results coincide with the number constraints found with D1-UCD as seen in Table 2.4. While for the IEEE-118 case, similar results are obtained when $\Gamma \geq 12\%$.

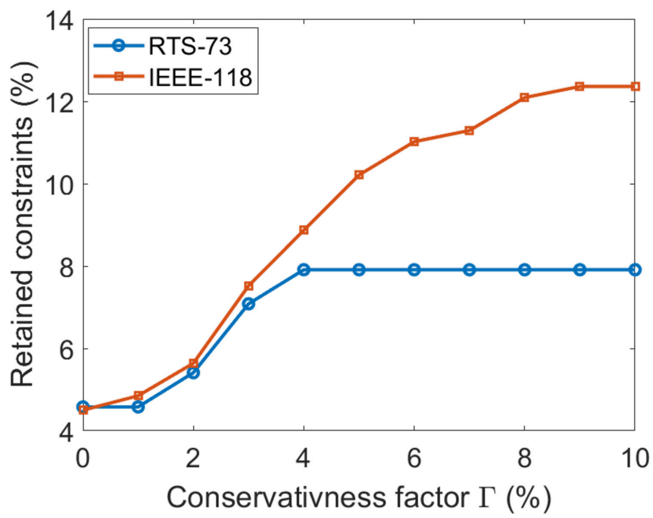

Figure 2.5: Retained umbrella constraints in CD+D1-UCD as a function of Γ.

2.4.9 Congested Case Study

Motivated by the previous case study CASE500_pserc in subsection 2.4.7, where the network is very light loading condition of the test system. Testing the fidelity of our proposed approach becomes imperative due to the noticeable slowdown in the solution time of the complete UC problem when operating within a congested network. Therefore, We show the proposed approach's efficiency for a congested CASE500_pserc test system. The congested test system is obtained by multiplying the original line capacities [137] with a factor equals 0.7. The set of 1466 line constraints has been divided into 8 equal blocks in an arbitrary manner. We use $\eta = 0.035$ for the test system with the nominal loading level given in [137]. The cost upper bound and DPUS ($K = 50$ principal components) have been determined with 7200 net demand vectors, while 240 instances were retained for testing.

Table 2.10: Congested CASE500_pserc Results

Method	Screening time (s)	Retained constraints (%)	Reduced UC compute time (%)	Cost error (%)	Number of infeasibilities
BA	910	14.05	15.7	0	0
CG	–	9.40 (−33.0%)	123.8 (+689%)	0	0
B-UCD	190 (−79.1%)	14.05 (0%)	15.7 (0%)	0	0
D1-UCD	298 (−67.2%)	11.65 (−22.3%)	11.7 (−25.8%)	0	0
CD-UCD	419 (−53.9%)	12.96 (−7.8%)	13.5 (−14.0%)	0	0
CD+D1-UCD	379 (−58.3%)	7.30 (−48.1%)	7.9 (−49.7%)	0	0
CD+D1-UCD ($\Gamma = -10\%$)	410 (−54.9%)	5.04 (−64.1%)	10.9 (−30.5%)	0.008	32 (13.3% of test instances)

Generally, the percentage of retained constraints and the UC computation time reduction in Table 2.10 are larger compared to results in the normal congested case in Table 2.7 and Table 2.9. The CG method adds 9.4% of the network constraints, but it requires more time compared to the full UC since a UC instance has to be solved several times. The BA and B-UCD approaches retained 14% of the network constraints with an advantage of B-UCD with a screening time lower by 79.1%. Furthermore, the performance of D1-UCD surprisingly outperforms CD-UCD in terms of retrieved constraints by retaining 11.6% and 12.9%, respectively. This is a direct result of the impact of shrinking the uncertainty set which reveals a higher influence compared to cost-driven constraints with Box uncertainty set. Lastly, considering the cost-driven CD+D1-UCD, imposing a data-driven uncertainty set ($P_1(\mathcal{S}, K)$) combined with the cost-driven constraints reduces screening time and retained constraints by 58.3% and 48.1% compared to the BA, respectively. Indeed, the method CD+D1-UCD obtains the lowest UC solution time with a percentage of 8% with respect to the full UC problem. This result emphasizes the power of the synergistic impact of CD and D1 which involves the largest improvement across all other methods that produces no infeasible instances or cost error.

Lastly, we are showing through the conservativeness factor Γ how poor tuning of the cost upper bound can have negative consequences on the adequacy of constraint screening. In this case, we are forcing Γ to be -10% with the expected consequence of seeing valid constraints being screened out.[9] Indeed, with $\Gamma = -10\%$ the number of retained constraints drops along with the screening time by 64% and 54.9% with respect to the BA, respectively. Similar drops are observed with respect to the other screening approaches as seen in Table 2.10. As expected, with tighter cost upper bounds essential constraints end up being left out as evidenced by the cost errors and nonzero number of infeasible UC solutions. This "over-screening" problem can be managed by the user by tuning of the conservatism parameters $\Delta\sigma$ and Γ and by carefully validating reduced UC solutions against the full original UC. The fact that $\Delta\sigma$ and Γ are available here is an advantage over the proposal of [108]. Here

[9] In fact, here the first fitted line segment of the three piecewise linear regression was not adjusted with Γ to avoid CD+D1-UCD being infeasible.

the price to pay by increasing conservatism parameters is larger retained constraint counts, which come with the benefit of increasing the likelihood that the reduced UC solutions are consistently feasible for the original UC.

2.4.10 Real-World Case Study

To demonstrate the effectiveness of the suggested method in a practical case study, this section evaluates the simulation outcomes of various techniques applied to a model of the Texas power system [139]. The power system being examined consists of 2000 buses and 3206 lines. The generating units data has been modified to make the UC more challenging, as suggested in [88]. We use $\eta = 0.035$ for the test system with the nominal loading level given in [137]. The cost upper bound and DPUS have been determined with 7200 net demand vectors, while 240 instances were retained for testing. All UC instances are computed with an optimality gap of 1%. For UCD with polyhedral uncertainty sets, we consider keeping $K = 50$ principal components when determining $P_1(\mathcal{S}, K)$. Line-based decomposition is used when running all versions of UCD (B-UCD, D1-UCD, CD-UCD, ED+D1-UCD). Without loss of generality, we generated 14 sub-problems each containing 458 line flow constraints as explained in Appendix A.

Table 2.11 provides the relevant experimental results. One main observation that needs to be highlighted is that all six methods under consideration yield the same optimal UC cost as the full UC for the 240 instances in the test set. Furthermore, no infeasibility cases were recorded in this case study. As a result, the performance of these methods, is evaluated and compared based on screening time, the percentage of constraints retained, and the reduced UC compute time relative to the time taken to solve the complete UC problem. Our proposed approaches except for B-UCD — which yields the same result as BA — outperform Roald's method in terms of network constraint removal. Although the tightest screening approach CD+D1-UCD has retained a slightly higher percentage of retained constraints compared to the CG approach. Nevertheless, CD+D1-UCD and also CD-UCD provide faster UC computation time with respect to the BA and CG approaches. Indeed, when compared to

Table 2.11: Texas Power System Results

Method	Screening time (s)	Retained constraints (%)	Reduced UC compute time (%)
BA	118,190	4.28	3.80
CG	–	0.46 (−89.1%)	1.90 (−51.1%)
B-UCD	18,967 (−83.9%)	4.28 (0%)	3.90 (+3.2%)
D1-UCD	37,637 (−68.1%)	2.60 (−39.3%)	1.80 (−52.6%)
CD-UCD	24,861 (−78.9%)	1.30 (−68.4%)	1.60 (−57.9%)
CD+D1-UCD	17,585 (−85.1%)	0.60 (−86.2%)	1.56 (−59.0%)

Roald's method, the reduced UC solution time achieved by CD-UCD and CD+D1-UCD are 57.9% and 59% lower, respectively. Similarly, the CG approach shows 51.1% reduction in UC solution time computational time compared to Roald's method.

2.4.11 Enhanced CD-UCD comparison with CD-UCD and CD+D1-UCD

Lastly, we study how the enhanced cost-driven upper bound (ECD-UCD), (2.32) and (2.33), compares to the original CD-UCD. This study is performed by imposing a box uncertainty set and the $P_1(\mathcal{S}, K)$ DPUS. The intuition behind ECD-UCD is that in the conventional cost upper bound (2.29), all integer solutions for the UC are considered for both cheap and expensive generators for a given range of net demand (2.31). Nevertheless, we argue that it is more advantageous to adjust this upper bound to eliminate certain feasible yet sub-optimal UC integer solutions. In this section, we assess the relative benefits in terms of screening time and retained constraints between the base CD-UCD, (2.29)–(2.31), and ECD-UCD, which replaces (2.29)–(2.31) with (2.30),(2.31), (2.32) and (2.33).

Using ECD-UCD with the box uncertainty set leads to noteworthy computational improvements in screening time, exhibiting improvements over CD-UCD ranging from 14.7% to 65.9% across the four test case; see Table 2.12. Likewise, ECD-UCD with DPUS also shows considerable improvement over CD+D1-UCD in terms of screening time ranging

Table 2.12: Comparison of the Enhanced CD-UCD (ECD-UCD) with CD-UCD

	$(CD - ECD)/CD$ (%)			
Measures	Screening time (%)		Retained constraints (%)	
Uncertainty set	Box	DPUS	Box	DPUS
RTS-73	61.9	34	14.1	0
IEEE-118	65.9	23.6	23.5	0
Congested CASE500_pserc	14.7	31.9	28.5	24.2
Texas	60.7	28.3	12.3	11.6

from 23.6% to 34% across the four test cases.

In addition, generally we observe a decrease in number of retained constraints with ECD-UCD and ECD+D1-UCD in comparison to CD-UCD and CD+D1-UCD. No improvement is found when applying ECD+D1-UCD over CD+D1-UCD for IEEE-RTS-73 and IEEE-118 test systems—albeit the same number of constraints are identified in a fraction of the computation time. Improvements in screening results are more significant with the box uncertainty set. On the other hand, we notice that as the test power systems get larger, the use of DPUS yields similar screening performance to what is offered by box uncertainty sets.

2.5 Summary

A widespread observation in power system operation and planning optimization is that only a very small proportion of transmission line limitations are ever binding. In this chapter, we proposed a data-driven umbrella constraint discovery approach that takes advantage of historical information to disregard redundant constraints in unit commitment problem formulations robust to uncertain net demand (demand less non-dispatchable generation).

This approach requires first a characterization of polyhedral uncertainty sets using historical net demand observations and their past forecasts along with principal component analysis. We demonstrated how data-driven polyhedral uncertainty sets offer a good robustness compromise in comparison to cruder box-like uncertainty sets since they acknowledge cross-node correlations between demand and non-dispatchable generation.

Furthermore, we presented a proposal to refine the process of umbrella constraint discovery with the objective of predicting which of the umbrella constraints will be active in a unit commitment instance. With that prediction at hand, we demonstrate significant unit commitment solution speed-ups. This refinement is rendered possible by recognizing that the original set of umbrella constraints of a problem will intersect with a set of production cost upper bounds, whose computation is based on historical unit commitment solutions.

Chapter 3

Integrating Learning and Constraint Generation for Security-Constrained Unit Commitment Acceleration

In this chapter, we extend the single-period unit commitment formulation from chapter 2 by incorporating line contingencies where a single transmission line is unavailable ($N-1$) security. The security-constrained unit commitment (SCUC) problem is one of the fundamental tools for power systems operational planning and real-time operation. Conventionally, this problem requires the online solution of a mixed-integer optimization problem, which faces computational requirements limitations in real-world power systems due to its inherent large size. Although pure optimization-based methods, such as iterative constraint generation, provide optimal solutions when given enough time, the substantial time required to use them in online applications hinders their implementation in large systems. On the other hand, practically speaking SCUC is solved repeatedly with only minor changes in input data. Thus, we consider the auxiliary procedure of learning essential solution characteristics from the previous optimal solutions as functions of the input parameters. In this chapter, we integrate learning and constraint generation to develop a computationally-efficient and rigorous approach for implementing faster security-constrained unit commitment for online applications while preserving its feasibility and optimality. Our proposed method is based on learning offline relevant sets of constraints from which the optimal solution can be obtained efficiently. Then online, we can predict relevant constraint sets and warm-start the constraint generation method. The advantage of this procedure is much faster than conventional constraint generation approaches while still preserving the feasibility and optimality of full-fidelity constraint generation. We conduct case studies to demonstrate the effectiveness of the proposed approach.

3.1 Introduction

Security-constrained unit commitment is a fundamental tool for all major independent system operators in the US, such as ISO New England, CAISO and PJM, for the daily operation of power systems [140, 141]. The goal of the SCUC problem is to minimize system operational cost as offered by generators, while satisfying generation, network, and security constraints. As mentioned in chapter 1, SCUC is generally formulated as a mixed-integer linear programming problem, which belongs to the class of NP-hard problems even if a single time period is considered [18]. Hence, solving this problem in online applications becomes computationally challenging.

One distinctive aspect of power systems operation is that the SCUC problem is solved repeatedly at least every hour or even more often in response to variations in the operating conditions because of uncertainty in demand and renewable energy production [89]. Therefore, the resulting problem size quickly becomes computationally intractable with increasing system size and more complex contingency scenarios. The main computational cumbersomeness of the SCUC problem is the number of post-contingency scenarios and their associated constraints and variables [8, 23, 89, 103].

As argued in the introduction of the thesis, extensive research efforts have been devoted to simplifying and accelerating the traditional optimization algorithms for MILP problems through machine learning techniques [71,72]. By learning an effective and fast approximation

Table 3.1: Comparison of CG and ML Methods

Property	CG	ML
Paradigm	model-based	data-driven
Constraints handling in the optimization	mature✓	immature
Online computational complexity	high	low✓
Guaranteeing solution feasibility	yes✓	no
Preserving the optimality of solution	yes✓	no

of some underlying heavy computations, the resulting ML models, once well-trained, can significantly reduce the online computational burden of the original optimization problems. Our objective in this chapter is to develop a framework that enables the SCUC problem to be solved in a more efficient manner by utilizing machine learning methods. We leverage an interpretable classification algorithm for constraint learning and integrate the constraint learning outcome with a constraint generation approach. Constraint learning here refers to the learning process of a subset of constraints based on statistical data.

Moreover, we can see from the discussion in Section 1.6 of Chapter 1 that the properties of CG and ML are clearly complementary (see Table 3.1). The key outcome from Table 3.1 and discussion in Section 1.4 of Chapter 1 is that substituting SCUC with ML predictions does not ensure the provision of optimal operating points that will not violate any line flow limits [68] for future instances. Evaluating the worst-case performance using discrete samples from the entire training and test dataset establishes solely an empirical lower bound for the worst-case guarantee [68]. In contrast, the optimization method consistently ensures both solution feasibility and optimality. Therefore, in this chapter we integrate ML and CG to develop a computationally efficient and rigorous solution for accelerating the SCUC problem in online mode. We aim to fully leverage the benefits of both techniques while overcoming their respective drawbacks.

3.2 Motivation

In a general MILP problem $Q[\mathcal{J}]$ with set of inequality constraints $\mathcal{J}$, we denote $z = (x, y)$ as the decision variable vector defined by the continuous variables $x \in \mathbb{R}^v$ and integer variables $y \in \mathbb{Z}^w$. We assume $Q[\mathcal{J}]$ is feasible and bounded, and its optimal solution $z^*[\mathcal{J}]$ is unique[1]. However, it is important to note that if multiple optimal solutions emerge, our proposal only requires the retention of a single solution. The feasible region defined by constraints in $\mathcal{J}$ includes the subset of binding constraints $\mathcal{B} \subseteq \mathcal{J}$.

In a continuous linear programming problem where y vector does not exist, the binding constraints set $\mathcal{B}$ can be obtained based on the optimal solution $z^*[\mathcal{J}]$. Hence, the optimal objective values of $Q[\mathcal{J}]$ can be obtained through the reduced problem $Q[\mathcal{B}]$ i.e., $Q[\mathcal{B}] = Q[\mathcal{J}]$. On the other hand, for a MILP problem, a subset of constraints $\mathcal{S} \subseteq \mathcal{J}$ is defined as the *invariant constraint set* if the optimal objective values of problems $Q[\mathcal{J}]$ and $Q[\mathcal{S}]$ are equal [142]. In fact, as argued in the introduction of the thesis that minimal feasible region includes binding constraints and critical non-binding constraints. The set of binding constraints of a MILP does not necessarily entail the optimal objective value as that of the full problem. In MILP, the invariant constraint set comprises not just the binding constraints, but also some of the non-binding ones namely the critical non-binding constraints. Hence, we can state that for MILP problems $\mathcal{B} \subseteq \mathcal{S}$ [28, 142]. These critical non-binding constraints are essential for MILP problem-solving, as removing them from the original feasible region would compromise the feasibility and optimality of the resulting solution. In other words, the reduced problem $Q[\mathcal{B}]$ does not guarantee the optimality of the produced solution as the original problem $Q[\mathcal{J}]$. The goal of this chapter is to show that a reduced problem with fewer constraints generally requires less computational effort, making it more suitable for online applications in SCUC while focusing on defining an invariant constraint set for SCUC.

[1]The unique optimal solution in a MILP is a strong assumption that has been made to motivate the application in this chapter.

3.3 Security-Constrained Unit Commitment

3.3.1 Assumptions

For expository purposes, we use a simplified single-period security-constrained unit commitment optimization problem. Most of the current research publications that suggest techniques to filter network constraints focus on single-period problems [33, 79, 88, 106, 110]. Furthermore, we model line contingencies and their effects with line outage distribution factors (LODF) as in [8, 23, 33, 110] to the single-period unit commitment.

3.3.2 Problem Formulation

The optimization problem corresponding to this simplified SCUC is a MILP formulated as:

$$\min_{u,g,q} \sum_{m \in \mathcal{M}} c_m g_m \tag{3.1}$$

Subject to:

$$q_n = \sum_{m \in \mathcal{M}_n} g_m - d_n, \quad \forall n \in \mathcal{N} \tag{3.2}$$

$$\sum_{n=1}^{N} q_n = 0 \tag{3.3}$$

$$u_m g_m^{\min} \leq g_m \leq u_m g_m^{\max}, \quad \forall m \in \mathcal{M} \tag{3.4}$$

$$-\overline{f}_l^0 \leq \sum_{n=1}^{N} h_{ln}^0 q_n \leq \overline{f}_l^0, \quad \forall l \in \mathcal{L} \tag{3.5}$$

$$-\overline{f}_l^c \leq \sum_{n=1}^{N} h_{ln}^c q_n \leq \overline{f}_l^c, \quad \forall l, c \in \mathcal{L}, \mathcal{C} \tag{3.6}$$

$$u_m \in \{0, 1\}, \quad \forall m \in \mathcal{M} \tag{3.7}$$

Decision variables include the commitment status of the generating units u_m, the power output schedules g_m, the net power injections at each node q_n. The objective function (3.1) minimizes the total generation cost. Constraint (3.2) computes the net injected power at each node, while constraint (3.3) ensures power balance in the system. Constraint (3.4) imposes limits on generator outputs. Constraints (3.5) and (3.6) enforce the power flow limits for the base case i.e., normal operating condition and every contingency using PTDFs and LODFs, respectively. The symbols $\overline{f}_l^0$ and $\overline{f}_l^c$ represent the maximum power flow limits on line l in pre- and post-contingency outage states. Finally, (3.6) defines the binary variables of the generating units. For a more compact formulation, constraints (3.5) and (3.6), which define the feasible region of net injected power vector given base and contingency PTDFs matrices, and the transmission flow limits can be reformulated as follows:

$$\mathcal{F}(H, \bar{f}) = \{q : -\bar{f} \leq Hq \leq \bar{f}\} \tag{3.8}$$

where

$$H = \begin{bmatrix} H^0 \\ H^1 \\ \vdots \\ H^C \end{bmatrix}, \quad \bar{f} = \begin{bmatrix} \bar{f}^0 \\ \bar{f}^1 \\ \vdots \\ \bar{f}^C \end{bmatrix} \tag{3.9}$$

Here the PTDF matrix $H^0 \in \mathbb{R}^{L \times N}$ (h_{ln}^0 are the lnth elements of the matrix H^0) is a linear mapping of nodal power injections vector q_n to power flows vector $\overline{f}^0$. In order to represent the maximum and minimum values of the feasible region $\mathcal{F}(H, \bar{f})$, every contingency PTDF matrix starting from H^1 and going all the way to H^C adds $2(L-1)$ linear inequalities to the SCUC problem. Furthermore, with the imposition of the $N-1$ security criterion, the feasible region $\mathcal{F}(H, \bar{f})$ is defined by $2(L + C(L-1))$ inequalities. For a detailed explanation of the contingency PTDF matrices and their derivation, please refer to [110].

Here, we consider the set of line constraints that construct the feasible region in (3.8) is reformulated by the compact form ($A \in \mathbb{R}^{I \times N}$, $\bar{\boldsymbol{f}} \in \mathbb{R}^{I \times 1}$). The number of columns of A corresponds to the number of buses in the network, N, while its rows (as well as that of $\bar{\boldsymbol{f}}$)) are defined with a set of indices $\mathcal{I}$ of size I such that $I = 2(L + C(L-1))$ which corresponds for all the line limits in both pre- and post-contingency states such that [110]:

$$\mathcal{F}(A, \bar{\boldsymbol{f}}, \mathcal{I}) = \Big\{ q \in \mathbb{R}^N : A_i q \leq \bar{\boldsymbol{f}}_i, \forall i \in \mathcal{I} \Big\} \tag{3.10}$$

where A_i is the i-th row of matrix A and $\bar{\boldsymbol{f}}_i$ is the i-th entry of vector $\bar{\boldsymbol{f}}$. Nevertheless, it has been proven that only a portion of these inequalities is required to adequately define the SCUC problem, thus reducing the computational complexity of SCUC. For brevity, we can refer to feasible region in equation (3.10) as $\mathcal{F}(A, \bar{\boldsymbol{f}})$.

3.3.3 Constraint Generation Algorithm

This chapter tackles the deterministic SCUC problem which is solved based on the standard CG approach. Leveraging the fact that a candidate SCUC solution can easily be checked for feasibility, the standard CG approach adds constraints in an iterative way to a reduced base problem, which is a unit commitment problem with no transmission constraints [8]. The CG approach is an iterative technique where violated constraints from the original SCUC are gradually added to the reduced one until the solution to the latter is feasible in the former [102]; see Fig. 3.1. The interested reader may refer to the constraint generation approach that has been applied to large-scale robust optimization in unit commitment and OPF problems [143, 144].

3.4 Learning-Based SCUC Constraint Generation

Next, we seek to demonstrate that the results of a CG algorithm can be predicted for a SCUC. We posit that it is possible to use a predicted invariant constraint set, $\hat{\mathcal{S}}$. The predicted invariant constraint set can be obtained by having learned which constraints are part of the invariant set in the past. With such a set readily on hand, it is, therefore, possible to solve the full SCUC with a limited number of CG iterations—at least one if $\hat{\mathcal{S}} = \mathcal{S}$, and more if $\hat{\mathcal{S}} \subset \mathcal{S}$.

The elaboration of a learning-based CG algorithm requires both offline training and testing phases based on the outputs of past SCUC runs and/or simulated SCUC runs. As

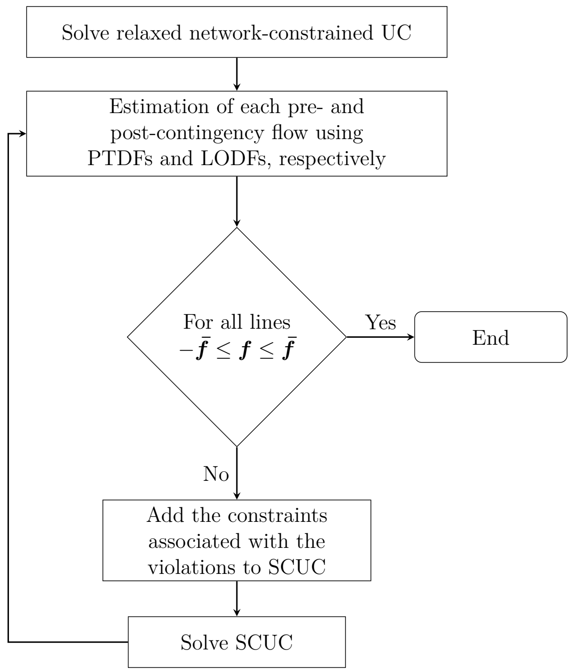

Figure 3.1: Constraint generation algorithm.

explained in the introduction, discovering an invariant constraint set can be difficult for the SCUC. Therefore, the development of an effective method for acquiring knowledge about an invariant constraint set $\mathcal{S} \subseteq \mathcal{I}$ remains an important research question.

3.4.1 Invariant Constraint Set Identification

We adopt the algorithm proposed in [28] to define the invariant set of a SCUC problem instance. This methodology seeks to identify an invariant constraint set, $\mathcal{S}_t$, for each training instance t. To compute the invariant constraint set $\mathcal{S}_t$ for a previously solved instance t, we follow these steps:

Step 1. We begin by initializing $\mathcal{S}_t$ with its set of binding constraints, $\mathcal{B}_t$.

Step 2. Next, a reduced SCUC problem denoted $\mathcal{UC}_{\boldsymbol{d}_t}[\mathcal{S}_t]$ is solved providing the optimal net power injections solution vector $q^*_{\boldsymbol{d}_t}[\mathcal{S}_t]$.

Algorithm 2: Identifying an invariant constraint set

Data: Historical or simulated net demand and its corresponding SCUC solution
Result: Invariant constraint set

1 Initialize $\mathcal{S}_t = \mathcal{B}_t$;
2 Solve $\mathcal{UC}_{\boldsymbol{d}_t}[\mathcal{S}_t]$ with solution $q^*_{\boldsymbol{d}_t}[\mathcal{S}_t]$;
3 **if** $\max_{i \in \mathcal{I} \setminus \mathcal{S}_t} \left\{ A_i^\top q^*_{\boldsymbol{d}_t}[\mathcal{S}_t] - \bar{\boldsymbol{f}}_i \right\} > 0$ **then**
4 $\quad \mathcal{S}_t := \mathcal{S}_t \cup \left\{ \arg\max_{i \in \mathcal{I} \setminus \mathcal{S}_t} \left\{ A_i^\top q^*_{\boldsymbol{d}_t}[\mathcal{S}_t] - \bar{\boldsymbol{f}}_i \right\} \right\}$;
5 $\quad$ go to step 2;
6 **else**
7 $\quad$ go to step 9;
8 **end if**
9 end;

Step 3. In the case that all the initial constraints in $\mathcal{F}(A, \bar{\boldsymbol{f}})$ are met, i.e., $A_i q^*_{\boldsymbol{d}_t}[\mathcal{S}_t] \leq \bar{\boldsymbol{f}}_i, \forall i \in \mathcal{I} \setminus \mathcal{S}_t$, then the algorithm terminates.

Step 4. Otherwise, the violated constraint or constraints are included in the set $\mathcal{S}_t$, and we return to Step 2.

The identification of the invariant constraint set method is summarized in Algorithm 2.

3.4.2 Training Data Generation

The premise of our proposal is that historical nodal net demand data indexed by previously solved instances $t = 1, ..., T$ and their corresponding SCUC invariant sets $(\boldsymbol{d_t}, \mathcal{S}_t)$ can be used to train a machine learning model capable of predicting the invariant constraint set for some unseen operating conditions. The predicted invariant constraint set is denoted by $\hat{\mathcal{S}}_{\tilde{t}}$, where $\tilde{t}$ is a test sample to be considered in the test phase.

Despite the availability of various machine learning methods, the K-nearest neighbors (KNN) algorithm [66] was chosen due to its clarity, interpretability, and its acceptance in the power systems community. Other classification methods such as support vector machines, decision trees, and neural networks could also be used for this task. A study utilizes the

KNN algorithm to distinguish if a line constraint belongs to an invariant set or not during time period t, using net demand data.

The training of the KNN model and the resulting construction of the invariant set $\mathcal{S}_t$ is cast as a binary classification problem. In the context of the KNN algorithm, the term "training" refers to the process of feeding the model with a labeled dataset. This labeled dataset is essential for the algorithm to learn the characteristics and patterns of the data [2]. Accordingly, we assign a label $s_t^i = 1$ or $s_t^i = 0$ to each line constraint $i \in \mathcal{I}$ in the SCUC problem instance t, based on whether the line constraint is in the invariant set $\mathcal{S}_t$ or not, respectively. This process makes sure all binding and critically non-binding constraints are included in $\mathcal{S}_t$ thus insuring that if the SCUC solved for $\boldsymbol{d_t}$ and $\mathcal{S}_t$ would return the same optimal solution that would have been obtained with the full set of constraints $\mathcal{I}$.

Unlike in classical classification training algorithms, here the focus is on SCUC performance, not classification or regression accuracy. The most commonly used Euclidean distance has been chosen as a distance metric to train KNN classifiers offline. The selection of the parameter K plays a critical role in KNN classification. A small value of K can increase the prediction sensitivity to noise, whereas a large value of K can result in over-generalization. Therefore, we consider multiple values of K to train offline different KNN models to be deployed next in the testing phase.

3.4.3 Testing

In the testing phase, each constraint $i \in \mathcal{I}$ in an unseen problem instance will be assigned the label $s_{\tilde{t}}^i = 1$ if the machine learning model predicts that the constraint i is in $\mathcal{S}_{\tilde{t}}$, or $s_{\tilde{t}}^i = 0$ otherwise.

It is widely recognized that the performance of machine learning models heavily relies on how data is split into training and testing samples. In order to achieve consistent out-of-sample results, this chapter employs the *leave-one-out technique*; the reader may refer

[2] Unlike training a neural network for instance, where the model optimizes a set of parameters to make predictions on unseen data, training the KNN model involves storing the entire dataset.

to [66] for more details. Specifically, the chapter assumes that there is a database of T previously solved SCUC instances, and that the optimal solution for each instance is unique. The leave-one-out strategy involves running T iterations of the KNN predictions, where in each iteration, one MILP instance is chosen to be the test set. During each iteration, the approach selects one SCUC instance and designates it as the test set $\{\tilde{t}\}$ to be run in the online phase. The remaining $T-1$ instances constitute the training set, $\{1,\ldots,T\}\backslash\{\tilde{t}\}$. Note that the training phase includes $T-1$ time instances that were performed offline. The subsequent step is to make online predictions for the invariant constraint set for the kept test instance using the trained model. This predicted set is then used to initialize or warm-start the constraint generation algorithm, resulting in the optimal solution for the test instance.

3.5 Computational Experiments

All the computations reported next were carried out on an Intel(R) Core(TM) i7-11700K CPU @ 3.60 GHz and 64 GB of RAM platform. The optimization problems were solved using the commercial MIP solver CPLEX. The Invariant constraint set training and testing using KNN classification is carried out using ML software from MATLAB [145].

3.5.1 Test Systems

Points of comparison

We compare the chapter's proposed approach with two other algorithms. The first algorithm is the standard constraint generation algorithm in Fig. 3.1 that ignores any information provided by the data and only adds violated constraints at each iteration; it is denoted as CG. The second algorithm uses the binding constraint set, $\mathcal{B}$, to warm-start the constraint generation method as suggested in [88]. This method is denoted as the B-CG algorithm. The proposed approach, which uses a prediction of the invariant constraint set $\mathcal{S}$ to warm-start the constraint generation, is denoted as S-CG.

Performance metrics

We assess the performance of the proposed approach over T runs in terms of the following metrics:

- The number of constraints included in the reduced SCUC. It is given by two values: the minimum and maximum number of constraints. These values are denoted as $\alpha_{\min}$ and $\alpha_{\max}$, respectively.
- The minimum and maximum number of CG iterations executed for the various strategies (CG, B-CG, and S-CG), averaged over all test instances. The notation used is $\beta_{\min}$ and $\beta_{\max}$ to denote the minimum and maximum values, respectively.
- The percentage of test instances that can be solved with only one iteration of the constraint generation method is denoted as τ.
- The fraction (in percent) of the SCUC online computation time required in comparison to that of the fully-constrained original SCUC, denoted by δ.

Test environment

In this subsection, we test our proposed methodology in a number of IEEE test networks from the MATPOWER database [137]. Also, generator marginal costs c_m have been modified so that they vary in the range $[15, 40]$ \$/MWh. We generate T net load instances of dimension $N^\star$, where $N^\star$ is the number of nodes with uncertain net demand such that $N^\star \leq N$ which are then consigned to matrix $\boldsymbol{d}$. The net demand at each node n is sampled randomly from a uniform distribution within a certain range $\mathcal{U} = [\Delta_{\min} d_n^0, \Delta_{\max} d_n^0]$, where d_n^0 is the nominal net demand taken from [137]. In addition, an alternative method is utilized for generating T samples of the net loads, where the net loads follow a multivariate normal distribution. In this case, for each net load d_n, the mean value is set at $\mu_n = lf * d_n^0$ and its standard deviation at $\sigma_n = \zeta * d_n^0$, where lf is the loading factor. We further sample correlations across net loads uniformly from $[0, 1]$ and use it to create the covariance matrix. In both cases, we generate 2000 time instances, and we apply the leave-one-out strategy for testing. We train the KNN model for different numbers of k neighbors and investigate the impact on performance metrics.

3.6 Computational Results

3.6.1 IEEE RTS-73 Test System

Here, we run two scenarios: one where net load is uniformly distributed, and a second where it is normally-distributed. For uniformly-distributed scenario, we generate 2000 load data instances in the range $\mathcal{U} = [0.6, 1]d_n^0$. For the normally-distributed scenario, the loading factor $lf = 0.8$ and $\zeta = 0.045$. The total number of line constraints generated by the SCUC problem for this system is 26896. In the no-contingency state, we have $120 \times 2 = 240$ constraints. In each contingency, we have $119 \times 2 = 238$ constraints. Given that we are examining only 112 contingencies [3], the total number of constraints arising from lines, for operation under no-contingency and contingency states is $240+112\times238 = 26896$ constraints. Considering the two cases, We run 2000 instances for the SCUC problem offline to identify the binding and invariant constraint sets in the training set. The invariant constraints set were generated using all the violated constraints [4] at each iteration for each simulated instance t as in Algorithm 2.

In this section, we have generated box plots to compare the binding and invariant constraints resulting from solving T instances of SCUC problem offline as shown in Fig 3.2. In each box plot, the middle red line represents the median, while the lower and upper edges of the box represent the 25th and 75th percentiles, respectively. The whiskers extend to the furthest data points that are not considered outliers, and any outliers are displayed separately using the + marker symbol. From Fig 3.2, we notice that one of the percentiles in $\mathcal{B}$ and $\mathcal{S}$ coincide with the median which reveals minimal variations in the binding and

[3] We had to disregard the potential failure of 8 branches which lead to infeasible SCUC solutions.
[4] This corresponds to the max operator in step 3 in algorithm 2

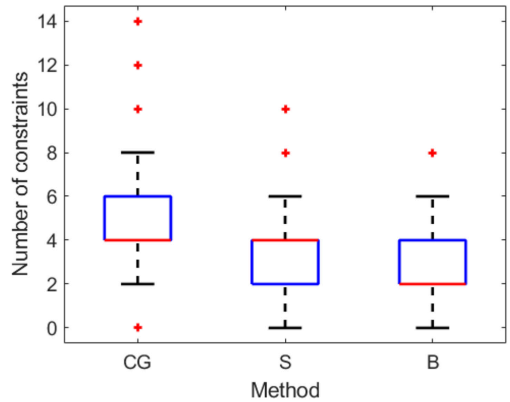

Figure 3.2: IEEE RTS-73 – Box plot of the number of constraints in each method from training set; uniformly-distributed net load

Table 3.2: IEEE RTS-73 – Testing results for uniformly-distributed net loads

Method	k	$[\alpha_{\min}, \alpha_{\max}]$	$[\beta_{\min}, \beta_{\max}]$	$\tau(\%)$	$\delta(\%)$
CG	-	$[0, 14]$	$[1, 4]$	0.2	110.93
B-CG	1	$[2, 16]$	$[1, 3]$	88.25	50.31
	5	$[2, 16]$	$[1, 3]$	98.4	43.8
	100	$[14, 16]$	$[1, 2]$	99.95	42.59
S-CG	1	$[2, 24]$	$[1, 3]$	99.85	42.95
	5	$[24, 24]$	$[1, 1]$	100	42.8
	100	$[24, 24]$	$[1, 1]$	100	42.6

invariant set across the simulated instances T. Also, we can see that the median number of constraints in the invariant set in the training set is four constraints, while the number of binding constraints is two at the median. Note that we demonstrate the number of constraints in the CG approach in Fig 3.2 along with the binding and invariant sets from training instances, but we are deploying the CG approach to be compared with warm-started B-CG and S-CG approaches in the testing phase.

We train KNN predictors for $k \in \{1, 5, 10\}$ using the information provided by sets $\mathcal{B}$ and $\mathcal{S}$ in Fig 3.2 for B-CG and S-CG approaches. In the testing phase, we can see from Table 3.2

that the reduced problems generated from the three algorithms have 99.9% fewer constraints compared to the original SCUC problem. Moreover, when considering various values of k for KNN, both B-CG and S-CG require only 50% or less of the original computation time in the full SCUC problem. Notice that the CG approach is more computationally demanding than solving the full SCUC problem in this case. The main outcome of Table 3.2 is that the larger k is, the more conservative we are, which means the larger number of retained constraints and consequently fewer iterations are needed to recover the optimal solution. Also, more than 88% and 99% of the test instances only needed a single iteration to recover the optimal solution considering B-CG and S-CG approaches, respectively. Finally, the number of invariant constraints in S-CG is relatively larger than the number of retained constraints from the other two algorithms.

For a normally-distributed net load scenario, we train KNN models for $k \in \{1, 5, 100\}$ using the information provided by sets $\mathcal{B}$ and $\mathcal{S}$ in Fig 3.3. From Table 3.3, the maximum number of retained constraints from the CG algorithm is approximately twice the maximum number of constraints resulted from the warm-started CG algorithms. Also, Table 3.3 shows that the maximum number of iterations with S-CG is two, where sometimes four iterations are necessary with the CG algorithm which results in higher computational time as compared to the S-CG algorithm. For B-CG, the computational cost of the algorithm varies based on the value of k. The higher the value of k, the fewer iterations are needed and, consequently, the necessary compute time is reduced. In fact, the B-CG approach that warm-started with the predicted binding constraints set needs more iterations to recover some invariant constraints to achieve optimality. Finally, Fig 3.3 illustrates the statistical properties of the retained constraints from all training samples before running the prediction. Notice that the SCUC problem with normally-distributed net loads has slightly higher constraints as shown in Fig 3.3 compared to the uniformly-distributed net loads case in Fig 3.2.

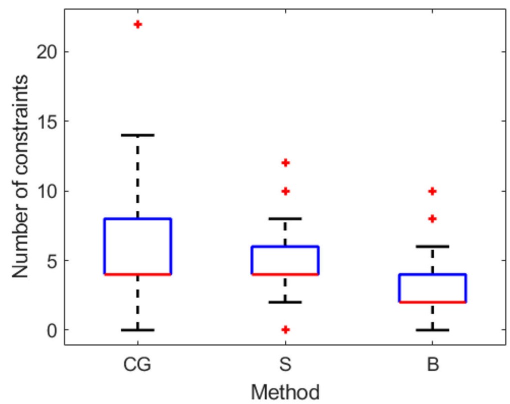

Figure 3.3: IEEE RTS-73 – Box plot of the number of constraints in each method from training set; normally-distributed net load

Table 3.3: IEEE RTS-73 – Testing results for normally-distributed net loads

Method	k	$[\alpha_{\min}, \alpha_{\max}]$	$[\beta_{\min}, \beta_{\max}]$	$\tau(\%)$	$\delta(\%)$
CG	-	$[0, 22]$	$[1, 4]$	0.06	104.31
B-CG	1	$[0, 10]$	$[1, 3]$	77.05	59.73
	5	$[0, 10]$	$[1, 3]$	83.4	55.9
	100	$[2, 10]$	$[1, 3]$	90.9	51.02
S-CG	1	$[0, 12]$	$[1, 2]$	99.85	43.5
	5	$[0, 12]$	$[1, 1]$	100	43.2
	100	$[12, 12]$	$[1, 1]$	100	43.2

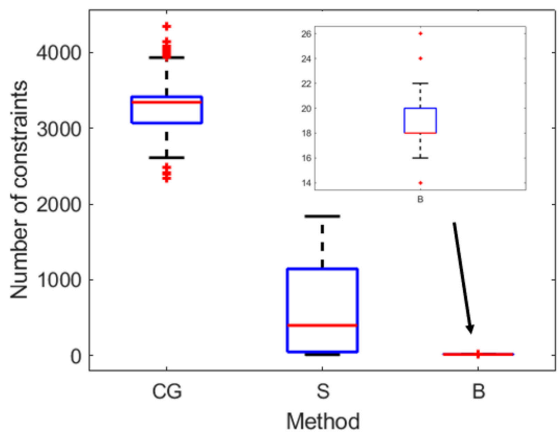

Figure 3.4: IEEE 118 – Box plot of the number of constraints in each method from training set; uniformly-distributed net load

3.6.2 IEEE-118 Test System

Like with the IEEE RTS-73 case, we also run two net load scenarios: uniform and normal distributions. For uniformly-distributed net loads, we generate 2000 load data instances in the range $[0.6, 1]d_n^0$. For normally-distributed net loads, the loading factor equals 0.8 and $\zeta = 0.05$. The training data for uniformly- and normally-distributed net loads are collated in Fig 3.4 and Fig 3.5, respectively.

Due to the high number of invariant constraints found from algorithm 2, we train KNN predictor models for $k \in \{5, 10, 500\}$ with a small adjustment. In fact, the max operator threshold in algorithm 2 in step 3 controls how many violated constraints will be added to the invariant constraints set in the training phase. Here, we investigate the impact of selecting only 70 and 100 of the total number of invariant constraints in each instance for the S-CG algorithm in normal and uniform scenarios, respectively. These subsets of constraints are randomly selected from the invariant constraints for each simulated training instance t. The testing cases are collated in Table 3.4 and Table 3.5 for the uniformly- and normally-distributed net load cases, respectively.

Additionally, when we examine the amount of CG iterations used in both B-CG and

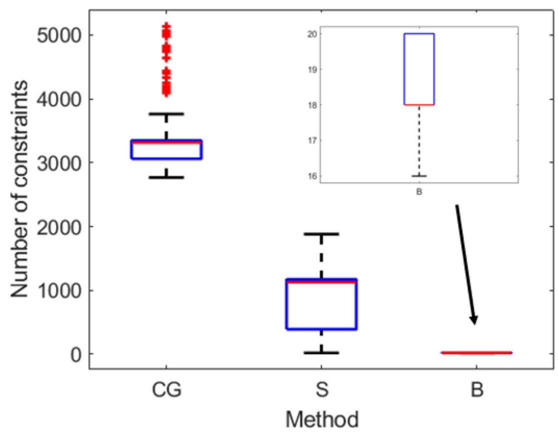

Figure 3.5: IEEE 118 – Box plot of the number of constraints in each method from training set; normally-distributed net load

S-CG approaches under a uniform distribution scenario, it becomes evident that the B-CG requires at the most two iterations compared to the S-CG which needed only one, regardless of the values of k. The total number of binding constraints across all the simulated instances in the training phase in Fig 3.4 is 48 constraints. In the testing phase, Table 3.4 shows that α_{max} value is 52 with different values of k. These four added constraints on top of the binding constraints in B-CG are necessary and sufficient critical non-binding constraints to recover the optimal solution. Additionally, randomly selecting invariant constraints from each training instance significantly increases the size of the invariant constraint set in the S-CG approach.

However, the results from Table 3.4 indicate a slightly different conclusion. Both B-CG and S-CG are able to converge using a maximum of three iterations. In fact, the impact of randomly selecting a subset of invariant constraints [5] has been reflected in the low percentage of instances which needed only one iteration compared to B-CG approach (77% to 93%). This result is necessary to reflect how the warm starting set is a crucial factor in the speed of the convergence of the data-driven CG approach. Some instances of the S-CG approach

[5]The selection procedure is performed randomly from the invariant constraints set which includes both binding and critical non-binding constraints.

Table 3.4: IEEE-118 – Testing results for uniformly-distributed net loads

Method	k	$[\alpha_{\min}, \alpha_{\max}]$	$[\beta_{\min}, \beta_{\max}]$	$\tau(\%)$	$\delta(\%)$
CG	-	$[2338, 4346]$	$[3, 4]$	0	33.34
B-CG	5	$[48, 52]$	$[1, 2]$	99.85	11.95
	10	$[48, 52]$	$[1, 2]$	99.85	11.94
	500	$[48, 52]$	$[1, 2]$	99.85	11.94
S-CG	5	$[212, 228]$	$[1, 1]$	100	11.95
	10	$[212, 228]$	$[1, 1]$	100	11.94
	500	$[228, 228]$	$[1, 1]$	100	11.89

Table 3.5: IEEE-118 – Testing results for normally-distributed net loads

Method	k	$[\alpha_{\min}, \alpha_{\max}]$	$[\beta_{\min}, \beta_{\max}]$	$\tau(\%)$	$\delta(\%)$
CG	-	$[2768, 5144]$	$[2, 4]$	0	39.32
B-CG	5	$[30, 70]$	$[1, 3]$	93.05	11.2
	10	$[30, 70]$	$[1, 3]$	93.05	11.1
	500	$[30, 70]$	$[1, 3]$	93.05	11.3
S-CG	5	$[78, 114]$	$[1, 3]$	77.7	12.39
	10	$[78, 114]$	$[1, 3]$	77.7	12.37
	500	$[88, 114]$	$[1, 3]$	77.7	12.35

needed more iterations to recover some binding and essential critical non-binding constraints that were missed during the random selection procedure. Compared to the B-CG which also needed three iterations to uncover some critical non-binding constraints that were not provided in the training instances in Fig 3.5. The S-CG with a randomly selected invariant constraint set still provides competitive results in terms of the number of iterations and the total number of constraints with CG approach.

Note that the choice of the number of neighbors, K, is connected to the confidence level in relaxing line capacity constraints that are input to the CG approach. A larger K indicates a more conservative approach, resulting in the retention of more constraints and, consequently, fewer iterations in online computation. While increasing the number of neighbors enhances the conservativeness of the proposed method, there are situations where recovering the original solution of SCUC becomes impossible solely from the learned constraints, even with a sufficiently large value of K, without running the CG approach online. This challenge is notably evident in the B-CG approach, where a specific network constraint might be a critical non-binding constraint across all historical data points. Regardless of the chosen value for K, the B-CG approach consistently removes such line flow constraints, potentially resulting in inaccurate solutions for certain operating conditions without running the CG approach. Therefore, this chapter emphasizes on defining invariant constraints set.

Overall, addressing the SCUC problem and achieving an optimal solution for a large-scale network can pose significant challenges. The advantage of the warm-started CG approach is that the online time needed to find the set of binding and critical non-binding constraints has been moved to be performed offline in the training phase. For a system operator or planner, the machine learning model can be trained using a year's worth of training data, and then run the SCUC in the next (unseen) year with considerable speed improvements. Hence, the system operator or planner in the testing phase with the warm-started CG approach would be able to distinguish the new potential binding and critical non-binding constraints. Also, other machine learning models such as graphical neural networks can be deployed to enhance prediction accuracy by utilizing existing network structures embodied in PTDF and LODF matrices along with demand data correlation. Ultimately, the suggested method has the potential for further expansion into multi-period SCUC for large-scale networks, presenting a more formidable challenge. Consequently, the advantages of the proposed approach are expected to become even more prominent in such a context.

3.7 Summary

The computational burden of using traditional algorithms to solve the SCUC for online applications—like security-constrained day-ahead and (possibly in the future) real-time electricity market clearing problems—can make it difficult to achieve optimality when a limited time window is available to run market-clearing algorithms. While some machine learning techniques have been used to speed up SCUC solutions, these methods may produce sub-optimal or even infeasible solutions. In this chapter, we proposed a machine-learning-assisted warm-start constraint generation algorithm that can achieve optimal SCUC solutions in a significantly shorter amount of time. Our approach is based on identifying invariant constraint sets from previous instances of the SCUC in an offline fashion. As a result, much fewer iterations are needed to run the SCUC constraint generation algorithm since a great majority of them have already been predicted. This generally leads to significant SCUC solution time speed-ups, a necessary feature for future low-carbon power systems.

Chapter 4

Cost-Aware Bound Tightening for Constraint Screening in AC OPF

In this chapter, we address the constraint screening problem using the bound tightening technique in the context of the OPF problem formulated with a full ac power flow characterization. As discussed in Chapter 1, the classic AC-OPF problem is both non-linear, nonconvex, and therefore NP-hard. Due to the non-convexity of the AC-OPF, we investigate line constraint screening under different convex relaxations of the problem. In this chapter, we introduce a valid inequality constraint that is directly connected to the objective function of the AC-OPF in the bound-tightening optimization-based screening approach. We employ *constraint learning* to augment an upper-bound cost-driven constraint derived by fitting an appropriate regression model using past instances of the AC-OPF problem. Hence, we reduce the conservativeness of the screening approach using the available historical data and thus lead to a tighter AC-OPF formulation.

4.1 Introduction

The optimal power flow (OPF) problem seeks to find optimal operating conditions subject to physical and engineering constraints of power systems [33, 55]. The OPF incorporates physical constraints to represent power flow phenomena and constraints such as voltage, generator, and line flow limits. The ac optimal power flow (AC-OPF) problem is both nonlinear, nonconvex and therefore NP-hard [55]. Furthermore, the number of variables and constraints becomes large as network size increases, posing more computational challenges for large realistic systems.

Despite the fact that all constraints in the OPF problem must be satisfied for a solution to be feasible, power system operators' experience and past research have shown that only a small proportion of the problem's inequality constraints (especially line flow limits) can be potentially binding (i.e., satisfied with equality) at the optimal solution [33]. As a result, it is widely common to screen out redundant constraints in order to reduce the problem size and speed up computations.

Umbrella constraint discovery is a pioneer constraint screening algorithm which has been proposed for DC-OPF problems to filter out redundant constraints [33]. Another dominant technique is *optimization-based bound tightening* (OBBT) which was proposed primarily to enhance the quality of convex relaxations of OPF problems [118,119]. The general procedure of OBBT is performed by minimizing or maximizing the desired variable while considering the constraints of the relaxation. This approach has been extended to screen out line flow constraints in DC-OPF, unit commitment [106] and AC-OPF [121] problems. Using OBBT, the authors of [106, 121] identify line flow limits that will never become active by solving one minimization and one maximization optimization problem associated with each line flow limit. In a broader sense, several constraints are satisfied indirectly through other constraints in the problem, allowing them to be eliminated confidently before requesting a solver's assistance.

At the same time, several convex relaxations of the AC-OPF problem have garnered substantial attention for various reasons. These relaxations include the quadratic convex relaxation (QCR) [118], the semidefinite relaxation (SDR) [146], and the second-order cone relaxation (SOCR) [147]. Generally, convex relaxations are only approximations of the original nonconvex optimization problem; they offer a limit on the best possible global optimal value of the AC-OPF problem. The advantage of convex relaxations with respect to constraint screening problems is that relaxations provide a lower (optimistic) objective bound (assuming the problem is a minimization; the converse applies if one is solving a maximization). Therefore, if the limit provided by a relaxation falls within the set boundaries for the restricted variable, we can be confident that the constraint is unnecessary or redundant in the original problem [121].

In this chapter, we propose a refinement to OBBT for AC-OPF constraint screening. First, instead of attempting to solve OBBT with the nonconvex AC-OPF problem directly, we utilize a convex relaxation to establish an upper bound on the global solution. Second, rather than identifying only redundant line constraints as suggested in [121], we propose a valid upper bound inequality constraint that embodies prior economical information to filter out even more redundant constraints. This refinement distinguishes between redundant, active, and inactive constraints in the AC-OPF problem. Finally, we apply the proposed method on state-of-the-art convex relaxations [148] to compare the relative effectiveness of the our proposal. The main contributions of this chapter are twofold:

1. To investigate constraints screening for the AC-OPF problem and show how different convex relaxations yield varying outcomes. We provide a comparative analysis to determine the conservativeness of various convex relaxations in terms of constraint screening.

2. To improve the OBBT method to identify not only redundant constraints but also inactive ones, thus leading to lighter AC-OPF formulations.

4.2 AC Optimal Power Flow Formulation

Consider a typical power system which consists of a set of $\mathcal{N} = \{1, \ldots, n\}$ buses (a subset of which have generators denoted by the set $\mathcal{G}$) and $\mathcal{L} = \{1, \ldots, l\}$ branches. Every node $k \in \mathcal{N}$ in the network has three properties, voltage $v_k = V_k \angle \delta_k$, power generation $s_{G_k} = p_{G_k} + jq_{G_k}$, and power consumption $s_{D_k} = p_{D_k} + jq_{D_k}$, all of which are complex numbers because of the AC power's oscillatory characteristics. Each branch $\ell \in \mathcal{L}$ has a series admittance

$y_\ell = g_\ell + jb_\ell$ and a total shunt susceptance b'_ℓ. We denote each bus's shunt conductance and susceptance as g'_k and b'_k, respectively. Each branch $\ell \in \mathcal{L}$ has a *from* end k and a *to* end m such that we denote $\ell = (k, m)$. From these we have active and reactive power flows for each branch ℓ leaving its *from* end—$p_{f\ell}, q_{f\ell}$—and corresponding flows at its *to* end—$p_{t\ell}, q_{t\ell}$. Lastly, in the case where a branch ℓ is a tap-changing transformer, we denote its off-nominal setting with the symbol t_ℓ. The AC-OPF problem is formulated as specified in [148, 149]:

$$\min \sum_{g \in \mathcal{G}} c_{g2} p_{Gg}^2 + c_{g1} p_{Gg} + c_{g0} \tag{4.1}$$

where variables $\boldsymbol{p}_G, \boldsymbol{q}_G \in \mathbb{R}^{|\mathcal{G}|}, \boldsymbol{p}_f, \boldsymbol{q}_f, \boldsymbol{p}_t, \boldsymbol{q}_t, \boldsymbol{t} \in \mathbb{R}^{|\mathcal{L}|}$, and $\boldsymbol{v} \in \mathbb{C}^{|\mathcal{N}|}$, is subject to:

$$\begin{aligned} &\sum_{g \in \mathcal{G}_k} p_{Gg} - p_{Dk} - g'_k \left|v_k\right|^2 \\ &\qquad = \sum_{\ell=(k,m) \in \mathcal{L}} p_{f\ell} + \sum_{\ell=(m,k) \in \mathcal{L}} p_{t\ell}, \quad \forall k \in \mathcal{N} \end{aligned} \tag{4.2}$$

$$\begin{aligned} &\sum_{g \in \mathcal{G}_k} q_{G_g} - q_{Dk} + b'_k \left|v_k\right|^2 \\ &\qquad = \sum_{\ell=(k,m) \in \mathcal{L}} q_{f\ell} + \sum_{\ell=(m,k) \in \mathcal{L}} q_{t\ell}, \quad \forall k \in \mathcal{N} \end{aligned} \tag{4.3}$$

$$\begin{aligned} &\frac{v_k}{t_\ell} \left[\left(j \frac{b'_\ell}{2} + y_\ell \right) \frac{v_k}{t_\ell} - y_\ell v_m \right]^* \\ &\qquad\qquad = p_{f\ell} + j q_{f\ell}, \quad \forall \ell = (k, m) \in \mathcal{L} \end{aligned} \tag{4.4}$$

$$\begin{aligned} &v_m \left[- y_\ell \frac{v_\ell}{t_\ell} + \left(j \frac{b_\ell}{2} + y_\ell \right) v_m \right]^* \\ &\qquad\qquad = p_{t\ell} + j q_{t\ell}, \quad \forall \ell = (k, m) \in \mathcal{L} \end{aligned} \tag{4.5}$$

$$\underline{p}_{G_g} \leq p_{G_g} \leq \overline{p}_{G_g}, \; \underline{q}_{Gg} \leq q_{G_g} \leq \overline{q}_{Gg}, \quad \forall g \in \mathcal{G} \tag{4.6}$$

$$|p_{f\ell} + jq_{f\ell}| \leq \bar{s}_\ell, \ |p_{t\ell} + jq_{t\ell}| \leq \bar{s}_\ell, \quad \forall \ell \in \mathcal{L} \tag{4.7}$$

$$\underline{v}_k \leq |v_k| \leq \overline{v}_k, \quad \forall k \in \mathcal{N} \tag{4.8}$$

$$\angle v_1 = 0 \tag{4.9}$$

The objective function (4.1) minimizes the total production cost, with c_{g2}, c_{g1} and c_{g0} denoting the coefficients for a quadratic cost function for all $g \in \mathcal{G}$. Constraints (4.2)–(4.3) represent the nodal power balance equations for active and reactive powers, respectively. Constraints (4.4)–(4.5) represent the active and reactive power flow equations in each branch. In addition to these physical laws, operational constraints (4.6)–(4.9) are required in AC power flows. Constraints (4.6)–(4.7) impose limits on generator active and reactive power outputs and line thermal limits, respectively. We assume that $\underline{v}_k > 0$ for all $k \in \mathcal{N}$ in (4.9). Constraint (4.10) specifies, without loss of generality, node $k = 1$ as the reference.

Constraints (4.4) and (4.5) are nonlinear and nonconvex; this makes problem (4.1)–(4.9) difficult to solve and, in fact, NP-hard [55]. Applying local methods to this problem provides no guarantees on the optimality of any solution found. Moreover, it is intractable to solve to global optimality for large-scale instances. Hence, techniques aiming at convexifying and reducing the dimensions of this problem are part of one's arsenal in the hope of efficiently finding a good local optimal solution to this problem.

4.3 Line Flow Constraint Screening

4.3.1 Existing Optimization-based Screening Approaches

This chapter proposes a screening method for line thermal limits adapted to the AC-OPF problem. The method uses optimizations to determine each line's minimum and maximum power flow values subject to all other constraints. If those flows are within the specified line flow limits, the limits are considered to be redundant and can be eliminated. However, if the flows reach established limits, the constraint is non-redundant. The method first assesses the binding potential of constraints based on the other problem constraints without considering generation cost functions.

Here we formulate the OBBT problem. It involves the solution of two maximization and two minimization problems for each line flow constraint across a range of load fluctuations. The constraint screening problem objective (4.11) aims to minimize and to maximize active and reactive power flows while considering all the remaining constraints of the original OPF (4.2)–(4.10), including added load variability constraints (4.12)–(4.13). The optimization problem includes additional decision variables for every active load p_{D_k} and reactive load q_{D_k} for each $k \in \mathcal{N}$. We assume that the power losses are small in typical meshed transmission networks, which means $p_{f\ell} \approx -p_{t\ell}$, while a similar assumption applies to reactive power flows. Hence, we consider only one line end (*to*) for the optimization problems in (4.11). The parameter λ specifies load uncertainty ranges, and $p^{\circ}_{D_k}$ and $q^{\circ}_{D_k}$ refer respectively to nominal nodal active and reactive power loadings.

$$\min_{\boldsymbol{v},\boldsymbol{t},\boldsymbol{p}_G,\boldsymbol{q}_G,\boldsymbol{p}_D,\boldsymbol{q}_D} / \max_{\boldsymbol{v},\boldsymbol{t},\boldsymbol{p}_G,\boldsymbol{q}_G,\boldsymbol{p}_D,\boldsymbol{q}_D} p_{t\ell}/q_{t\ell} \tag{4.10}$$

subject to:

$$\text{Constraints} \quad (4.2) - (4.9) \tag{4.11}$$

$$(1-\lambda)p^{o}_{D_k} \leq p_{D_k} \leq (1+\lambda)p^{o}_{D_k}, \quad \forall k \in \mathcal{N} \tag{4.12}$$

$$(1-\lambda)q^{o}_{D_k} \leq q_{D_k} \leq (1+\lambda)q^{o}_{D_k}, \quad \forall k \in \mathcal{N} \tag{4.13}$$

When the optimal solution of (4.10)–(4.13) (whether one is maximizing or minimizing and is optimizing either one of $p_{t\ell}$ or $q_{t\ell}$) is such that $|p^{\star}_{t\ell} + jq^{\star}_{t\ell}| = \bar{s}_{\ell}$, it indicates that the flow limit for line ℓ is non-redundant. On the other hand, if flows are strictly within their allowable range, the corresponding bounds are redundant and could be ignored when solving (4.1)–(4.10). We will refer to this formulation as the benchmark approach (BA).

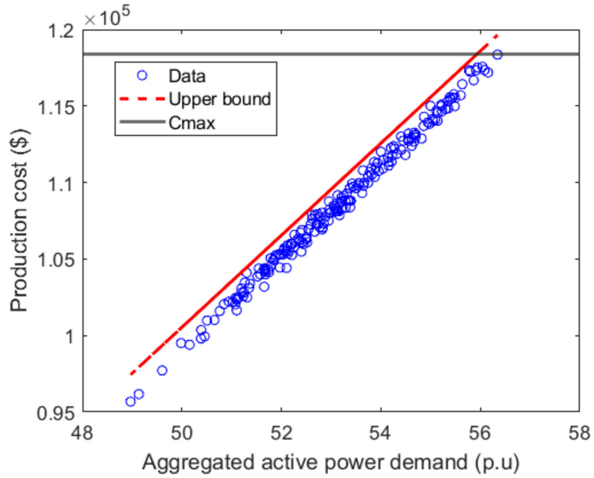

Figure 4.1: Observed production cost against system net load.

4.3.2 Cost-Driven Constraint Screening

To further the power of OBBT in screening line flow constraints, we propose to add an extra valid inequality whose role is to capture the effect of the original problem's objective function (4.1) as part of constraint screening. For this, we add the constraint

$$\sum_{g \in \mathcal{G}} c_{g2} p_{Gg}^2 + c_{g1} p_{Gg} + c_{g0} \leq \bar{C} \tag{4.14}$$

to (4.10)–(4.13). This constraint, by putting an upper bound on the operational cost, ends up identifying line flow constraints which are not only non-redundant but also potentially binding in the original problem. This is the case because (4.14) limits the allowable power generation in a way similar the objective function (4.1) is attempting to minimize cost. We note here that the right-hand side of (4.14) $\bar{C}$ is a function of the forecasted net load in the power system, and it reflects expected system-level operating costs for the given net load forecast. Also, $\bar{C}$ would be set slightly higher than historically-observed system costs for similar loading levels to lower the risk of infeasibility of OBBT.

Fig. 4.1 provides an illustration of the total operating cost as a function of the aggregated active power demand for 200 prior problem instances of (4.1)–(4.9), with $C^{\max}$ being the highest observed cost. It is not surprising that various allocations of demand among network buses may result in different operating costs, even if the aggregated net demand values are similar. In fact, one could argue that setting $\overline{C} = C^{\max}$ is a possible option; however, it is all but too conservative. In fact, for low net demand values, the actual operating cost would be much lower than this upper bound. This implies that the constraint-screening capability with (4.14) would not be superior to that of (4.10)–(4.13) in such a scenario. Therefore, to maximize the benefits of the valid inequality, we make $C^{\max}$ dependent on the active power demand. By doing this, it is possible to obtain tighter upper bounds for all net demand levels, which would enable a larger number of line capacity constraints to be screened out.

Next, we will explain the reasons behind our modeling choice for estimating the function $\overline{C}(\boldsymbol{p}_D)$, where $\boldsymbol{p}_D$ is the active power demand vector. To minimize the complexity of the model and the possibility of over-fitting, we opt to make the upper-bound $\overline{C}$ dependent on the aggregated active power demand only $D = \sum_{k\in\mathcal{N}} p_{D_k}$, instead of utilizing all nodal active power demands as explanatory variables. Furthermore, to ensure that problems (4.10)–(4.13) remain manageable and computationally tractable, we choose to approximate the relationship between the upper-bound $C^{\max}$ and the aggregated net demand D using a linear function [108]. The upper bound for an aggregate net demand D can be thus computed as:

$$\overline{C}(D) = (1 + \Delta\sigma)a_0 + (1 + \Gamma)b_0 D \tag{4.15}$$

where a_0 and b_0 are the intercept and slope of the linear function. Obviously, here there is some tuning to be carried out in determining the parameters a_0 and b_0 of the proposed cost upper bound, while $\Delta\sigma$ and Γ are user-specified conservativeness parameters as defined previously in chapter 2.

Hence, we cast the cost-driven optimization-based screening as follows:

$$\min / \max\, p_{t\ell}/q_{t\ell} \tag{4.16}$$

subject to:

$$\text{Constraints } (4.2) - (4.9), (4.12) - (4.13) \tag{4.17}$$

$$\sum_{g \in \mathcal{G}} c_{g2} p_{Gg}^2 + c_{g1} p_{Gg} + c_{g0} \leq (1 + \Delta\sigma) a_0 + (1 + \Gamma) b_0 D \tag{4.18}$$

$$D = \sum_{k \in \mathcal{N}} p_{D_k} \tag{4.19}$$

$$D^{\min} \leq D \leq D^{\max} \tag{4.20}$$

The minimum and maximum aggregate net demand is denoted by $D^{\min}$ and $D^{\max}$, respectively. We will refer to this approach as cost-driven (CD) optimization-based bound tightening constraint screening. We also introduce a different version of the cost-driven approach where the cost upper bound —i.e. the right-hand side of constraint (4.14)— is modeled as $\overline{C}(D) = C^{\max}$. In this case, the cost upper bound limit represents the maximum observed cost and is not a function of aggregate net demand. We refer to this this approach as the naive cost-driven (NCD) approach.

4.4 AC-OPF Convex Relaxations

As argued in the introduction, globally solving problem (4.1)–(4.9) is challenging, as the AC-OPF problem is NP-hard. Convex relaxations of the AC-OPF problem have garnered substantial attention in recent years. Convex relaxation extends the nonconvex AC-OPF feasible space to become convex by adding infeasible points while including all the feasible points of the original AC-OPF. Actually, utilizing convex relaxation to solve AC-OPF presents numerous advantages. Firstly, they have the potential to achieve global optimality. Secondly, being relaxations, they offer a bound on the global optimal value of the AC-OPF problem. Thirdly, if any of these relaxations proves infeasible, it indicates that the original AC-OPF problem is also infeasible. Integrating these features with powerful convex optimization tools used in industry, like Gurobi [150] and Mosek [151], opens new venues to develop new efficient approaches and algorithms for the AC-OPF problem.

For the constraint screening approach, we use convex relaxations to bound its possible (if feasible) global solution. If the limit of the relaxed bound falls within the set limits of the constrained quantity, then we can be certain that a constraint under study through OBBT is redundant. We will compare the performance of four state-of-the-art convex relaxations namely, the QCR relaxation [118], the SDR relaxation [146], the SOCR relaxation [147], and the tight-and-cheap relaxation (TCR) [149]. In the optimization-based screening approach, we substitute the original AC-OPF set of constraints in (4.11) with each convex relaxation. The interested reader is invited to consult [118, 146, 147, 149] for detailed descriptions of each of those formulations.

4.4.1 Semidefinite Relaxation (SDR)

Assuming $V = vv^H$, the AC-OPF problem (4.1)–(4.9) can be reformulated as follows:

$$\min \sum_{g\in\mathcal{G}} c_{g2} p_{Gg}^2 + c_{g1} p_{Gg} + c_{g0} \tag{4.21}$$

subject to:

$$\text{Constraints } (4.6), (4.7), (4.9) \tag{4.22}$$

$$\begin{aligned} &\sum_{g\in\mathcal{G}_k} p_{Gg} - p_{Dk} - g'_k V_{kk} \\ &= \sum_{\ell=(k,m)\in\mathcal{L}} p_{f\ell} + \sum_{\ell=(m,k)\in\mathcal{L}} p_{t\ell}, \quad k \in \mathcal{N} \end{aligned} \tag{4.23}$$

$$\begin{aligned} &\sum_{g\in\mathcal{G}_k} q_{Gg} - q_{Dk} + b'_k V_{kk} \\ &= \sum_{\ell=(k,m)\in\mathcal{L}} q_{f\ell} + \sum_{\ell=(m,k)\in\mathcal{L}} q_{t\ell}, \quad k \in \mathcal{N} \end{aligned} \tag{4.24}$$

$$\begin{aligned} &\frac{1}{|t_\ell|^2}\left(-j\frac{b'_\ell}{2} + y_\ell^*\right) V_{kk} - \frac{y_\ell^*}{t_\ell} V_{km} \\ &= p_{f\ell} + jq_{f\ell}, \quad \ell = (k,m) \in \mathcal{L} \end{aligned} \tag{4.25}$$

$$
\begin{aligned}
& -\frac{y_\ell^*}{t_\ell^*} V_{mk} + \left(-j\frac{b_\ell'}{2} + y_\ell^*\right) V_{mm} \\
& = p_{t\ell} + jq_{t\ell}, \quad \ell = (k,m) \in \mathcal{L}
\end{aligned}
\tag{4.26}
$$

$$
\underline{v}_k^2 \leq V_{kk} \leq \overline{v}_k^2, \qquad k \in \mathcal{N} \tag{4.27}
$$

$$
|\mathrm{Im}\,(V_{km})| \leq \mathrm{Re}\,(V_{km}) \tan \bar{\delta}_\ell, \qquad \ell = (k,m) \in \mathcal{L}, \tag{4.28}
$$

$$
V = vv^H \tag{4.29}
$$

We denote the phase angle difference as $|\angle v_k - \angle v_m| \leq \bar{\delta}_\ell, \forall \ell = (k,m) \in \mathcal{L}$ such that $0 < \bar{\delta}_\ell < \pi/2$ for all $\ell \in \mathcal{L}$. Therefore, we added the constraint (4.28) to the formulation. The nonconvexity of problem (4.21)–(4.29) is seen with the constraint (4.29). It can be shown that $V = vv^H$ if and only if $V \succeq 0$[1] and $\mathrm{rank}(V) = 1$. However, standard semidefinite relaxation is derived by eliminating the rank constraint which is non-convex [146].

4.4.2 Second-order Cone Relaxation (SOCR)

Different relaxations have been derived by manipulating the nonconvex constraint (4.29) in different ways. For instance, the second-order cone relaxation (SOCR) [152] has been derived by relaxing $V \succeq 0$ in SDR by $|\mathcal{L}|$ constraints in the matrix as follow:

$$
V_{\{k,m\}} = \begin{bmatrix} V_{kk} & V_{km} \\ V_{km}^* & V_{mm} \end{bmatrix} \succeq 0, \forall (k,m) \in \mathcal{L} \tag{4.30}
$$

Hence, constraint (4.29) in SDR will be replaced by (4.30) which leads to a new formulation called SOCR.

4.4.3 Tight-and-Cheap Relaxation (TCR)

Inspired by the SDR formulation, and to enhance the computational complexity of SDR for large-scale power systems, the authors of [149] derived a computational cheaper reformulation

[1] The symbol $\succeq$ means *positive semidefinite*.

of the semidefinite relaxation. The constraint (4.30) has been replaced using the following constraint

$$\begin{bmatrix} 1 & v_k^* & v_m^* \\ v_k & V_{kk} & V_{km} \\ v_m & V_{km}^* & V_{mm} \end{bmatrix} \succeq 0, \forall \ell = (k,m) \in \mathcal{L} \tag{4.31}$$

combined with the reformulation-linearization technique for the reference bus

$$\mathrm{Re}\,(v_1) \geq \frac{V_{11} + \underline{v}_1 \bar{v}_1}{\underline{v}_1 + \bar{v}_1}, \quad \mathrm{Im}\,(v_1) = 0 \tag{4.32}$$

Hence, constraint (4.29) in SDR formulation has been replaced by combining (4.31) and (4.32) which leads to TCR formulation.

4.4.4 Quadratic Convex Relaxation (QCR)

Finally, an alternative convex relaxation with similar benefits as that of the TCR is the quadratic convex relaxation (QCR). We note also that the QCR can serve as an intriguing substitute for the SDR because it is computationally cheaper. The previous relaxations preserved the relation between V and v in constraint (4.29) in a rectangular form. The polar coordinates of voltage variable v in constraint (4.29) is given by $\mathrm{v}_k = |v_k|$ and $\theta_k = \angle v_k$ for all $k \in \mathcal{N}$. Hence, the connection between polar voltage variables v, θ and the voltage V can be given by [153]:

$$V_{kk} = \mathrm{v}_k^2 \qquad \forall k \in \mathcal{N}, \tag{4.33}$$

$$\mathrm{Re}\,(V_{km}) = \mathrm{v}_k \mathrm{v}_m \cos\left(\theta_k - \theta_m\right) \qquad \forall \ell = (k,m) \in \mathcal{L}, \tag{4.34}$$

$$\mathrm{Im}\,(V_{km}) = \mathrm{v}_k \mathrm{v}_m \sin\left(\theta_k - \theta_m\right) \qquad \forall \ell = (k,m) \in \mathcal{L}, \tag{4.35}$$

Next, we introduce auxiliary variables as suggested in [148]: $w_\ell = \mathrm{v}_k \mathrm{v}_m, \tilde{c}_\ell = \cos\left(\theta_k - \theta_m\right)$

and $\tilde{s}_\ell = \sin(\theta_k - \theta_m)$ for all $\ell = (k, m) \in \mathcal{L}$. The QCR model addresses the non-convexity of equations (4.33)–(4.35) by composing convex envelopes of these equations [120]. We introduce the preliminaries for deriving the convex relaxation of these non-convex equations in Appendix C, we use $\langle . \rangle$ notation to refer to it. The interested reader may refer to [120,154] for a detailed explanation of this relaxation. We introduce QCR by relaxing non-convex nonlinear equations (4.33)–(4.35) as done in [148]:

$$\mathrm{V}_{kk} = \left\langle \mathrm{v}_k^2 \right\rangle, \qquad \forall k \in \mathcal{N}, \tag{4.36}$$

$$\mathrm{Re}\left(\mathrm{V}_{km}\right) = \left\langle w_\ell \bar{c}_\ell \right\rangle, \qquad \forall \ell = (k, m) \in \mathcal{L}, \tag{4.37}$$

$$\mathrm{Im}\left(\mathrm{V}_{km}\right) = \left\langle w_\ell \bar{s}_\ell \right\rangle, \qquad \forall \ell = (k, m) \in \mathcal{L}, \tag{4.38}$$

$$w_\ell = \left\langle \mathrm{v}_k \mathrm{v}_m \right\rangle, \qquad \forall \ell = (k, m) \in \mathcal{L}, \tag{4.39}$$

$$\bar{c}_\ell = \left\langle \cos\left(\theta_k - \theta_m\right) \right\rangle, \qquad \forall \ell = (k, m) \in \mathcal{L}, \tag{4.40}$$

$$\bar{s}_\ell = \left\langle \sin\left(\theta_k - \theta_m\right) \right\rangle, \qquad \forall \ell = (k, m) \in \mathcal{L}, \tag{4.41}$$

$$\theta_1 = 0 \tag{4.42}$$

The QCR relaxation will add the set of constraints (4.36)–(4.42) and (4.30) to the SDR formulation in subsection 4.4.1 to construct the QCR formulation.

4.5 Case Studies

4.5.1 Computational Setup

This section demonstrates the methods described in section 4.3 and section 4.4 for various PGLib-OPF test cases [138]. The implementation of all convex relaxations were based on the CONICOPF package in [148]. We solved all the relaxations in MATLAB using CVX 2.2 with the solver MOSEK 9.1.9 and its default precision and parameters. All the computations were carried out on an Intel(R) Core(TM) i7-11700K CPU @ 3.60 GHz and 64 GB of RAM.

4.5.2 Results: Fixed Load

We consider the first scenario in which the active and reactive powers in (4.12) and (4.13) are unique. Specifically, the elements in $\boldsymbol{p}_D$ and $\boldsymbol{q}_D$ are given by the dataset [138] (which is assumed to be known). In this case, we will only be able to assess the benchmark and NCD approaches.

Also, the original AC-OPF problem was solved using the MATPOWER-solver MIPS 7.0 to calculate the historical cost upper bound $\bar{C}$. Notice that when the demand is fixed, the CD approach becomes equivalent to the NCD approach. Moreover, to avoid an over-tight cost upper bound, which could lead to infeasibility of (4.11)–(4.14), we set a conservativeness factor to 2% [2] of the historical cost values, which we then applied as an additional component on top of the historical cost values to establish the upper bound C^{max}. In all cases here, we consider load variability of $\lambda = 0$ around the nominal load values. All tap changers $\boldsymbol{t}$ are set to their nominal levels and are not optimized.

The results in Table 4.1 summarize how the proposed constraint screening approach works *with* (WB) and *without* (WTB) the addition of the cost upper bound (4.14) for the four convex relaxations under consideration.

Firstly, all convex relaxations show a considerable enhanced constraint screening performance with cost-driven tightening in comparison to the approach without cost-driven tightening. Secondly, the SDR reveals the highest constraint screening ability with an average of 83% and 77% superfluous constraint elimination with and without bound tightening, respectively. This outcome complies with the fact that the SDR is the tightest relaxation among those tested. Screening results for all other relaxations are compared to those obtained with the SDR. SOCR is the weakest relaxation among the others considering the screening approaches. TCR dominates QCR in five out of seven instances for WB, while for WTB, TCR outperforms QCR in four out of seven instances. In fact, TCR has achieved an optimum enhancement in terms of redundancy removal considering the WB approach in comparison to the WTB approach by an average of 40%.

[2] For cases 'case5_pjm' and 'case118_ieee', the conservativeness factor is set to 10% and 5%, respectively.

Table 4.1: Proportion (%) of Redundant Line Flow Constraints Identified for Different Convex Relaxations – Fixed Load

Method	SDR	TCR (%)	QCR (%)	SOCR (%)	SDR	TCR (%)	QCR (%)	SOCR (%)	SDR	TCR	QCR	SOCR
Test case	Without Bound Tightening (WTB)				With Bound Tightening (WB)				(WB-WTB)/WTB (%)			
case5_pjm	50	16 (−67%)	0 (−100%)	0 (−100%)	50	33 (−33%)	0 (−100%)	0 (−100%)	0	100	0	0
case14_ieee	100	100 (−0%)	95 (−5%)	75 (−25%)	100	100 (−0%)	95 (−5%)	90 (−10%)	0	0	0	20
case24_ rts	90	66 (−27%)	68 (−24%)	21 (−77%)	95	95 (−0%)	87 (−8%)	45 (−53%)	6	44	27	113
case39_epri	74	48 (−35%)	41 (−44%)	30 (−59)	91	61 (33%)	41 (55%)	35 (−62)	24	27	0	14
case57_ieee	99	95 (−4%)	86 (−13%)	69 (−35%)	100	98 (−3%)	91 (−9%)	83 (−18%)	1	3	6	20
case73_ieee_rts	75	33 (−56%)	56 (−26%)	18 (−77%)	92	67 (−27%)	69 (−25%)	28 (−70%)	22	100	24	57
case118_ieee	52	19 (−64%)	23 (−55%)	13 (−57%)	56	20 (−63%)	26 (−54%)	13 (−77%)	8	9	12	0
Average	**77**	**54** (−**36**%)	**53** (−**38**%)	**32** (−**63**%)	**83**	**68** (−**23**%)	**59** (−**36**%)	**42**(−**56**%)	−**9**	−**40**	−**10**	−**32**

4.5.3 Results: Variable Load

We will now explore a different scenario where the net demand elements $\boldsymbol{p}_D$ and $\boldsymbol{q}_D$ are not limited to a single element. The goal here is to examine the cost-driven OBBT capabilities in the case of demand variation. For active load p_{D_k} and reactive load q_{D_k} for each $k \in \mathcal{N}$, we consider a uniform demand variation between the nominal base case values in [138] to 80% of their nominal values. This means that positive active and reactive demands vary within 80% and 100% of their nominal value. For characterizing the cost-driven constraint (4.18) in subsection 4.3.2, we generate a synthetic random loading factor vector in the range [0.8, 1.0], consisting of 48 sorted elements. The loading factor is multiplied by the net load $p_{D_k} + jq_{D_k}$ for each $k \in \mathcal{N}$ to simulate 48 time instances for the AC-OPF problem. For the production cost upper bound setting, we set $\Delta = 3.3$ and $\Gamma = 0$ for all test networks. For testing the computational enhancement of the reduced AC-OPF, we test on 24 time instances generated using the same approach used for determining cost-driven constraint. All these models were implemented using a single-period AC-OPF problem with no inter-temporal constraints.

We will compare three optimization-based screening approaches: BA, NCD, and CD, under three convex relaxations. These results have been recorded in Table 4.2 for different PGLib-OPF test cases. We discard the SOCR from the comparison as a result of poor performance in Table 4.1. From Table 4.2, the NCD approach with SDR and QCR has achieved a negligible enhancement in terms of superfluous constraint elimination with respect to the BA approach with an average of 2% and 3%, respectively. While the TCR increases the percentage of redundant constraint elimination approximately by an average of 16% across all test cases with respect to BA approach under the NCD approach. Moreover, across all convex relaxations, the CD approach demonstrates notably improved constraint screening performance compared to the other two approaches. The TCR under the CD approach results in a 92% increase in the percentage of superfluous constraint elimination compared to the BA approach under the same relaxation. While SDR and QCR under the CD approach increase the percentage of the superfluous constraint elimination by 44% and 54%, respectively with respect to their BA approaches. The outcomes of this comparison across standard test cases

Table 4.2: Percentage of Redundant Line Flow Constraints Identified From Each Convex Relaxation – Variable Load

Method	SDR	TCR	QCR	SDR	TCR	QCR	SDR	TCR	QCR
Test case	BA approach			NCD			CD		
case5_pjm	50	0	0	50	33	0	83	83	50
case24_rts	79	55	58	82	55	58	82	61	58
case30	59	46	29	59	46	34	93	90	34
case30_as	10	5	2	12	5	2	56	49	22
case57_ieee	95	85	81	95	85	81	99	98	88
case118_ieee	46	14	18	46	14	18	83	77	46
Average (change %)	**56**	**34**	**31**	**57** (2%)	**40** (16%)	**32** (3%)	**83** (44%)	**76** (92%)	**50** (54%)

indicate that the SDR relaxation offers a tighter relaxation, allowing for the exclusion of a significantly larger number of constraints.

Furthermore, Fig. 4.2 shows the percentage of change in a few case studies which drives this improvement in constraint screening capabilities considering both NCD and CD approaches with respect to the BA approach. In the case of case30_as network, the CD approach significantly increases the superfluous constraints by approximately 480% when compared to the BA approach using SDR relaxation. While for the same network, TCR and QCR approaches achieve an increase in the constraint redundancy removal percentage by 800% and 900% compared to their BA approches, respectively. Also, for the 118_IEEE test system, TCR, QCR, and SDR combined with CD approach increase the constraint elimination by 450%, 160%, and 80%, respectively. In contrast, the conservative cost-driven optimization-based screening demonstrates either no discernible difference or only minor enhancement concerning redundant constraint removal when compared to the BA approach. Finally, we used 24 testing time instances to check whether the reduced AC-OPF problem for each convex relaxation produces the same solution as the original relaxation or not. All the testing instances for the three convex relaxations verify that the cost-driven constraint screening does not affect the optimality gap [3] resulting from the full

[3] optimality gap is calculated as the percentage difference between the lower bound obtained from a convex relaxation and the upper bound provided by MIPS

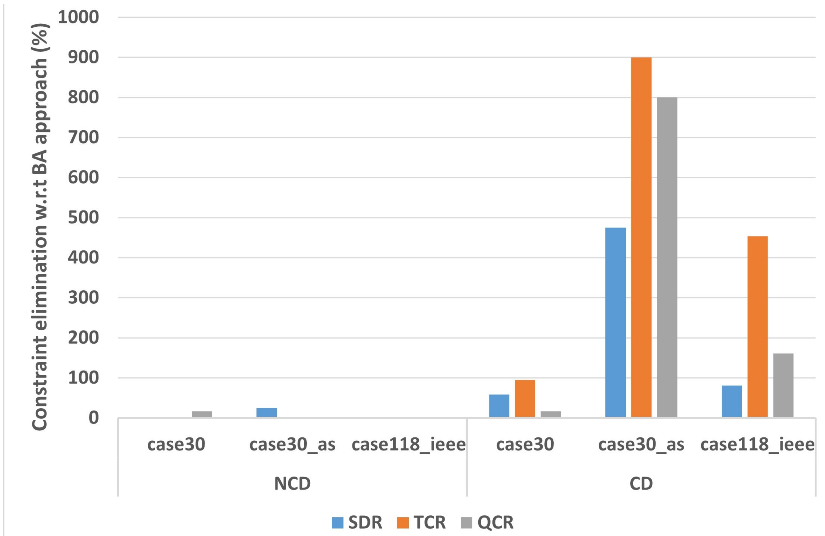

Figure 4.2: Percentage change of redundant constraints in NCD and CD approaches compared to BA approach.

convex relaxation solution while it considerably enhancing the computation time.

4.5.4 Computational Advantage of Constraint Screening for AC-OPF

Eliminating unnecessary constraints decreases the size of optimization problems. In this context, we explore the computational benefits of employing the cost-driven constraint screening approach outlined in subsection 4.5.2 for solving reduced AC-OPF problems. We will assess the solution time of the simplified AC-OPF problem, obtained by removing unnecessary constraints, in comparison to the full AC-OPF problem for each convex relaxation. Here, we will examine the computation complexity for the case of fixed load in subsection 4.5.2. We apply the outcomes derived from the bound tightening scenario in Table 4.1 to solve a reduced AC-OPF problem for a single-demand instance. Additionally, we solve the full AC-OPF under the same convex relaxation. Fig. 4.3 shows the percentage difference in CPU time needed to solve the simplified AC-OPF in comparison to the full

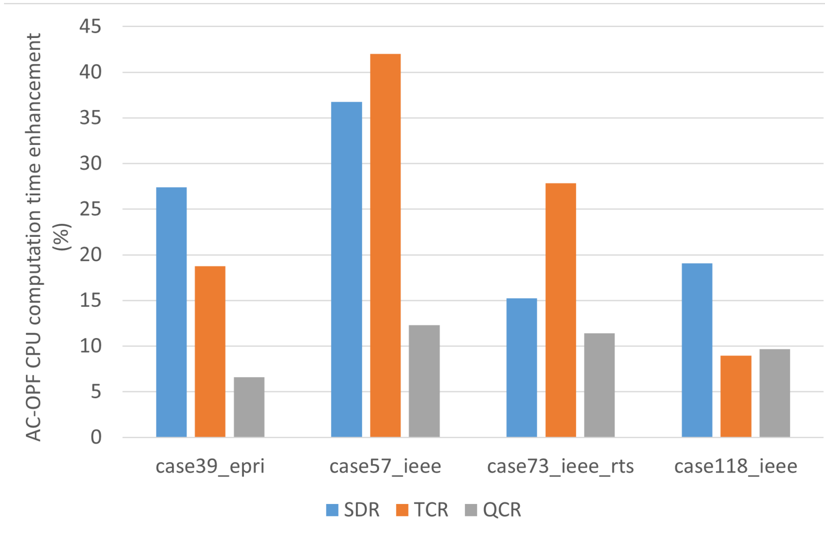

Figure 4.3: Computation advantage of reduced AC-OPF with respect to full ACOPF – Fixed Load

AC-OPF problem under each convex relaxation. We observe that QCR relaxation reveals the lowest computation time enhancement with respect to full AC-OPF. The computation savings for QCR compute time is less than 12% for all test instances reported in Fig. 4.3. Conversely, the SDR and the TCR show a considerable time reduction in AC-OPF compute time. The reduced AC-OPF with the SDR illustrates a decrease in the solution time ranging from 19% to 36% across the test networks. Furthermore, the TCR with constraint elimination demonstrates a reduction in the solution time ranging from 9% and 41%.

4.5.5 Computational Complexity of Screening for AC-OPF

OBBT—with and without a cost upper bound—entails having to run two minimizations and two maximizations for each branch in a sequential manner for transmission line constraint screening. The total CPU screening time across the three different approaches, namely the benchmark approach, the naive cost-driven approach, and the cost-driven approach

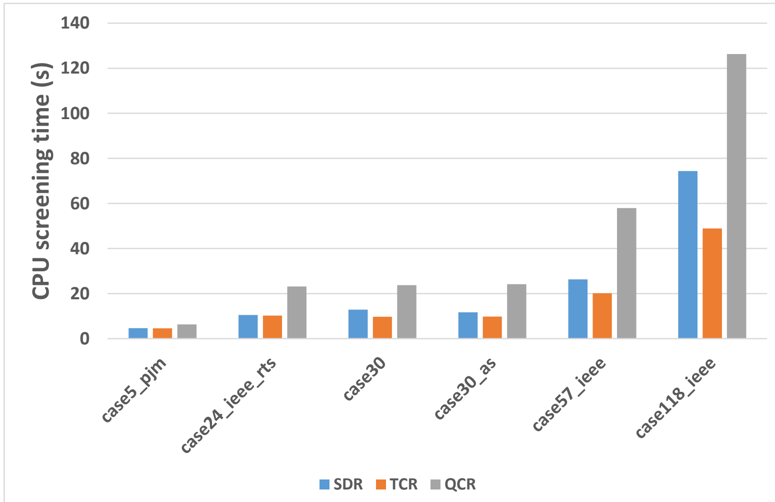

Figure 4.4: Screening time under CD approach.

is relatively the same for the test cases under the study for the variable load scenario. Therefore, we will analyze the screening time considering the cost-driven OBBT approach i.e. CD approach. It is clearly shown from Fig. 4.4 that among the three convex relaxations considered, the screening time is proportional to the size of the network. Also, the QCR revealed the highest screening computational cost. TCR's computational time is slightly faster than SDR for small-size test systems, but it is considerably faster than SDR for larger systems.

Overall, the cost-driven constraint screening approach has augmented the economical aspect of the objective function into the conventional OBBT. The computational effort for cost-driven OBBT is similar to the conventional one. The cost-driven OBBT constraint screening does not jeopardize the lower-bound solution revealed by the original convex relaxation. The outcomes of this evaluation across standard test cases indicate that the SDR relaxation proves to be the tighter relaxation as it allows for the exclusion of a significantly larger number of constraints. The encouraging reduction in computational time achieved through the screening of line constraints can be expanded to encompass the screening of other constraints as well. More specifically, voltage constraints represent cumbersome for the solver as they are more dense constraints compared to line constraints. Besides eliminating the constraints only, variables can also be removed if they are associated with redundant or inactive constraints and are not part of the objective function.

4.6 Summary

We have extended the cost upper bound proposal from Chapter 2 to constraint screening of convex relaxations of the AC-OPF. Cost-driven constraints clearly enhanced the screening capabilities of the standard optimization-based bound tightening (OBBT) method and provides a future venue to embodied critical information from non-convex AC-OPF into convex relaxations. Using PGLib-OPF test cases with up to 118 buses, we show that on average, SDR dominates other relaxations. Furthermore, for the test cases with and without bound tightening, TCR is stronger than QCR. Results show that cost-driven constraint-reduced AC-OPF convex relaxations obtain better solution time performance than the original unscreened relaxations.

Chapter 5

Flexibility Characterization in the Demand Space: A Data-Driven Inverse Optimization Approach

Chapters 2 and 3 presented and validated different approaches for managing the flexibility of conventional generators to meet net loads using the unit commitment. This chapter presents a framework for quantifying and characterizing the existing system flexibility for given unit commitment solutions and network topologies under uncertain net load. In this chapter, we propose a novel data-driven inverse optimization framework for flexibility characterization of power systems in the demand space along with its geometric intuition. The approach captures the spatial correlation of multi-site renewable generation and load using polyhedral uncertainty sets. Moreover, the framework projects the uncertainty on the feasibility region of power systems in the demand space, which are also called *loadability sets*. By using inverse optimization, we succeed in inferring system flexibility adequacy or lack thereof.

5.1 Introduction

The shares of renewable energy resources (RES) have increased significantly in the last decade and will grow at even faster paces as economies decarbonize and electrify. This large-scale, uncertain, and volatile renewable generation creates many challenges to power system operations. Power system flexibility is defined as the system's ability to accommodate any component outage or variation in its net load (*i.e.*, demand less non-dispatchable generation) to keep the system secure [2]. The increasing integration of renewable energy sources into large-scale power systems necessitates adequate flexible resources to address the real-time imbalances between generation and demand. Diverse flexibility resources, such as conventional controllable power plants, energy storage, and demand response, can effectively address the requirements for flexibility.

In general, quantifying power system flexibility for bulk power system operation with renewable energy sources can be classified into two main categories [51]. The first category focuses on the robust generation scheduling problem, aiming to handle the pre-specified uncertainty as previously addressed in chapter 2. The second category addresses a different problem: assessing the extent to which available resources can manage net load uncertainty. This involves evaluating the system's flexibility under the given operating conditions. In this chapter, our focus will be on assessing flexibility from the perspective of the second category.

Explicit flexibility assessment is characterized mainly through the use of region-based geometrical approaches. A pioneering study proposed the concept of *do-not-exceed (DNE) limits* to define the maximum variations of uncertain parameters a system can accommodate using robust optimization [155]. These limits leverage unambiguously the utilization of renewable resources while treating uncertainty sets as a decision variable. Further enhancements of the DNE dispatch method has been proposed considering corrective topology control actions [156], and using historical data of wind power realizations [157]. Along similar lines, the dispatchable region concept was introduced to characterize flexibility regions explicitly. The authors of [158] characterized the dispatchable region of wind generation and revealed its geometry to be a polytope in uncertainty space. This concept was generalized in [159] to include a full ac network model. Another form of dispatchable region was optimized using energy and reserve scheduling based on an affine redispatch policy [160]. The flexibility set determination approach proposed in [161] infers a polytope describing the allowed deviations from current system state in generation and tie lines spaces. Likewise, reference [162] estimated the size of a power system's feasible region in generation space under different levels of uncertainties.

Similar research directions have expanded to quantify flexibility using various metrics. Zhao *et al.* [163] suggested a flexibility measure based on a system's DNE region. They defined a binary flexibility metric to check if the largest variation of uncertainty is within the admissible range or not. Another flexibility framework has quantified insufficient flexibility by power imbalance event magnitude and frequency [164]. There is a family of publications [52, 165–167] that investigated wind generation admissibility assessment using two-stage robust optimization. In these publications, wind accommodation capabilities under a given solution UC strategy is assessed using expected load shedding and wind curtailment.

However, most of the previous work was built on budget-constrained polyhedral uncertainty sets and neglected spatial and temporal trends in historical data [52, 165, 166]. Another drawback of budget-constrained uncertainty modeling is the combinatorial growth of vertices needed to represent the uncertainty set with respect to the uncertain parameters [48]. A more accurate way of modeling uncertainty is to calculate the convex hull of spatial and temporal scenarios for wind generation admissibility assessment [167]. The empirical study in [114] does not recommend the use of the convex hull for wind and photovoltaics in dimensions higher than four—a number too small for practical applications—because of inherent computational costs.

From a broader perspective, the majority of region-based flexibility assessment methods have assessed and visualised dispatchable regions in either generation or uncertainty spaces considering system operational constraints regardless of the uncertainty impacts of the RES output [158, 159, 168]. Moreover, when the dimensionality of the uncertainty grows, these regions cannot be easily visualized. This chapter's proposal attempts to fill this research gap by developing a comprehensive flexibility assessment framework under deep penetration of renewables, leveraging the advantages of region-based approaches and metric-based methods. In this context, the proposed method is considered a complement to energy and reserve scheduling problems [48, 50], and belongs to the latter type of flexibility assessments such as [51]. The framework relies on a given unit commitment strategy, and consequently assesses the impact of the uncertainty of RES outputs at a given operating condition.

Compared to previous work, our proposal has the following features. First, it extends the notion of RES accommodation assessment proposed in [155, 158, 165], which maps feasibility regions from the generation-demand space to the demand space only using the loadability set approach [125, 128, 169]. Second, it captures the spatial correlation of multiple renewable generation sites and loads using data-driven polyhedral uncertainty sets. In addition, a novel data-driven inverse optimization problem formulation is proposed to identify existing system flexibility for uncertainty mitigation by exploring the feasibility region of a linear programming (LP)-relaxation i.e loadability set. Finally, this assessment is meant to be quantitatively indicative of how much "room" exists in the bulk power system to handle net load uncertainty for given unit commitment solutions and network topologies. In cases where flexibility is found to be inadequate, the inverse optimization problem is able to quantify the "shortest distance" to flexibility adequacy.

The main benefit of our work proposed in this chapter is summarized as follows.

1. We revisit the loadability set characterization and implicitly incorporate the data-driven uncertainty set to redefine the loadability set.

2. We propose a unified framework to characterize power system flexibility explicitly and geometrically in the demand space using a data-driven inverse optimization technique (DDIO).

3. We present a solution methodology for DDIO which considers uncertainty sets which may or may not intersect its feasibility region along with its geometric intuition.

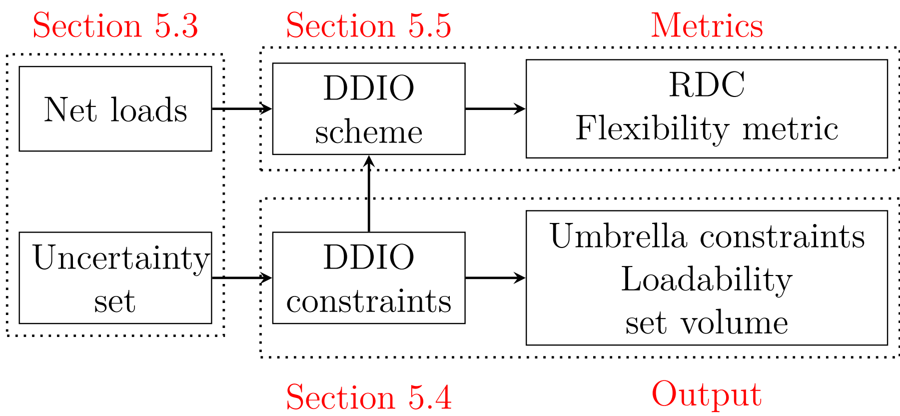

Figure 5.1: Overview of the method proposed in this chapter

4. We propose a framework that has the ability to assess *both* excessive and inadequate system flexibility by assessing how far operating points are from their feasibility region boundaries.

An overview of our proposed method in this chapter is shown in Fig. 5.1.

5.2 Data-Driven Nodal Net Load Uncertainty Set

In this chapter, we will use the previously developed uncertainty set DPUS $P_2(S, K)$ as described in subsection 2.3.1 in chapter 2. For brevity, we will refer to DPUS $P_2(S, K)$ as PUS in this chapter. Without reinventing the wheel here, assuming that the number of historical forecast error data points is large and reflects a good sample of a diversity of operating conditions, we argue that $PUS(\mathcal{S}, K)$ is time invariant. Therefore, we posit that PUS shifted by a vector of nodal net load forecasts looking into the future (*i.e.*, not historical, like μ in chapter 2) d^0 is an adequate representation of possible future net load

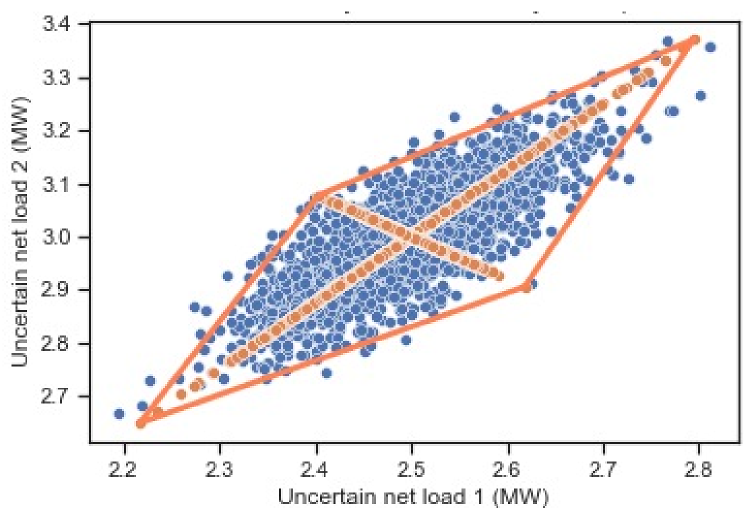

Figure 5.2: Two-dimensional polyhedral uncertainty set.

and its uncertainty. Otherwise said, we define the forward-looking net load PUS as

$$P(\mathcal{S}, K) = \left\{ \mathbf{E} \in \mathbb{R}^N \mid \mathbf{E} = d^0 + \sum_{k=1}^{K} \left(\omega_k^+ \mathcal{S}_k^+ + \omega_k^- \mathcal{S}_k^- \right), \right. \\ \sum_{k=1}^{K} \left(\omega_k^+ + \omega_k^- \right) = 1, \\ \left. 0 \leq \omega_k^+ \leq 1,\ 0 \leq \omega_k^- \leq 1, \forall k \right\} \tag{5.1}$$

Fig. 5.2 illustrates the construction of PUS in a two-node power system. In this example, we see the original historical net load forecast error data, represented by blue dots, and the data projected onto two of its principal components (orange dots). By inspection, the rhombus-shaped envelope, whose principal axes correspond to the principal components of the data, encapsulates the vast majority of the original data. Moreover, the vertices of this rhombus correspond to the extrema of the data projection into the retained principle components as previously mentioned in chapter 2. Moreover, we notice here that $d^0 = \begin{bmatrix} 2.5 & 3.0 \end{bmatrix}^\top$ MW is the forecast net load at nodes 1 and 2, respectively.

Compared to the conventional convex hull encapsulation approach [48], the number of edges of the PUS depends on the chosen number of retained principal components K, which can be at most $2N$, Moreover, PUS can be represented using 2^K linear constraints.

In the context of this chapter, we sought to determine the smallest possible *loadability sets*. The reason why one would want to find the smallest loadability set is to be able to reliably test whether or not a net demand vector would be feasible in a given network-constrained generation scheduling or dispatch problem. If a loadability set is loose (like $P_1(\mathcal{S}, K)$ in comparison to $P_2(\mathcal{S}, K)$), there is a chance that some net demand vectors may be deemed feasible while, in fact, they are not.

5.3 Net load forecast errors Uncertainty Accommodation Assessment Framework

5.3.1 Introduction

The standard two-stage robust unit commitment with a single uncertainty set [48] determines in the first-stage the generators' commitment status, energy and reserve schedules. The second-stage finds the minimum cost redispatch solution given the worst uncertainty realization. This computationally-heavy approach goes against existing industry practice, where stress tests are applied *ex-post* as offline validation procedures [48].

Next, we present, starting from a first-stage unit commitment solution, how much uncertainty can be handled by a power system. For expository purposes, we use a relaxed linear optimization of the second-stage assuming first-stage variables are known, as it is usually the case in most RES admissibility assessment frameworks [52, 155, 158, 165, 166].

5.3.2 Problem Formulation

A net load admissibility framework evaluates quantitatively how much demand less non-dispatchable renewables can be accommodated by the bulk power system given a specific

UC solution without causing any operational infeasibility.

We formulate the following linear optimization problem, which optimizes net load admissibility as a function of the first-stage unit commitment solution, expressed by the collection of the tuples $\zeta_m = (u_m, g_m^0 + r_m^{\uparrow}, g_m^0 - r_m^{\downarrow})$ for each of the system's dispatchable generators $m \in \mathcal{M} = \{1, \dots, M\}$. Specifically, ζ_m contains: u_m its commitment status (on/off), g_m^0 its scheduled power output, and $r_m^{\uparrow}$ and $r_m^{\downarrow}$ respectively its scheduled up- and down-reserves.

$$f(\zeta_1, \dots, \zeta_M) = \min_{\hat{g}, q, \epsilon, d} \sum_{n=1}^{N} \gamma \, |\epsilon_n| \tag{5.2}$$

Subject to:

$$q_n + \epsilon_n = \hat{g}_n - d_n, \qquad \forall n \in \mathcal{N} \tag{5.3}$$

$$\sum_{n=1}^{N} q_n = 0 \tag{5.4}$$

$$\hat{g}_n \leq \sum_{m \in \mathcal{M}_n} \left(g_m^0 + r_m^{\uparrow} \right), \qquad \forall n \in \mathcal{N} \tag{5.5}$$

$$\hat{g}_n \geq \sum_{m \in \mathcal{M}_n} \left(g_m^0 - r_m^{\downarrow} \right), \qquad \forall n \in \mathcal{N} \tag{5.6}$$

$$\sum_{m \in \mathcal{M}_n} \left(g_m^0 - r_m^{\downarrow} \right) \geq \sum_{m \in \mathcal{M}_n} g_m^{\min} u_m, \qquad \forall n \in \mathcal{N} \tag{5.7}$$

$$\sum_{m \in \mathcal{M}_n} \left(g_m^0 + r_m^{\uparrow} \right) \leq \sum_{m \in \mathcal{M}_n} g_m^{\max} u_m, \qquad \forall n \in \mathcal{N} \tag{5.8}$$

$$-f_l^{\max} \leq \sum_{n=1}^{N} h_{ln} q_n \leq f_l^{\max}, \qquad \forall l \in \mathcal{L} \tag{5.9}$$

$$d_n^{\min} \leq d_n \leq d_n^{\max}, \qquad \forall n \in \mathcal{N} \tag{5.10}$$

The objective function (5.2) minimizes the "cost" of total power imbalance, which consists of renewable curtailment and load shedding, as captured by the slack variables ϵ_n and weighed by an imbalance price γ. Constraint (5.3) determines the net power injection at each bus, while constraint (5.4) guarantees power balance across the system. The dispatchable generation capacity limits, and up and down reserves limits are defined by constraints (5.5)–(5.8), respectively. Constraint (5.9) enforces flow limits on the transmission lines. Finally, net load vector limits are enforced using minimum and maximum limits, as denoted by $d_n^{\min}$ and $d_n^{\max}$, respectively. We will refer to this model as the benchmark approach (BA) for evaluating net load admissibility.

5.3.3 Limitations of the Benchmark Net Load Admissibility Assessment Approach

The BA calculates allowable generation reserve deployment variables bus-per-bus $\hat{g}_n = \sum_{m \in \mathcal{M}_n} g_m$, net power injections q_n, allowable net loads d_n and their possible curtailment ϵ_n, $\forall n \in \mathcal{N}$ based on the specified range of net loads set in (5.10).

The first drawback of the BA relates to the modeling of net load range limits (5.10), which is a simple box in N-dimensional space. This constraint may lead to sub-optimal or even incorrect admissibility assessments because it ignores the spatial correlation which may exist among net loads at different locations of a power system. Instead, we argue in favor of the use of a PUS, $d_n \in P_2(\mathcal{S}, K)$ as described in section 5.2 which captures those correlations.

Another shortcoming of the BA occurs when the N-dimensional box of net loads (5.10) is big enough that none of the inequality constraints (5.5)–(5.9) are active. In this case, the objective function of the BA equals zero, which means that the power system has sufficient reserve and transmission capacity to handle all allowable net load values. In these cases, one may argue that too much flexibility—in the form of reserves—was scheduled, which may be grossly uneconomical. On the other hand, there may also be cases where the margin offered by scheduled flexibility resources and available transmission capacity with respect to the range of net loads is in fact very small. These are risky situations, where simple errors in characterizing the net load range, may lead to infeasibility, albeit the original flexibility assessment having come back with a positive outcome.

Clearly, the BA fails to assess the possible risks associated with poorly-assessed uncertainty that might lead to infeasibility. In this chapter, we will propose a framework that has the ability to assess *both* excessive and inadequate system flexibility by assessing how far operating points are from their feasibility region boundaries. We recall that the aim of flexibility assessment methods such as ours and [52, 165–167] is to estimate possible power imbalances; they do not calculate optimal reserve deployment such as dispatch problems [48, 50].

5.3.4 Feasibility Region Projection onto the Demand Space

The first step in recasting the BA, is to determine its corresponding *loadability set*. The loadability set of a power system is a set of net load realizations that can be supplied by generation while respecting all transmission and reserve capacity limits [169]. A loadability set in the generation-demand space, $\Xi_{gd}(\zeta)$, is characterized as a function of $\zeta = [\zeta_1 \ \cdots \ \zeta_M]^\top$, a specific unit commitment solution

$$\Xi_{gd}(\zeta) = \{(g, d) \mid (5.5) - (5.10)\} \tag{5.11}$$

On the other hand, the loadability set, $\Xi_d(\zeta)$, is the projection of $\Xi_{gd}(\zeta)$ onto demand space only. It is defined as

$$\Xi_d(\zeta) = \{d \mid \exists (g, d) \in \Xi_{gd}(\zeta)\} \tag{5.12}$$

The loadability set $\Xi_{gd}(\zeta)$ is a relaxation of the BA original feasibility region. It enforces all its inequalities, but ignores its equality constraints. Alternatively, $\Xi_d(\zeta)$ describes which net load vectors can be supported by a power system considering a specific unit commitment instance ζ. As seen in [128] and [125], the projection process whereby we pass from $\Xi_{gd}(\zeta)$ to $\Xi_d(\zeta)$ involves the generation of large numbers of constraints, many of which are redundant.

To counter the explosion in the number of redundant constraints associated with the mapping of $\Xi_{gd}(\zeta)$ onto $\Xi_d(\zeta)$, we adopt the iterative approach for determining the minimal representation of the loadability set proposed by [125]. This approach combines the *umbrella constraint discovery* (UCD) algorithm and the Fourier–Motzkin elimination (FME) method as follows. First, we identify network constraints which are *umbrella*—i.e., which are non-redundant in the BA and effectively contribute in shaping its feasibility region—, and we rule out the corresponding redundant network constraints. Second, we construct the loadability set in the generation-demand space considering the dispatchable generators capabilities and umbrella network constraints only. The loadability set constraints are mapped from the generation-demand space onto the demand space by removing the generator variables one by one using FME [128]. After each elimination, redundant constraints are identified and removed to keep the number of constraints as small as possible. We terminate the procedure once all dispatchable generator variables have been eliminated.

5.4 Explicit Flexibility Characterization by Inverse Optimization

In this section, inspired by recent advances in data-driven inverse optimization techniques [170–172], we present how inverse optimization can be used to address the flexibility assessment problem. Inverse optimization describes the "reverse" process of the conventional mathematical optimization. An inverse optimization problem takes decisions or observations as input and determines the objective function and/or the constraints that render these decisions/observations approximately or exactly optimal. In fact, the classical inverse optimization framework implicitly posits the existence of parameter values that render the provided solution optimal [173]. Yet, in numerous applications, it might be impractical to find parameter values that precisely accomplish this goal exactly [174].

The goal of inverse optimization (IO) shares similarities with certain machine learning approaches. Both IO and ML seek to infer the unknown parameters of a model using observable data. Nevertheless, a significant differentiation exists in the aspect that IO's model corresponds to the forward optimization, while its parameters carry meaningful interpretability [175]. In our context, starting from an observable solution of an operational planning problem, we can infer the critical constraint given an uncertain net load vector.

In this case, IO offers a basic framework to do so.

5.4.1 Generalized Inverse Linear Optimization Problems

Here, we introduce a general inverse optimization (GIO) model [172] for a linear optimization problem without making any explicit assumptions regarding its feasibility as in [170]. First, we start from a linear optimization problem which is called the *forward problem* (FO). Let $c, x \in \mathbb{R}^N$ denote cost and decision vectors, respectively. Let $A \in \mathbb{R}^{J \times N}$, and $b \in \mathbb{R}^J$ denote the constraint and the right hand side vector, respectively.[1]

$$\mathrm{FO}\,(c) : \min c^\top x \tag{5.13}$$

Subject to:

$$Ax \geq b \tag{5.14}$$

Assuming that the forward problem does not have redundant constraints, given a decision $\hat{x} \in \mathbb{R}^N$ and for a r-norm ($r \geq 1$), the single observation *generalized inverse linear optimization problem* (GIO) is

$$\mathrm{GIO}_r\,(\hat{x}) : \min_{c,y,s} \|s\|_r \tag{5.15}$$

Subject to:

$$A^\top y = c, \quad y \geq 0 \tag{5.16}$$

$$c^\top \hat{x} = b^\top y + c^\top s \tag{5.17}$$

$$A\,(\hat{x} - s) \geq b \tag{5.18}$$

$$\|c\|_1 = 1 \tag{5.19}$$

The objective function (5.15) minimizes the error (perturbation) vector $s \in \mathbb{R}^N$ using an arbitrary r-norm, which provides a natural measure of error in the space of decision

[1] We are using dimensions J and N in a generic sense here; at this stage, there is no explicit connection with prior developments presented earlier in the chapter and the thesis.

variables. In the GIO, $y \in \mathbb{R}^J$ represents the vector of dual variables of the forward problem's inequality constraints. Constraints in (5.16) enforces the dual feasibility of the forward problem. Constraint (5.17) connects the cost vector of the forward problem and its dual variables' vector, including the perturbation vector whose value may have to be non-zero to satisfy strong duality of the forward problem for the given $\hat{x}$. Constraint (5.18) enforces primal feasibility of the perturbed decisions $\hat{x} - s$. Finally, constraint (5.19) normalizes of the cost vector to prevent it from collapsing to the trivial solution, which is zero.

5.4.2 GIO for Flexibility Assessment

Consider a power system's feasible space whose minimum realization loadability set has been determined ($\mathcal{D}(\zeta)$) based on (5.5)–(5.10), or, more accurately, by imposing $d \in PUS(\mathcal{S})$ in lieu of (5.10). We demonstrate next how GIO can assess the "distance" of any d to the boundaries of $\mathcal{D}(\zeta)$. We posit that knowledge of how far (or near) an operating point is to the boundary of its feasibility region is highly valuable to power system operators and planners alike. With such knowledge at hand, one could seek to extend that distance for increased robustness or try to reduce it, when excessively large, to aim for more economical system operations.

We now consider some instance d^0 (as $\hat{x}$ in the general case), as well as vectors α'_j and β'_j, $j \in \mathcal{J}' = \{1, \ldots, J'\}$—exogenously determined by calculating $\mathcal{D}(\zeta)$—vectors to form the input data set to infer GIO variables. Aiming for a more compact notation, we stack the J' inequalities of $\mathcal{D}(\zeta)$ into an $\mathbb{R}^{J' \times N}$ matrix A (whose rows are $(\alpha'_j)^\top$, $\forall j \in \mathcal{J}'$) and a $\mathbb{R}^{J' \times 1}$ vector b (whose rows are β'_j, $\forall j \in \mathcal{J}'$); from these we now have $\mathcal{D}(\zeta) = \{d \in \mathbb{R}^N \mid Ad \geq b\}$.

Therefore, we define the data-driven inverse optimization problem (DDIO) for flexibility assessment

$$\mathrm{DDIO}_r\left(d^0, \zeta\right) : \min_{c,y,s} \|s\|_r \tag{5.20}$$

Subject to:

$$A^\top y = c, \quad y \geq 0 \tag{5.21}$$

$$c^\top \left(d^0 - s\right) = b^\top y \tag{5.22}$$

$$A\left(d^0 - s\right) \geq b \tag{5.23}$$

$$\|c\|_1 = 1 \tag{5.24}$$

When the objective function of DDIO is equal to zero, this means d^0 is optimal. In the case where $\mathcal{D}(\zeta)$ is a polytope and if $\|s\|_r = 0$, it effectively means that d^0 is on one of the boundaries of $\mathcal{D}(\zeta)$ (hence optimal for the forward linear program with some c). Otherwise, d^0 is interior or exterior to $\mathcal{D}(\zeta)$. In fact, it is possible to construct a c that puts d^0 on an edge of $\mathcal{D}(\zeta)$, that is where the pair $(d^0 - s, y)$ in constraint (5.22) satisfies the strong duality with respect to c. Therefore, the vector $s \neq 0$, and the norm of s can be interpreted as a measure of distance to the closest boundary of $\mathcal{D}(\zeta)$ (based on an appropriately chosen norm).

We note that DDIO (5.20)–(5.24) is a nonlinear, non-convex optimization problem because of the of the $c^\top s$ term in the strong duality constraint (5.22). In the next subsection, we will propose a computationally efficient method to solve DDIO in reasonable time using off-the-shelf optimization software.

To overcome the non-convexity of (5.22), we leverage the feasibility projection problem structure described in [171, 172] to solve the inverse problem. The problem can be decomposed into $j = 1, \ldots, J'$ linear sub-problems

$$\min_{s_j} \|s_j\|_r \tag{5.25}$$

Subject to:

$$A(d^0 - s_j) \geq b \tag{5.26}$$

$$\left(\alpha'_j\right)^\top (d^0 - s_j) = \beta'_j \tag{5.27}$$

and then picking out the smallest $\|s_j\|_r$ over all $j \in \mathcal{J}'$. The problem (5.25)–(5.27) finds the shortest distance between the net load forecast d^0 and each of the constraints $j \in \mathcal{J}'$. The vector s_j that is found has to be consistent with all constraints (5.26), and it has to

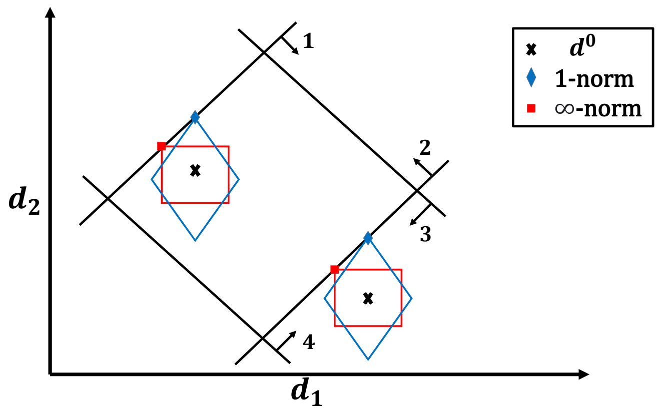

Figure 5.3: Geometrical interpretation of inverse optimization solution methodology.

bring d^0 in contact with constraint j as per (5.27). Picking out the constraint or constraints $j^* \in \mathcal{J}^* \subseteq \mathcal{J}'$ with the shortest distance finds the closest point to the boundary of $\mathcal{D}(\zeta)$ with respect to d^0. The first and infinity norms in feasibility projection problem (5.25)–(5.27) can be linearised as in [176]. A geometrical illustration of (5.25)–(5.27) is shown in Fig. 5.3. Here d^0 can be in the interior of $\mathcal{D}(\zeta)$, or its exterior, and, based on the specific choice of a vector norm, we can determine how far d^0 is from its boundary.

The authors of [170] demonstrate that the corresponding DDIO cost vector can be determined analytically

$$c^* = \frac{\alpha'_{j^*}}{\left\|\alpha'_{j^*}\right\|_1} \tag{5.28}$$

where j^* is the index of the constraint selected by (5.25)–(5.27). Although obtaining this cost vector is an integral part of solving DDIO, it does not offer further information on flexibility adequacy. Nevertheless, it opens up a potential avenue for future research.

5.4.3 Flexibility Assessment Through DDIO

As just seen, DDIO is capable of determining the shortest distance between a net load vector d^0 and the boundaries of a power system's loadibility set $\mathcal{D}(\zeta)$. Moreover, it is able to identify which constraint or constraints of $\mathcal{D}(\zeta)$ are either violated (if d^0 is exterior) or close to be violated (if d^0 is interior). Therefore, loosely speaking, a net load forecast is "flexibility adequate" if d^0 is in the interior of $\mathcal{D}(\zeta)$ and has a large distance to its boundaries.

Based on these observations, we thus propose flexibility metrics based DDIO results:

- Analytical flexibility metric ρ_r: Inspired by [170], we argue that

$$\rho_r\left(d^0, \zeta\right) = 1 - \frac{\|s_{j^*}\|_r}{(1/J')\sum_{j=1}^{J'} \|s_j\|_r} \tag{5.29}$$

  is a useful indicator of the relative security of the net load d^0. It weighs the shortest distance between d^0 to the boundaries of $\mathcal{D}(\zeta)$ relative to the average of boundary distances. The indicator $\rho_r \to 1$ if d^0 is close to one or more boundaries (i.e., system flexibility is in tight supply and/or may not be transmittable to all portions of the network), or it would tend to zero if it is somewhat in the center of $\mathcal{D}(\zeta)$ (i.e., system flexibility is plenty and can be adequately transmitted across the network). We distinguish one weakness of ρ_r, however. As formulated here, it is not possible to distinguish whether or not s_j is used to bring d^0 to a boundary of $\mathcal{D}(\zeta)$ from the inside or the outside. In fact, we would argue that ρ_r is useful when $d^0 \in \mathcal{D}(\zeta)$. For cases where $d^0 \notin \mathcal{D}(\zeta)$, we propose the next metric.

- Net demand curtailed (NDC): In case there exists one or more $j \in \mathcal{J}'$ such that $(\alpha'_j)^\top d^0 < \beta'_j$ (i.e., $d^0 \notin \mathcal{D}(\zeta)$), net demand may need to be curtailed as indicated by the components of s_j. Defining the subset of violated boundaries of $\mathcal{D}(\zeta)$, $\tilde{\mathcal{J}} = \{j \in \mathcal{J}' \mid (\alpha'_j)^\top d^0 < \beta'_j\}$, we have

$$\text{NDC} = \sum_{j \in \tilde{\mathcal{J}}} \sum_{n=1}^{N} s_{jn} \tag{5.30}$$

  where we note that if NDC > 0 demand has to be shed, and if NDC < 0 non-dispatchable generation has to be curtailed.

We will see in the next section how the choice of norm can influence values of ρ_r and NDC. Moreover, the advised reader may be tempted to suggest computing the volume of the loadability set as a way to assess flexibility adequacy. As exposed in [177], this would be prohibitive from a computational point of view. The computational effort required to obtain the volume of a polytope increases very rapidly with its number of vertices. In addition, we recall from [128] that the number of vertices of loadability sets tends to grow very rapidly with successive applications of Fourier-Motzkin elimination. Therefore, it would be ill-advised to pursue this objective here. In our case studies presented next, we will nonetheless compute the volume of $\mathcal{D}(\zeta)$ for comparison purposes; however, we shall use an approach based on Monte Carlo simulations rather than compute volumes analytically [114].

5.5 Case Studies

In this section, we illustrate how the use of forward-looking net load PUS and its coupling with DDIO can work to assess post-unit commitment flexibility adequacy.

5.5.1 Procedure for Constructing Correlated Net Load Forecast Error Time Series

We generate N synthetic spatially-correlated net load time series of length T, which are then consigned to matrix W. They consist of historic net load forecasts $\mu \in \mathbb{R}^{T\times N}$, which correspond to the nominal demand values from the data sets in [137]. These are superimposed with zero-mean normally-distributed forecast errors with spatial correlation given by the covariance matrix Σ. Here, we take the approach outlined in [136], where errors are assumed to be proportional to forecasts and whose variance and correlation are adjusted with an uncertainty level parameter $\eta \in [0, 1]$. This way, the diagonal elements of Σ are $\sigma_{nn}^2 = (\eta\mu_n)^2$ for all $n \in \mathcal{N}$, and, as proposed in [133], its off-diagonal elements are given by $\sigma_{nn'}^2 = \eta^2\alpha\mu_n\mu_{n'}$, for all $n \neq n' \in \mathcal{N}$, and where $\alpha \in [-1, 1]$ is an adjustable correlation coefficient.

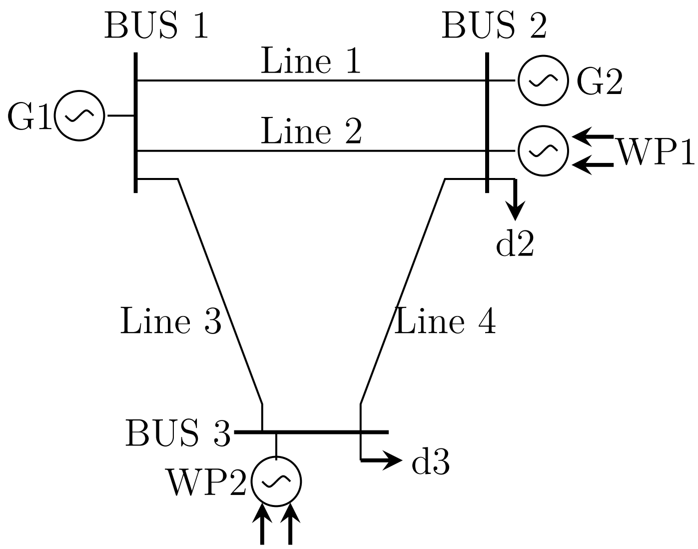

Figure 5.4: Three-bus test system

5.5.2 Three-Bus Test System

Here we use the three-bus test system from [128] depicted in Fig. 5.4. We had a slight modification by adding two wind farms at buses 2 and 3, and neglecting the two generators ramping constraints [125]. The two conventional generators are identical, each with maximum and minimum capacity limits set at 250 MW and 100 MW, respectively. Each line in the system has the same per unit series reactance. The line capacities for lines $l = 1, 2, 3, 4$ are as follows: 100 MW, 100 MW, 60 MW, and 80 MW, respectively. We consider two scenarios whose past forecasted net loads were 320 and 50 MW (Scenario 1) and 240 and 40 MW (Scenario 2) at buses 2 and 3, respectively. We generated $T = 4000$ time instances for each scenario as seen in Fig. 4 (a) for Scenario 1. In Scenario 1, net loads have an uncertainty level η of 0.067 per unit and a correlation coefficient α of 0.8. For Scenario 2, $\eta = 0.1$ per unit with $\alpha = 0.7$. We assume that the penalty for load shedding and renewable generation spillage is $\gamma = \$1000$ per MWh.

We define three intact loadability sets which do not assume net load forecast errors and its uncertainty; that is, they exclude (5.1) and (5.10) and only require that net loads be strictly

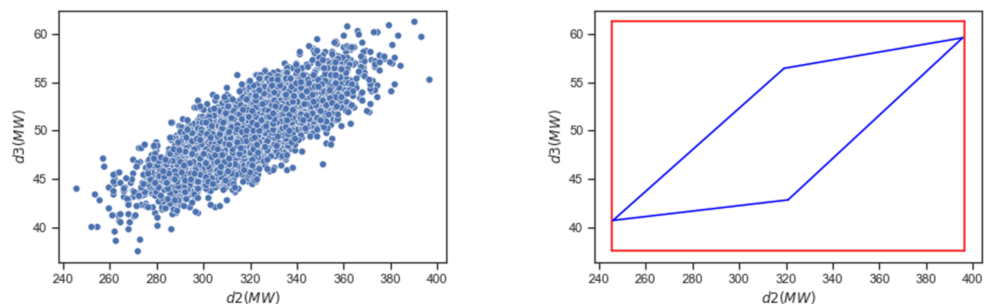

(a) (b)

Figure 5.5: (a) Scatter plot of net loads for Scenario 1; (b) Uncertainty sets for Scenario 1.

Table 5.1: Uncertainty and Loadability Set Volumes

	Volume (MW^2)			
	Uncertainty set		Loadability set	
Scenario	PUS	Box	PUS$\mathcal{D}(\zeta_3)$	Box$\mathcal{D}(\zeta_3)$
1	1163	3950	936	3520
2	1929	4740	1810	4530

positive. These sets are called $\mathcal{D}(\zeta_1) = \mathcal{D}(u_1 = 1, u_2 = 0)$, $\mathcal{D}(\zeta_2) = \mathcal{D}(u_1 = 0, u_2 = 1)$ and $\mathcal{D}(\zeta_3) = \mathcal{D}(u_1 = 1, u_1 = 1)$, and they are described by six, five, and six constraints, respectively. Moreover, for these we constructed loadability sets based on both PUS and box uncertainty sets, and we refer to them as PUS$\mathcal{D}$ and Box$\mathcal{D}$, respectively.

Uncertainty and Loadability Sets' Volume

In Fig. 5.5 (b), one can see the PUS for the data from Scenario 1 (blue rhombus); in addition, we provide the box set corresponding to (5.10) (red rectangle). By inspection, we see that the PUS can effectively capture the spatial correlation between the net loads, while being less conservative than the boxed uncertainty set. In Table. 5.1, we provide the volume (areas here) for the two scenarios considering PUS and box-shaped uncertainty modeling. The conservative box uncertainty set is 3.4 and 2.45 larger than PUS for Scenarios 1 and 2, respectively. Also, in Table 5.1 we characterize the loadability sets considering

Table 5.2: Performance of Flexibility Assessment Strategies

Scenario	Method	NDC
1	DDIO^1	98.527 (0.0%)
	DDIO^∞	147.48 (+50%)
	BA	98.527
2	DDIO^1	39.065 (0.0%)
	DDIO^∞	39.065 (0.0%)
	BA	39.065

the two generators are committed on, the network constraints and data-driven uncertainty sets. For Scenario 1, the loadability sets $\mathrm{PUS}\mathcal{D}(\zeta_3)$ and $\mathrm{Box}\mathcal{D}(\zeta_3)$ are characterized by their uncertainty boundaries plus one constraint representing the umbrella line flow constraint after eliminating generator variables using FME and removing any redundancy using UCD. Similarly for Scenario 2, $\mathrm{PUS}\mathcal{D}(\zeta_3)$ and $\mathrm{Box}\mathcal{D}(\zeta_3)$ are characterised by their uncertainty sets and one constraint representing the boundary defined by the generator minimum capacity limits. Clearly, system constraints associated to respective loadability sets shave larger volumes from the box set in comparison to PUS in both scenarios. In fact, $\mathrm{Box}\mathcal{D}(\zeta_3)$ volume's was shaved off by 1.90 and 1.76 times more than $\mathrm{PUS}\mathcal{D}(\zeta_3)$ for Scenarios 1 and 2, respectively.

Flexibility Assessment Strategies' Performance

Table 5.2 displays the performance of three proposed methods for both scenarios and the loadability set $\mathcal{D}(\zeta_3)$. The percentage changes in NDC are taken with respect to the BA's optimal objective function value (which is equal to the amount of load and/or non-dispachable generation curtailed). Both scenarios emphasize that DDIO^1 (DDIO solved using the $r = 1$ norm) is able to assess net load curtailed in the same way as the BA. In the case of Scenario 1, DDIO^∞ shows an increase in NDC of 50% compared to DDIO^1 and the BA. The reason for this is that when using the $r = \infty$ norm for calculating the shortest distance to reach the loadability set boundary from d^0, DDIO is using all dimensions to get to the boundary. On the other hand, when the $r = 1$ norm is used, DDIO is using only one dimension, while neglecting the others. However, in the calculation of NDC in (5.30), all N components of s_j are used, which the the case in the calculation of

NDC and in the solution of DDIO[1].

Impacts of Generation Schedules on Flexibility Metrics

Here, the properties of the flexibility metric ρ_r are discussed under the three different loadability sets, $\mathcal{D}(\zeta_i); i = 1, 2, 3$. The variations of ρ_r under different generating conditions are shown in Fig. 5.6. For $r = \infty$, we can see how ρ_∞ varies for the three loadability sets as a unit-free quantity in the range $[0, 1]$. By inspection, the flexibility metric varies in a structured way inside the loadability set. It shows a non decreasing trend in a radial fashion as the loading moves from the interior towards the loadability set boundaries. Hence, for any d^0 and generation schedule ζ it is possible to obtain a normalized "flexibility score" indicating its degree of safety in terms of relative distance to the boundaries of loadability sets.

5.5.3 IEEE Reliability Test System

Next, we test the proposed approach on the 24-bus IEEE Reliability Test System (RTS). The data of the network, the nominal demand profile at each node, and the minimum and maximum power outputs of generators are adopted from MATPOWER [137]. Generating units ramp rate constraints are neglected as in [125]. We generated $T = 4000$ time instances of net load while varying uncertainty levels to generate synthetic polyhedral and box uncertainty sets. Lastly, we assume here that ζ corresponds to the RTS unit commitment where *all* its units are online.

Loadability Set Construction

Here, we consider a case where net load is uncertain at 17 of the 24 network nodes. Historical forecast errors are generated considering nominal loading levels with $\eta = 0.067$ and $\alpha = 0.7$. Polyhedral and box uncertainty sets are built to capture net load limits which are in turn used in characterizing the loadability sets of the RTS including its transmission limits.

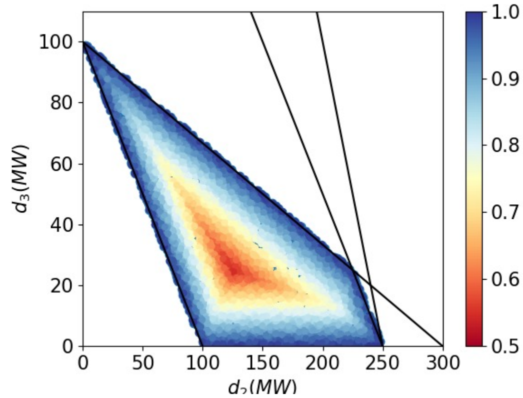

(a) $\mathcal{D}(\zeta_1)$

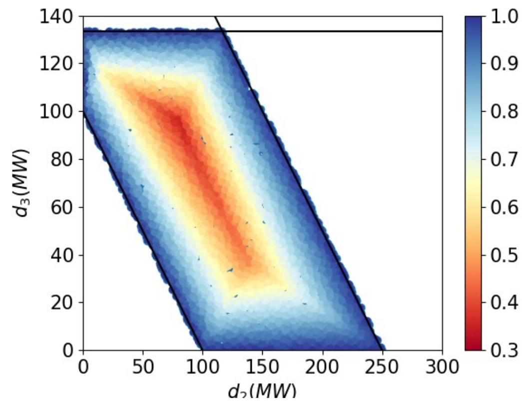

(b) $\mathcal{D}(\zeta_2)$

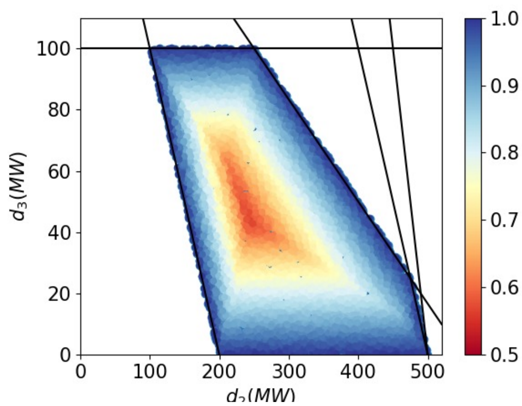

(c) $\mathcal{D}(\zeta_3)$

Figure 5.6: Flexibility metric ρ_∞ distribution across the intact loadability sets.

We construct the loadability set constraints (5.5)–(5.9) of the network along the polyhedral and box uncertainty sets in the generation-demand space considering all 10 generator nodes. For the polyhedral uncertainty set, we feed the UCD algorithm with corresponding net load limits along with the generation and network constraints as follows. First, we group uncertain net loads into three separate polyhedral sets: $P_1(\mathcal{S}, 6)$ for d_{1-6}, $P_2(\mathcal{S}, 6)$ for $d_{7-10,13-14}$, and $P_3(\mathcal{S}, 5)$ for $d_{15-16,18-20}$. Set $P_1(\mathcal{S}, 6)$ captures the uncertainty in net load seen at nodes 1–6, set $P_2(\mathcal{S}, 6)$ the uncertainty at nodes 7–10, 13 and 14, and finally $P_3(\mathcal{S}, 5)$ maps uncertainty at nodes 15, 16, 18–20 (for the grand total of 17 nodes). The construction of three separate PUS rather than a single one is driven by the need to limit the growth in the number of superfluous constraints when the FME algorithm is run. Hence, instead of having 2^{17} constraints considered simultaneously, much fewer constraints need to be assessed at the UCD stage: 2^6 (for P_1) + 2^6 (for P_2) + 2^5 (for P_3) = 160 native PUS constraints. We choose to keep all principal components of each set to ensure robustness of the resulting polyhedral uncertainty sets.

While there are ten generators in the RTS, we need to project only four generation variables at a time using FME to characterize each loadability set. This is a valid assumption since the maximum number of potentially active transmission constraints in the RTS is four, as shown in [125]. This is done while the remaining generators are pushed to one of their capacity limits with the aim of maximizing the resulting loadability set volumes. Going with the approach taken in [125], we assume the marginal units are located at buses 1, 7, 16 and 22. The four marginal units are eliminated one by one using FME, and after each elimination, the UCD algorithm removes superfluous constraints. Table 5.3 lists the numbers of remaining umbrella constraints after each marginal unit elimination for both the PUS and box uncertainty sets. We can see that the number of constraints required by the PUS uncertainty is greater than that needed by the box set. This is due to the fact that the PUS is much more surgical in bounding the uncertainty.

Table 5.3: Number of umbrella constraints describing the loadability sets by uncertainty set type

	No. of constraints identified	
	PUS$\mathcal{D}(\zeta)$	Box$\mathcal{D}(\zeta)$
In generation-demand space	209	87
After eliminating $\hat{g}_1$	200	77
After eliminating $\hat{g}_7$	180	55
After eliminating $\hat{g}_{16}$	178	53
After eliminating $\hat{g}_{22}$	176	51
In demand space	161	35

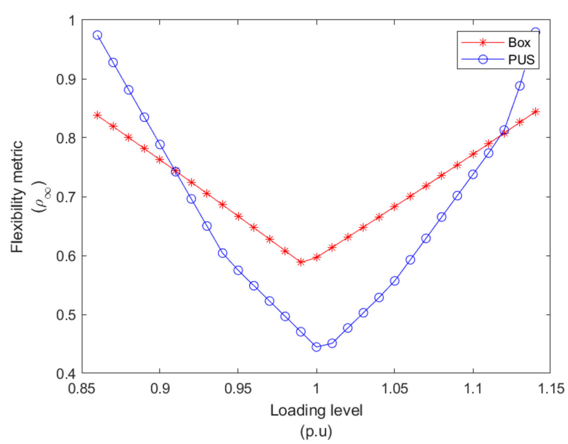

Figure 5.7: Flexibility metric for PUS$\mathcal{D}(\zeta)$ and Box$\mathcal{D}(\zeta)$.

Flexibility Assessment Strategies' Performance

Fig. 5.7 displays the flexibility metric ρ_∞ while varying the loading in the range of $\pm 14\%$ of the nominal loading level d_0. By inspection, we see that ρ_∞, when used with the PUS uncertainty set, performs much better at characterizing flexibility than when used on its corresponding box uncertainty set. The reason for this assessment is that ρ_∞ spans a much wider range under PUS than under the box set. This is a desirable feature because system operators would have a more sensitive assessment of prevailing levels of flexibility. In the case of the box set, variations in ρ_∞ are so narrow (≈ 0.25 about the base index, in comparison to ≈ 0.55 with the PUS). Moreover, it does not even get close to one as the system loading becomes more critical, a feature required to signal clearly flexibility inadequacy.

Level of Uncertainty Influence on Constraints Projections into the Demand Space

We consider next the RTS nominal loading level with different levels of uncertainty $\eta = \{0.033, 0.067, 0.1\}$ for modelling load variations and a correlation factor $\alpha = 0.7$. The line capacities are reduced by half to have a more congested network. In Table. 5.4 we notice an increasing trend in umbrella line flow constraints when the level of uncertainty grows. This happens because the system has to cover wider ranges of net loads which tends to increase the possibility of hitting one or more line flow limits.

In particular, for the case when $\eta = 0.067$ or 0.1, the box set retains a higher percentage of its line constraints in comparison with the PUS, by 77.78% and 66.67%, respectively. On the other hand, in the generation-demand space most generator constraints are expected to be umbrellas. Still, while considering the highest level uncertainty, the PUS retains only up to 22.7% of the total original constraints in comparison to 30.9% with the conventional box approach. This is a positive outcome indicating the superiority of the PUS approach. With fewer remaining constraints, the evaluation of ρ_r and NDC through DDIO is expected to be simpler and faster.

Finally, the proposed approach provides a novel way to quantify flexibility inadequacies in power systems. Using this information, one could identify which constraints are the most

Table 5.4: Percentage of Constraints Retained in the BA and its Corresponding Loadability Set After the Application of UCD

	PUS	Box	PUS	Box
η	Line constraints (% change)		Generation-demand space (% change)	
0.033	9.21	9.21 (0.0%)	20.6	23.7 (+15%)
0.067	11.84	21.05 (+77.78%)	20.6	27.8 (+34.95%)
0.100	15.78	26.31 (+66.67%)	22.7	30.9 (+36.12%)

critical for operation. Also, the selection of a particular norm to use might be determined by the specific application. For our case, we demonstrate how DDIO^1 outperforms DDIO^∞ by providing lower NDC for the three-bus test system. This chapter considers complementary to chapters 2 and 3, as it relies on a given unit commitment strategy, and consequently assesses the impact of the uncertain net loads at a given operating condition.

There are many practical considerations one has to take into when moving to use inverse optimization for power systems. For instance, the power systems operators and planners might have empirical knowledge about feasible observations (decision variables such as generator dispatch, demand response, energy storage and so on), but the explicit constraints of this underlying model are not well defined. The inverse optimization problem could be extended to determine the feasible region of an optimization problem that would result in a given set of observations being feasible and/or optimal. In other words, the inverse optimization approach could retrieve the constraint of a linear model, followed by proposing a feasible reformulation that is compact and tractable.

5.6 Summary

This chapter proposed a novel data-driven inverse optimization scheme for assessing flexibility explicitly in low-carbon power systems. Using historical demand data and its forecasts, polyhedral uncertainty sets can capture the spatial correlation of net loads and their forecasting errors. A new flexibility metric provides a useful numerical and visualization tool to assess how net load forecast errors are expected to be handled given committed flexible resources. Moreover, umbrella constraint discovery is used to determine the minimum number of constraints that shape the feasibility region and how that can be affected under correlated uncertainties. The framework unlocks the integration assessment of renewable generation with loadability set approaches by defining critical constraints. Several interesting potential applications could be explored on the basis on the inverse optimization scheme presented in the chapter. For example, one could assess how the flexibility metric ρ_r and NDC are affected by deploying energy storage assets or demand response programs.

Chapter 6

Conclusion

6.1 Thesis Overview

The accelerating decarbonization of society and its increasing reliance on electricity are posing significant challenges to electric power system operation and planning. As uncertainties—coming primarily from increases in variable and intermittent renewable energy sources (like solar and wind power generation) and new emerging uses of electricity (like electric vehicle charging)—become more prevalent in power systems, it is necessary for system operators to incorporate them into their operational planning problem formulations to maintain secure and economic operations. However, including uncertainties along with the complexity of large-scale practical power systems leads to models that are difficult to solve to high levels of accuracy within short computation timelines associated with day-ahead planning and real-time operations. Solving operational planning problems such as the unit commitment problem, security-constrained unit commitment and optimal power flow repeatedly in daily operation is necessary, but their associated large number of constraints can significantly increases their solution times and required fast memory. Previous research and empirical evidence indicate that only a small percentage of constraints are responsible for enclosing the feasible solution space of such problems; moreover, at their optima the number of associated binding constraints is even lower.

Led by these observations, in this thesis we sought to advance the state-of-the-art of *constraint screening* for power system operational planning problems. We demonstrated how *constraint learning* is essential to efficient constraint screening. Constraint learning uses machine learning models to predict which constraints are necessary and sufficient to represent the feasible space of planning problems on top of also predicting which ones would be potentially active at the problems' optima. Here the learning process is led by discovering insights from previous solved operations planning instances. Although constraint learning is time-consuming at the outset—due to offline training requirements—, its use to weed out unnecessary constraints in large operations planning problems leads to significant solution time savings for time-limited real-time computations.

Chapter 2 starts off with a critical review of state-of-the-art approaches used to quantify the uncertainty space of variable renewable energy and demand, called *net load* or *net demand*. Some approaches were found to be too conservative and negligent of multisite spatial correlations. Those overly robust approaches employ large multidimensional boxes set to encompass all credible net demand outcomes. On the other hand, convex hull approaches seek to enclose all credible net demand outcomes by drawing a convex polytope around historic net demand observations. Convex hull approaches are much less conservative than multidimensional boxes, and they are able to capture multisite correlations. However, they require the generation of overly large numbers of necessary bounding constraints.

To overcome the shortcomings of multidimensional boxes and convex hulls, we proposed the use of polyhedral uncertainty sets. These sets require a small number of constraints, and they are capable of capturing spatial correlations seen across multiple sites in a system. They offer coverage levels similar to those of convex hulls without the over conservatism of multidimensional boxes.

Second, the constraint screening problem, oftentimes called *umbrella constraint discovery*, is studied in the context of polyhedral uncertainty sets integrated in robust unit commitment problems. Inasmuch umbrella constraint discovery is useful in stripping down optimization problems like unit commitment to their bare bones in terms of constraint numbers, it is agnostic to the nature of the objective function of the original optimization problem. In light of this, we proposed to augment the umbrella constraint discovery problem with the addition of an upper bound[1] on the value of the objective function of the original minimization problem. In our case, this upper bound is found by fitting an appropriate regression model using past instances of the unit commitment problem.

With the addition of this upper bound in the umbrella constraint discovery problem, the constraints retained are no longer the constraints needed to describe minimally the feasible set of the unit commitment. They are the constraints which are expected to be *binding* at the optima of the problem. In practice, the ratio between the number of binding constraints to the total number constraints is very low. Knowing this, one expects that the number of retained constraints by our proposed constraint screening approach should be significantly lower. Therefore, if one runs a unit commitment subject only to its predicted binding constraints, significant solution speed ups should be achieved.

This property is proved to be the case when running computational experiments on standard test power systems. Moreover, we showed how the use of polyhedral uncertainty sets lead to improved constraint screening performance when compared to other state-of-the-art approaches.

In that vein, Chapter 3 proposed an interpretable machine learning algorithm for real-time constraint generation for security-constrained unit commitment problems. The proposed algorithm predicts which constraints would be generated as part the iterative simultaneous feasibility test which is used to identify and correct constraint violations in practical security-constrained unit commitment problems. With a good prediction of such constraints, it is possible to warm start the problem's simultaneous feasibility test process and reduce the number of iterations needed to complete the process. The algorithm provides the same feasibility and the same optimality as the full simultaneous feasibility test process and its associated constraint generation. Alike in Chapter 2, we illustrated performance enhancements for security-constrained unit commitment solution applied on

[1] It should be a lower bound if the optimization problem is a maximization.

several standard test systems of increasing sizes.

In Chapter 4, constraint learning is extended to address the challenging environment associated with the ac optimal power flow. Knowing that the AC-OPF problem is NP-hard, constraint learning is applied to convex relaxations of this problem rather than to its original non-convex version. The approach taken sought to tighten convex relaxation bounds with the assistance of economic information obtained from past optimal power flow runs, thus identifying active and inactive constraints of convex relaxations. Experimental results obtained from AC-OPF runs on the PGLib-OPF test cases showed important speed-ups for large cases, a vital need to bring AC-OPF formulations to practical settings.

Throughout the thesis, constraint screening and learning have been underlined as essential in carrying out generation planning problems for practical power systems close to real time. Finding out ahead of time which constraints will determine the optimal solution is great; however, it is not enough for the prudent operator. This is why, in Chapter 5, we developed a novel approach to determine the *distance* of an optimization problem solution to its non-binding constraints, or even its violated constraints in cases when problems are infeasible. Here, the notion of "distance" to a problem's constraints is associated with the ability of the power system to respond to uncertain events, i.e., how *flexible* it is. For this purpose, we proposed system flexibility metrics which are calculated by solving an associated inverse optimization problem. We showed if this approach is used on the loadability set of a power system, it is able to ascertain the feasibility of a net demand vector, and it is able to identify which constraints are closest to that net demand vector.

6.2 Recommendations for Future Work

This thesis did shed light on constraint learning and its direct application to constraint screening for several power system operations planning problems: unit commitment, security-constrained unit commitment, and optimal power flow. Furthermore, we did introduce a novel way to characterize flexibility explicitly in power system operation. Yet, several areas remain open for future research.

- In this thesis, we model the upper-bound cost-driven constraint based on the aggregate demand using a linear regression model. However, the dual problem of the unit commitment and the Lagrangian multipliers can provide insights into the economic impacts of relaxing or tightening specific constraints. Utilizing location marginal prices information with all nodal net loads using advanced machine learning techniques might provide guarantees on the constraints screening outcome for identifying the binding constraints.

- One could explore applying sensitivity analysis to discover how umbrella constraints respond to changes in the objective function for the unit commitment problem. This analysis would shed light on the transition of constraints from being inactive to becoming active constraints. This information is crucial for system operators as it enables them to promptly identify if a line constraint has the potential to be a binding constraint if any changes occur in the system.

- The optimization with constraint learning approach can be extended to another important problem which is optimal transmission switching, this problem is NP-hard and can greatly benefit from the computational enhancement.

- An important area for future research involves exploring how systems planners can integrate the identification of binding constraints and critical non-binding constraints into long-term investment planning studies for power systems with high renewable energy penetration.

- From a methodological standpoint, this thesis's research opens up numerous avenues for future exploration. One of the most intriguing areas is the future application of inverse optimization technique to power systems area, whether for flexibility assessment, optimal pricing for ancillary services, or any other potential use. The research conducted in this thesis only scratches the surface of inverse optimization and time series uncertainties, with a great deal of potential for improvement. For instance, exploiting vast amounts of data, allowing for cost and demand relationships by employing machine learning techniques, and obtaining robust solutions are just two of the many enhancements that need to be addressed. From a theoretical standpoint, additional mathematical foundations that characterize generalized inverse optimization problems' with multiple solutions could help better understand the models' fundamental characteristics.

Appendix A

UCD Decomposition

The computational burden of the UCD algorithm can be further reduced through a decomposition technique [125], also called *enhanced UCD (E-UCD)*, which searches for umbrella constraints in computationally-manageable constraint blocks $\mathcal{L}_\kappa$ of the initial optimization such that $\cup_\kappa \mathcal{L}_\kappa = \{1, \ldots, L\}$ and $\mathcal{L}_\kappa \cap \mathcal{L}_{\kappa'} = \emptyset$ for all $\kappa \neq \kappa'$. To perform this decomposition on UCD, one needs to consider the entire blocks of constraints (2.8)–(2.12) and (2.19)–(2.20) in addition to one of the blocks $\mathcal{L}_\kappa$ of the block of constraints in (2.13)–(2.18). Furthermore, this step can be executed by parallel processing to expedite the solution of UCD problem. Hence, we solve (A.1)–(A.8) for each $\mathcal{L}_\kappa$

$$\min \sum_{l' \in \mathcal{L}_\kappa} (v_{l'}^+ + v_{l'}^-) \tag{A.1}$$

Subject to:

$$(2.8) - (2.12), (2.19) - (2.20) \tag{A.2}$$

$$\sum_{n=1}^{N} h_{l'n} q_n + z_{l'}^{+} \geq f_{l'}^{\max}, \qquad \forall l' \in \mathcal{L}_{\kappa} \tag{A.3}$$

$$-\sum_{n=1}^{N} h_{l'n} q_n + z_{l'}^{-} \geq f_{l'}^{\max}, \qquad \forall l' \in \mathcal{L}_{\kappa} \tag{A.4}$$

$$v_{l'} - \frac{z_{l'}^{+}}{\Omega} \geq 0, \qquad \forall l' \in \mathcal{L}_{\kappa} \tag{A.5}$$

$$v_{l'}^{+} - \frac{z_{l'}^{-}}{\Omega} \geq 0, \qquad \forall l' \in \mathcal{L}_{\kappa} \tag{A.6}$$

$$z_{l'}^{+}, z_{l'}^{-} \geq 0, \qquad \forall l' \in \mathcal{L}_{\kappa} \tag{A.7}$$

$$v_{l'}^{+}, v_{l'}^{-} \in \{0, 1\}, \qquad \forall l' \in \mathcal{L}_{\kappa} \tag{A.8}$$

In this case, the number of binary variables induced for examining line constraints per subproblem is $2|\mathcal{L}_{\kappa}|$, where $|\mathcal{L}_{\kappa}|$ is the cardinality of the subset $\mathcal{L}_{\kappa}$. By considering all the umbrella constraints identified in each block, we obtain all the umbrella constraints of the original UC problem.

Appendix B

Piecewise Linear Cost Upper Bound Modelling

The cost-driven upper bound linear constraint in chatper 2 is extended using a piecewise linear set of constraints to capture net demand and cost data over different ranges of net demand. The minimum and maximum net demand for each segment is denoted by $D_s^{\min}$ and $D_s^{\max}$, and we introduce a binary variable y_s per segment s, which is equal to 1 if $y_s D_s^{\min} \leq D \leq y_s D_s^{\max}$, and to 0 otherwise. The total number of segments is denoted as S. The upper bound with multiple segments can be reformulated as follows:

$$\sum_{m \in \mathcal{M}} c_m g_m \leq \sum_{s=1}^{S} y_s \left((1 + \Delta_s \sigma_s) a_s + (1 + \Gamma) b_s D\right) \tag{B.1}$$

Due to the non-linearity of equation (B.1) which creates a non-convex set, we introduce a new variable r_s to linearize the product of binary and continuous variables using Big-M method.

$$\sum_{m\in\mathcal{M}} c_m g_m \leq \sum_{s=1}^{S}(1+\Delta_s\sigma_s)y_s a_s + \sum_{s=1}^{S}(1+\Gamma)r_s b_s \tag{B.2}$$

$$D = \sum_{n=1}^{N} d_n \tag{B.3}$$

$$r_s \leq y_s M \tag{B.4}$$

$$r_s \geq D + (y_s - 1)M \tag{B.5}$$

$$\sum_{s=1}^{S} y_s D_s^{\min} \leq D \leq \sum_{s=1}^{S} y_s D_s^{\max} \tag{B.6}$$

$$\sum_{s=1}^{S} y_s = 1 \tag{B.7}$$

$$y_s \in \{0,1\}, \quad s = 1,\ldots,S \tag{B.8}$$

Appendix C

Convex Envelopes Preliminaries for Quadratic Convex Relaxation

This Appendix is associated with the quadratic convex relaxation presented in chapter 4 and how the convex envelopes of the square and the product of variables are derived as detailed in [154].

Consider a real variable denoted as x, satisfying the inequality $\underline{x} \leq x \leq \overline{x}$, with $\underline{x} < \overline{x}$. If we define y as the square of x, i.e., $y = x^2$, then it holds that:

$$\langle y \rangle \equiv \begin{cases} y \geq x^2 \\ y \leq (\underline{x} + \overline{x})\,\overline{x} - \underline{x}\overline{x} \end{cases} \tag{C.1}$$

On the other hand, consider two real variables, denoted as x and y, satisfying the inequalities $\underline{x} \leq x \leq \overline{x}$ and $\underline{y} \leq y \leq \overline{y}$, where $\underline{x} < \overline{x}$ and $\underline{y} < \overline{y}$. If we define z as the product of x and y, i.e., $z = xy$, then it holds that:

$$\langle z \rangle \equiv \begin{cases} z \geq \underline{x}y + \underline{y}x - \underline{x}\underline{y} \\ z \geq \overline{x}y + \overline{y}x - \overline{x}\overline{y} \\ z \leq \underline{x}y + \overline{y}x - \underline{x}\overline{y} \\ z \leq \overline{x}y + \underline{y}x - \overline{x}\underline{y} \end{cases} \tag{C.2}$$

Finally, for convex envelopes for sine and cosine functions, suppose we have a real number t, subject to the condition $|t| \leq \bar{t}$, where $0 < \bar{t} < \frac{\pi}{2}$. Let $x = \cos t$ and $y = \sin t$. Then, for the given values of t and $\bar{t}$, the following inequalities hold [148]:

$$\cos \bar{t} \leq x \leq 1 - (1 - \cos \bar{t})\bar{t}^2 \tag{C.3}$$

$$\left| y - t \cos \frac{\bar{t}}{2} \right| \leq \sin \frac{\bar{t}}{2} - \frac{\bar{t}}{2} \cos \frac{\bar{t}}{2}. \tag{C.4}$$

References

[1] IEA, "IEA Renewables 2021, IEA, Paris, France." https://www.iea.org/reports/renewables-2021. Accessed: 2022-12-06.

[2] B. Mohandes, M. S. E. Moursi, N. Hatziargyriou, and S. El-Khatib, "A review of power system flexibility with high penetration of renewables," *IEEE Transactions on Power Systems*, vol. 34, no. 4, pp. 3140–3155, 2019.

[3] L. A. Roald, D. Pozo, A. Papavasiliou, D. K. Molzahn, J. Kazempour, and A. Conejo, "Power systems optimization under uncertainty: A review of methods and applications," *Electric Power Systems Research*, vol. 214, p. 108725, 2023.

[4] Q. P. Zheng, J. Wang, and A. L. Liu, "Stochastic optimization for unit commitment—a review," *IEEE Transactions on Power Systems*, vol. 30, no. 4, pp. 1913–1924, 2015.

[5] Energy Information Administration (EIA), "Wholesale electricity and natural gas market data." https://www.eia.gov/electricity/wholesale. Accessed: 2022-12-07.

[6] A. J. Ardakani, *Identification of Umbrella Constraints in Power Generation Scheduling Problems*. PhD thesis, McGill University, Aug 2014.

[7] G. Gutiérrez-Alcaraz, B. Díaz-López, J. M. Arroyo, and V. H. Hinojosa, "Large-scale preventive security-constrained unit commitment considering n-k line outages and transmission losses," *IEEE Transactions on Power Systems*, vol. 37, no. 3, pp. 2032–2041, 2022.

[8] A. S. S. Xavier, F. Qiu, F. Wang, and P. R. Thimmapuram, “Transmission constraint filtering in large-scale security-constrained unit commitment,” *IEEE Transactions on Power Systems*, vol. 34, no. 3, pp. 2457–2460, 2019.

[9] T. Zhao, H. Zhang, X. Liu, S. Yao, and P. Wang, “Resilient unit commitment for day-ahead market considering probabilistic impacts of hurricanes,” *IEEE Transactions on Power Systems*, vol. 36, no. 2, pp. 1082–1094, 2021.

[10] D. N. Trakas and N. D. Hatziargyriou, “Resilience constrained day-ahead unit commitment under extreme weather events,” *IEEE Transactions on Power Systems*, vol. 35, no. 2, pp. 1242–1253, 2020.

[11] H. Shayan and T. Amraee, “Network constrained unit commitment under cyber attacks driven overloads,” *IEEE Transactions on Smart Grid*, vol. 10, no. 6, pp. 6449–6460, 2019.

[12] X. Wu and A. J. Conejo, “An efficient tri-level optimization model for electric grid defense planning,” *IEEE Transactions on Power Systems*, vol. 32, no. 4, pp. 2984–2994, 2017.

[13] E. Lannoye, D. Flynn, and M. O’Malley, “Evaluation of power system flexibility,” *IEEE Transactions on Power Systems*, vol. 27, no. 2, pp. 922–931, 2012.

[14] B. Carlson, Y. Chen, M. Hong, R. Jones, K. Larson, X. Ma, P. Nieuwesteeg, H. Song, K. Sperry, M. Tackett, D. Taylor, J. Wan, and E. Zak, “MISO unlocks billions in savings through the application of operations research for energy and ancillary services markets,” *Interfaces*, vol. 42, no. 1, pp. 58–73, 2012.

[15] N. Yang, Z. Dong, L. Wu, L. Zhang, X. Shen, D. Chen, B. Zhu, and Y. Liu, “A comprehensive review of security-constrained unit commitment,” *Journal of Modern Power Systems and Clean Energy*, vol. 10, no. 3, pp. 562–576, 2022.

[16] Y. Chen, F. Pan, F. Qiu, A. S. Xavier, T. Zheng, M. Marwali, B. Knueven, Y. Guan, P. B. Luh, L. Wu, B. Yan, M. A. Bragin, H. Zhong, A. Giacomoni, R. Baldick, B. Gisin, Q. Gu, R. Philbrick, and F. Li, "Security-constrained unit commitment for electricity market: Modeling, solution methods, and future challenges," *IEEE Transactions on Power Systems*, pp. 1–14, 2022.

[17] W. Ackooij, I. Lopez, A. Frangioni, F. Lacalandra, and M. Tahanan, "Large-scale unit commitment under uncertainty: an updated literature survey," *Ann Oper Res*, vol. 271, p. 11–85, 2018.

[18] M. Anjos and A. Conejo, *Unit Commitment in Electric Energy Systems*. Foundations and trends in electric energy systems, 2017.

[19] B. Knueven, J. Ostrowski, and J.-P. Watson, "On mixed-integer programming formulations for the unit commitment problem," *INFORMS Journal on Computing*, vol. 32, no. 4, pp. 857–876, 2020.

[20] F. Bouffard, *Electricity market-clearing with stochastic security*. PhD thesis, McGill University, Feb 2006.

[21] P. Bendotti, P. Fouilhoux, and C. Rottner, "On the complexity of the unit commitment problem," *Ann Oper Res*, vol. 274, no. 1, pp. 119–130, 2019.

[22] A. J. Wood, B. F. Wollenberg, and G. B. Sheblé, *Power generation, Operation, and Control*. Wiley-Interscience, 2014.

[23] D. A. Tejada-Arango, P. Sánchez-Martın, and A. Ramos, "Security constrained unit commitment using line outage distribution factors," *IEEE Transactions on Power Systems*, vol. 33, no. 1, pp. 329–337, 2018.

[24] Z. Guo, R. L.-Y. Chen, N. Fan, and J.-P. Watson, "Contingency-constrained unit commitment with intervening time for system adjustments," *IEEE Transactions on Power Systems*, vol. 32, no. 4, pp. 3049–3059, 2017.

[25] V. H. Hinojosa, "Comparing corrective and preventive security-constrained DCOPF problems using linear shift-factors," *Energies*, vol. 13, no. 3, 2020.

[26] J. Zhu, *Optimization of Power System Operation.* Wiley, 2008.

[27] Y. Chen, D. Savageau, F. Wang, and A. Casto, "Voltage and local reliability commitment under electricity market operations," in *2016 IEEE Power and Energy Society General Meeting (PESGM)*, pp. 1–5, 2016.

[28] A. Jiménez-Cordero, J. M. Morales, and S. Pineda, "Warm-starting constraint generation for mixed-integer optimization: A machine learning approach," *Knowledge-Based Systems*, vol. 253, p. 109570, 2022.

[29] G. Morales-España, J. M. Latorre, and A. Ramos, "Tight and compact MILP formulation for the thermal unit commitment problem," *IEEE Transactions on Power Systems*, vol. 28, no. 4, pp. 4897–4908, 2013.

[30] D. A. Tejada-Arango, S. Lumbreras, P. Sánchez-Martín, and A. Ramos, "Which unit-commitment formulation is best? A comparison framework," *IEEE Transactions on Power Systems*, vol. 35, no. 4, pp. 2926–2936, 2020.

[31] J. Ostrowski, M. F. Anjos, and A. Vannelli, "Tight mixed integer linear programming formulations for the unit commitment problem," *IEEE Transactions on Power Systems*, vol. 27, no. 1, pp. 39–46, 2012.

[32] Q. Zhai, X. Guan, J. Cheng, and H. Wu, "Fast identification of inactive security constraints in scuc problems," *IEEE Transactions on Power Systems*, vol. 25, no. 4, pp. 1946–1954, 2010.

[33] A. J. Ardakani and F. Bouffard, "Acceleration of umbrella constraint discovery in generation scheduling problems," *IEEE Transactions on Power Systems*, vol. 30, no. 4, pp. 2100–2109, 2015.

[34] M. Carrion and J. Arroyo, "A computationally efficient mixed-integer linear formulation for the thermal unit commitment problem," *IEEE Transactions on Power Systems*, vol. 21, no. 3, pp. 1371–1378, 2006.

[35] N. Langrene, W. van Ackooij, and F. Breant, "Dynamic constraints for aggregated units: Formulation and application," *IEEE Transactions on Power Systems*, vol. 26, no. 3, pp. 1349–1356, 2011.

[36] K. Kim, A. Botterud, and F. Qiu, "Temporal decomposition for improved unit commitment in power system production cost modeling," *IEEE Transactions on Power Systems*, vol. 33, no. 5, pp. 5276–5287, 2018.

[37] M. J. Feizollahi, M. Costley, S. Ahmed, and S. Grijalva, "Large-scale decentralized unit commitment," *International Journal of Electrical Power & Energy Systems*, vol. 73, pp. 97–106, 2015.

[38] S. Pineda, R. Fernández-Blanco, and J. M. Morales, "Time-adaptive unit commitment," *IEEE Transactions on Power Systems*, vol. 34, no. 5, pp. 3869–3878, 2019.

[39] S. Y. Abujarad, M. Mustafa, and J. Jamian, "Recent approaches of unit commitment in the presence of intermittent renewable energy resources: A review," *Renewable and Sustainable Energy Reviews*, vol. 70, pp. 215–223, 2017.

[40] D. Bertsimas and M. Sim, "The price of robustness," *Operations Research*, vol. 52, no. 1, pp. 35–53, 2004.

[41] Y. Zhang, J. Wang, B. Zeng, and Z. Hu, "Chance-constrained two-stage unit commitment under uncertain load and wind power output using bilinear Benders decomposition," *IEEE Transactions on Power Systems*, vol. 32, no. 5, pp. 3637–3647, 2017.

[42] A. Shapiro, “Distributionally robust stochastic programming,” *SIAM Journal on Optimization*, vol. 27, pp. 2258–2275, Jan. 2017.

[43] A. Tuohy, P. Meibom, E. Denny, and M. O’Malley, “Unit commitment for systems with significant wind penetration,” *IEEE Transactions on Power Systems*, vol. 24, no. 2, pp. 592–601, 2009.

[44] P. Meibom, R. Barth, B. Hasche, H. Brand, C. Weber, and M. O’Malley, “Stochastic optimization model to study the operational impacts of high wind penetrations in Ireland,” *IEEE Transactions on Power Systems*, vol. 26, no. 3, pp. 1367–1379, 2011.

[45] A. Papavasiliou, S. S. Oren, and R. P. O’Neill, “Reserve requirements for wind power integration: A scenario-based stochastic programming framework,” *IEEE Transactions on Power Systems*, vol. 26, no. 4, pp. 2197–2206, 2011.

[46] H. Nosair and F. Bouffard, “Economic dispatch under uncertainty: The probabilistic envelopes approach,” *IEEE Transactions on Power Systems*, vol. 32, no. 3, pp. 1701–1710, 2017.

[47] D. Bertsimas, E. Litvinov, X. A. Sun, J. Zhao, and T. Zheng, “Adaptive robust optimization for the security constrained unit commitment problem,” *IEEE Transactions on Power Systems*, vol. 28, no. 1, pp. 52–63, 2013.

[48] A. Velloso, A. Street, D. Pozo, J. M. Arroyo, and N. G. Cobos, “Two-stage robust unit commitment for co-optimized electricity markets: An adaptive data-driven approach for scenario-based uncertainty sets,” *IEEE Transactions on Sustainable Energy*, vol. 11, no. 2, pp. 958–969, 2020.

[49] N. K. Dhaliwal, F. Bouffard, and M. J. O’Malley, “A fast flexibility-driven generation portfolio planning method for sustainable power systems,” *IEEE Transactions on Sustainable Energy*, vol. 12, no. 1, pp. 368–377, 2021.

[50] Y. Huo, F. Bouffard, and G. Joós, "Spatio-temporal flexibility management in low-carbon power systems," *IEEE Transactions on Sustainable Energy*, vol. 11, no. 4, pp. 2593–2605, 2020.

[51] W. Wei, Y. Chen, C. Wang, Q. Wu, and M. Shahidehpour, "Nodal flexibility requirements for tackling renewable power fluctuations," *IEEE Transactions on Power Systems*, vol. 36, no. 4, pp. 3227–3237, 2021.

[52] C. Wang, F. Liu, J. Wang, F. Qiu, W. Wei, S. Mei, and S. Lei, "Robust risk-constrained unit commitment with large-scale wind generation: An adjustable uncertainty set approach," *IEEE Transactions on Power Systems*, vol. 32, no. 1, pp. 723–733, 2017.

[53] K. Guerra, P. Haro, R. Gutiérrez, and A. Gómez-Barea, "Facing the high share of variable renewable energy in the power system: Flexibility and stability requirements," *Applied Energy*, vol. 310, p. 118561, 2022.

[54] C. Shao, X. Wang, M. Shahidehpour, X. Wang, and B. Wang, "Security-constrained unit commitment with flexible uncertainty set for variable wind power," *IEEE Transactions on Sustainable Energy*, vol. 8, no. 3, pp. 1237–1246, 2017.

[55] K. Lehmann, A. Grastien, and P. Van Hentenryck, "AC-feasibility on tree networks is NP-hard," *IEEE Transactions on Power Systems*, vol. 31, no. 1, pp. 798–801, 2016.

[56] S. Gopinath and H. L. Hijazi, "Benchmarking large-scale acopf solutions and optimality bounds," in *2022 IEEE Power & Energy Society General Meeting (PESGM)*, pp. 1–5, 2022.

[57] S. H. Low, "Convex relaxation of optimal power flow—part I: Formulations and equivalence," *IEEE Transactions on Control of Network Systems*, vol. 1, no. 1, pp. 15–27, 2014.

[58] S. H. Low, "Convex relaxation of optimal power flow—part II: Exactness," *IEEE Transactions on Control of Network Systems*, vol. 1, no. 2, pp. 177–189, 2014.

[59] D. K. Molzahn and I. A. Hiskens, "A survey of relaxations and approximations of the power flow equations," *Foundations and Trends in Electric Energy Systems*, vol. 4, no. 1-2, pp. 1–221, 2019.

[60] D. K. Molzahn and L. A. Roald, "Towards an ac optimal power flow algorithm with robust feasibility guarantees," in *2018 Power Systems Computation Conference (PSCC)*, pp. 1–7, 2018.

[61] A. Khotanzad, R. Afkhami-Rohani, and D. Maratukulam, "Annstlf-artificial neural network short-term load forecaster- generation three," *IEEE Transactions on Power Systems*, vol. 13, no. 4, pp. 1413–1422, 1998.

[62] S. Chatzivasileiadis, A. Venzke, J. Stiasny, and G. Misyris, "Machine learning in power systems: Is it time to trust it?," *IEEE Power and Energy Magazine*, vol. 20, no. 3, pp. 32–41, 2022.

[63] J. Xie, I. Alvarez-Fernandez, and W. Sun, "A review of machine learning applications in power system resilience," in *2020 IEEE Power & Energy Society General Meeting (PESGM)*, pp. 1–5, 2020.

[64] Y. Zhang, X. Shi, H. Zhang, Y. Cao, and V. Terzija, "Review on deep learning applications in frequency analysis and control of modern power system," *International Journal of Electrical Power & Energy Systems*, vol. 136, p. 107744, 2022.

[65] L. Duchesne, E. Karangelos, and L. Wehenkel, "Recent developments in machine learning for energy systems reliability management," *Proceedings of the IEEE*, vol. 108, no. 9, pp. 1656–1676, 2020.

[66] T. Hastie, R. Tibshirani, and J. Friedman, *The elements of statistical learning: data mining, inference and prediction.* Springer, 2 ed., 2009.

[67] R. S. Sutton and A. G. Barto, *Reinforcement Learning: An Introduction.* The MIT Press, second ed., 2018.

[68] A. Venzke, L. Halilbasic, U. Markovic, G. Hug, and S. Chatzivasileiadis, "Convex relaxations of chance constrained ac optimal power flow," *IEEE Transactions on Power Systems*, vol. 33, no. 3, pp. 2829–2841, 2018.

[69] R. Nellikkath and S. Chatzivasileiadis, "Physics-informed neural networks for ac optimal power flow," *Electric Power Systems Research*, vol. 212, p. 108412, 2022.

[70] B. Abbasi, T. Babaei, Z. Hosseinifard, K. Smith-Miles, and M. Dehghani, "Predicting solutions of large-scale optimization problems via machine learning: A case study in blood supply chain management," *Computers & Operations Research*, vol. 119, p. 104941, 2020.

[71] D. Bertsimas and B. Stellato, "Online mixed-integer optimization in milliseconds," *INFORMS Journal on Computing*, vol. 34, no. 4, pp. 2229–2248, 2022.

[72] Y. Bengio, A. Lodi, and A. Prouvost, "Machine learning for combinatorial optimization: A methodological tour d'horizon," *European Journal of Operational Research*, vol. 290, no. 2, pp. 405–421, 2021.

[73] J. Kotary, F. Fioretto, P. V. Hentenryck, and B. Wilder, "End-to-end constrained optimization learning: A survey," 2021.

[74] A. M. Alvarez, Q. Louveaux, and L. Wehenkel, "A machine learning-based approximation of strong branching," *INFORMS Journal on Computing*, vol. 29, no. 1, pp. 185–195, 2017.

[75] E. B. Khalil, B. Dilkina, G. L. Nemhauser, S. Ahmed, and Y. Shao, "Learning to run heuristics in tree search," in *Proceedings of the Twenty-Sixth International Joint Conference on Artificial Intelligence, IJCAI-17*, pp. 659–666, 2017.

[76] A. Chmiela, E. Khalil, A. Gleixner, A. Lodi, and S. Pokutta, "Learning to schedule heuristics in branch and bound," in *Advances in Neural Information Processing*

Systems (M. Ranzato, A. Beygelzimer, Y. Dauphin, P. Liang, and J. W. Vaughan, eds.), vol. 34, pp. 24235–24246, Curran Associates, Inc., 2021.

[77] A. Lodi and G. Zarpellon, "On learning and branching: a survey," *TOP*, vol. 25, pp. 207–236, June 2017.

[78] J. Wu, P. B. Luh, Y. Chen, B. Yan, and M. A. Bragin, "Synergistic integration of machine learning and mathematical optimization for unit commitment," *IEEE Transactions on Power Systems*, pp. 1–10, 2023.

[79] S. Pineda and J. Morales, "Is learning for the unit commitment problem a low-hanging fruit?," *Electric Power Systems Research*, vol. 207, p. 107851, 2022.

[80] S. Misra, L. Roald, and Y. Ng, "Learning for constrained optimization: Identifying optimal active constraint sets," *INFORMS Journal on Computing*, vol. 34, no. 1, pp. 463–480, 2022.

[81] N. Yang, C. Yang, C. Xing, D. Ye, J. Jia, D. Chen, X. Shen, Y. Huang, L. Zhang, and B. Zhu, "Deep learning-based SCUC decision-making: An intelligent data-driven approach with self-learning capabilities," *IET Generation, Transmission & Distribution*, vol. 16, no. 4, pp. 629–640, 2022.

[82] W. Chen, S. Park, M. Tanneau, and P. Van Hentenryck, "Learning optimization proxies for large-scale security-constrained economic dispatch," *Electric Power Systems Research*, vol. 213, p. 108566, 2022.

[83] X. Pan, T. Zhao, M. Chen, and S. Zhang, "DeepOPF: A deep neural network approach for security-constrained dc optimal power flow," *IEEE Transactions on Power Systems*, vol. 36, no. 3, pp. 1725–1735, 2021.

[84] A. Venzke, G. Qu, S. Low, and S. Chatzivasileiadis, "Learning optimal power flow: Worst-case guarantees for neural networks," in *2020 IEEE International*

Conference on Communications, Control, and Computing Technologies for Smart Grids (SmartGridComm), pp. 1–7, 2020.

[85] N. Papernot, P. McDaniel, S. Jha, M. Fredrikson, Z. B. Celik, and A. Swami, "The limitations of deep learning in adversarial settings," in *2016 IEEE European Symposium on Security and Privacy (EuroS&P)*, pp. 372–387, 2016.

[86] A. Venzke and S. Chatzivasileiadis, "Verification of neural network behaviour: Formal guarantees for power system applications," *IEEE Transactions on Smart Grid*, vol. 12, no. 1, pp. 383–397, 2021.

[87] Y. Chen, Y. Tan, and D. Deka, "Is machine learning in power systems vulnerable?," in *2018 IEEE International Conference on Communications, Control, and Computing Technologies for Smart Grids (SmartGridComm)*, pp. 1–6, 2018.

[88] S. Pineda, J. M. Morales, and A. Jiménez-Cordero, "Data-driven screening of network constraints for unit commitment," *IEEE Transactions on Power Systems*, vol. 35, no. 5, pp. 3695–3705, 2020.

[89] A. S. Xavier, F. Qiu, and S. Ahmed, "Learning to solve large-scale security-constrained unit commitment problems," *INFORMS Journal on Computing*, vol. 33, no. 2, pp. 739–756, 2021.

[90] D. Deka and S. Misra, "Learning for DC-OPF: Classifying active sets using neural nets," in *2019 IEEE Milan PowerTech*, pp. 1–6, 2019.

[91] A. Jahanbani Ardakani and F. Bouffard, "Prediction of umbrella constraints," in *2018 Power Systems Computation Conference (PSCC)*, pp. 1–7, 2018.

[92] F. Hasan, A. Kargarian, and J. Mohammadi, "Hybrid learning aided inactive constraints filtering algorithm to enhance ac OPF solution time," *IEEE Transactions on Industry Applications*, vol. 57, no. 2, pp. 1325–1334, 2021.

[93] A. O. Fajemisin, D. Maragno, and D. den Hertog, "Optimization with constraint learning: A framework and survey," *European Journal of Operational Research*, 2023.

[94] D. Maragno, H. Wiberg, D. Bertsimas, S. I. Birbil, D. d. Hertog, and A. Fajemisin, "Mixed-integer optimization with constraint learning," 2021.

[95] H. M. Wiberg, *Data-driven healthcare via constraint learning and analytics*. PhD thesis, Massachusetts Institute of Technology, May 2022.

[96] M. Ghorbanian, S. H. Dolatabadi, and P. Siano, "Big data issues in smart grids: A survey," *IEEE Systems Journal*, vol. 13, no. 4, pp. 4158–4168, 2019.

[97] A. J. Ardakani and F. Bouffard, "Identification of umbrella constraints in dc-based security-constrained optimal power flow," *IEEE Transactions on Power Systems*, vol. 28, no. 4, pp. 3924–3934, 2013.

[98] FERC2222, "Participation of distributed energy resource aggregations in markets operated by regional transmission organizations and independent system operators." `https://www.govinfo.gov/content/pkg/FR-2021-03-30/pdf/2021-06089.pdf`, note = Accessed: 2023-1-06.

[99] G. Byeon and P. Van Hentenryck, "Unit commitment with gas network awareness," *IEEE Transactions on Power Systems*, vol. 35, no. 2, pp. 1327–1339, 2020.

[100] Y. Chen, F. Pan, J. Holzer, E. Rothberg, Y. Ma, and A. Veeramany, "A high performance computing based market economics driven neighborhood search and polishing algorithm for security constrained unit commitment," *IEEE Transactions on Power Systems*, vol. 36, no. 1, pp. 292–302, 2021.

[101] B. Stott and E. Hobson, "Power system security control calculations using linear programming, part I," *IEEE Transactions on Power Apparatus and Systems*, vol. PAS-97, no. 5, pp. 1713–1720, 1978.

[102] Y. Fu, Z. Li, and L. Wu, "Modeling and solution of the large-scale security-constrained unit commitment," *IEEE Transactions on Power Systems*, vol. 28, no. 4, pp. 3524–3533, 2013.

[103] Y. Chen, A. Casto, F. Wang, Q. Wang, X. Wang, and J. Wan, "Improving large scale day-ahead security constrained unit commitment performance," *IEEE Transactions on Power Systems*, vol. 31, no. 6, pp. 4732–4743, 2016.

[104] Y. Dvorkin, P. Henneaux, D. S. Kirschen, and H. Pandžić, "Optimizing primary response in preventive security-constrained optimal power flow," *IEEE Systems Journal*, vol. 12, no. 1, pp. 414–423, 2018.

[105] A. Velloso, P. Van Hentenryck, and E. S. Johnson, "An exact and scalable problem decomposition for security-constrained optimal power flow," *Electric Power Systems Research*, vol. 195, p. 106677, 2021.

[106] L. A. Roald and D. K. Molzahn, "Implied constraint satisfaction in power system optimization: The impacts of load variations," in *2019 57th Annual Allerton Conference on Communication, Control, and Computing (Allerton)*, pp. 308–315, 2019.

[107] S. Zhang, H. Ye, F. Wang, Y. Chen, S. Rose, and Y. Ma, "Data-aided offline and online screening for security constraint," *IEEE Transactions on Power Systems*, vol. 36, no. 3, pp. 2614–2622, 2021.

[108] A. Porras, S. Pineda, J. M. Morales, and A. Jiménez-Cordero, "Cost-driven screening of network constraints for the unit commitment problem," *IEEE Transactions on Power Systems*, vol. 38, no. 1, pp. 42–51, 2023.

[109] D. Shchetinin, T. T. De Rubira, and G. Hug, "Efficient bound tightening techniques for convex relaxations of ac optimal power flow," *IEEE Transactions on Power Systems*, vol. 34, no. 5, pp. 3848–3857, 2019.

[110] R. Weinhold and R. Mieth, "Fast security-constrained optimal power flow through low-impact and redundancy screening," *IEEE Transactions on Power Systems*, vol. 35, no. 6, pp. 4574–4584, 2020.

[111] M. Szedlák, *Redundancy in Linear Systems: Combinatorics, Algorithms and Analysis.* PhD thesis, ETH Zurich, 2017.

[112] Z. Ma, H. Zhong, T. Cheng, J. Pi, and F. Meng, "Redundant and nonbinding transmission constraints identification method combining physical and economic insights of unit commitment," *IEEE Transactions on Power Systems*, vol. 36, no. 4, pp. 3487–3495, 2021.

[113] W. Wei and J. Wang, *Electric Power System with Renewable Generation*, pp. 21–161. Cham: Springer International Publishing, 2020.

[114] F. Golestaneh, P. Pinson, and H. B. Gooi, "Polyhedral predictive regions for power system applications," *IEEE Transactions on Power Systems*, vol. 34, no. 1, pp. 693–704, 2019.

[115] F. Golestaneh, P. Pinson, R. Azizipanah-Abarghooee, and H. B. Gooi, "Ellipsoidal prediction regions for multivariate uncertainty characterization," *IEEE Transactions on Power Systems*, vol. 33, no. 4, pp. 4519–4530, 2018.

[116] A. Lorca and X. A. Sun, "Multistage robust unit commitment with dynamic uncertainty sets and energy storage," *IEEE Transactions on Power Systems*, vol. 32, no. 3, pp. 1678–1688, 2017.

[117] P. Li, X. Guan, J. Wu, and X. Zhou, "Modeling dynamic spatial correlations of geographically distributed wind farms and constructing ellipsoidal uncertainty sets for optimization-based generation scheduling," *IEEE Transactions on Sustainable Energy*, vol. 6, no. 4, pp. 1594–1605, 2015.

[118] C. Coffrin, H. L. Hijazi, and P. Van Hentenryck, "Strengthening convex relaxations with bound tightening for power network optimization," in *21st Int. Conf. Principles and Practice of Constraint Programming*, pp. 39–57, Springer International Publishing, Aug. 2015.

[119] C. Chen, A. Atamtürk, and S. S. Oren, "Bound tightening for the alternating current optimal power flow problem," *IEEE Transactions on Power Systems*, vol. 31, no. 5, pp. 3729–3736, 2016.

[120] C. Coffrin, H. L. Hijazi, and P. Van Hentenryck, "Strengthening the SDP relaxation of ac power flows with convex envelopes, bound tightening, and valid inequalities," *IEEE Transactions on Power Systems*, vol. 32, no. 5, pp. 3549–3558, 2017.

[121] A. D. O. Aquino, L. A. Roald, and D. K. Molzahn, "Identifying redundant constraints for ac OPF: The challenges of local solutions, relaxation tightness, and approximation inaccuracy," in *2021 North American Power Symposium (NAPS)*, pp. 1–6, 2021.

[122] F. Hasan and A. Kargarian, "Topology-aware learning assisted branch and ramp constraints screening for dynamic economic dispatch," *IEEE Transactions on Power Systems*, vol. 37, no. 5, pp. 3495–3505, 2022.

[123] E. Prat and S. Chatzivasileiadis, "Learning active constraints to efficiently solve linear bilevel problems: Application to the generator strategic bidding problem," *IEEE Transactions on Power Systems*, pp. 1–11, 2022.

[124] A. V. Ramesh and X. Li, "Feasibility layer aided machine learning approach for day-ahead operations," *IEEE Transactions on Power Systems*, pp. 1–12, 2023.

[125] A. Abiri-Jahromi and F. Bouffard, "On the loadability sets of power systems—part II: Minimal representations," *IEEE Transactions on Power Systems*, vol. 32, no. 1, pp. 146–156, 2017.

[126] D. K. Molzahn, "Computing the feasible spaces of optimal power flow problems," *IEEE Transactions on Power Systems*, vol. 32, no. 6, pp. 4752–4763, 2017.

[127] A. N. Elmachtoub and P. Grigas, "Smart "predict, then optimize"," *Management Science*, vol. 68, no. 1, pp. 9–26, 2022.

[128] A. A. Jahromi and F. Bouffard, "On the loadability sets of power systems—part I: Characterization," *IEEE Transactions on Power Systems*, vol. 32, no. 1, pp. 137–145, 2017.

[129] V. H. Hinojosa and G. Gutiérrez-Alcaraz, "A computational comparison of 2 mathematical formulations to handle transmission network constraints in the unit commitment problem," *International Transactions on Electrical Energy Systems*, vol. 27, no. 8, p. e2332, 2017. e2332 ETEP-15-0458.R4.

[130] D. A. Pachamanova, "A robust optimization approach to finance," Ph.D. thesis, Sloan School of Management, Operations Research Center, Massachusetts Institute of Technology., Cambridge, MA, USA, 2002.

[131] D. D. Le, G. Gross, and A. Berizzi, "Probabilistic modeling of multisite wind farm production for scenario-based applications," *IEEE Transactions on Sustainable Energy*, vol. 6, no. 3, pp. 748–758, 2015.

[132] J. Ekström, M. Koivisto, I. Mellin, R. J. Millar, and M. Lehtonen, "A statistical model for hourly large-scale wind and photovoltaic generation in new locations," *IEEE Transactions on Sustainable Energy*, vol. 8, no. 4, pp. 1383–1393, 2017.

[133] M. Cheramin, R. L.-Y. Chen, J. Cheng, and A. Pinar, "Data-driven robust optimization using scenario-induced uncertainty sets," 2021.

[134] G. Gutiérrez-Alcaraz, B. Díaz-López, J. M. Arroyo, and V. H. Hinojosa, "Large-scale preventive security-constrained unit commitment considering n-k line outages and

transmission losses," *IEEE Transactions on Power Systems*, vol. 37, no. 3, pp. 2032–2041, 2022.

[135] S. Babaeinejadsarookolaee, A. Birchfield, R. D. Christie, C. Coffrin, C. DeMarco, R. Diao, M. Ferris, S. Fliscounakis, S. Greene, R. Huang, C. Josz, R. Korab, B. Lesieutre, J. Maeght, T. W. K. Mak, D. K. Molzahn, T. J. Overbye, P. Panciatici, B. Park, J. Snodgrass, A. Tbaileh, P. Van Hentenryck, and R. Zimmerman, "The power grid library for benchmarking ac optimal power flow algorithms," *arXiv*, 2019.

[136] A. Peña-Ordieres, D. K. Molzahn, L. A. Roald, and A. Wächter, "DC optimal power flow with joint chance constraints," *IEEE Transactions on Power Systems*, vol. 36, no. 1, pp. 147–158, 2021.

[137] R. D. Zimmerman, C. E. Murillo-Sánchez, and R. J. Thomas, "Matpower: Steady-state operations, planning, and analysis tools for power systems research and education," *IEEE Transactions on Power Systems*, vol. 26, no. 1, pp. 12–19, 2011.

[138] IEEE PES Task Force on Benchmarks for Validation of Emerging Power System Algorithms, "Pglib-opf: Benchmarks for the optimal power flow problem," *arXiv*, Aug 2019.

[139] A. B. Birchfield, T. Xu, K. M. Gegner, K. S. Shetye, and T. J. Overbye, "Grid structural characteristics as validation criteria for synthetic networks," *IEEE Transactions on Power Systems*, vol. 32, no. 4, pp. 3258–3265, 2017.

[140] X. A. Sun and Á. Lorca, *Robust Optimization in Electric Power Systems Operations*, pp. 227–258. Cham: Springer International Publishing, 2017.

[141] Q. P. Zheng, J. Wang, and A. L. Liu, "Stochastic optimization for unit commitment—a review," *IEEE Transactions on Power Systems*, vol. 30, no. 4, pp. 1913–1924, 2015.

[142] G. C. Calafiore, "Random convex programs," *SIAM Journal on Optimization*, vol. 20, no. 6, pp. 3427–3464, 2010.

[143] R. A. Jabr, "Adjustable robust OPF with renewable energy sources," *IEEE Transactions on Power Systems*, vol. 28, no. 4, pp. 4742–4751, 2013.

[144] A. Lorca, X. A. Sun, E. Litvinov, and T. Zheng, "Multistage adaptive robust optimization for the unit commitment problem," *Operations Research*, vol. 64, no. 1, pp. 32–51, 2016.

[145] M. Paluszek and S. Thomas, *MATLAB Machine Learning*. Apress Berkeley, CA, 2017.

[146] J. Lavaei and S. H. Low, "Zero duality gap in optimal power flow problem," *IEEE Transactions on Power Systems*, vol. 27, no. 1, pp. 92–107, 2012.

[147] B. Kocuk, S. S. Dey, and X. A. Sun, "Strong SOCP relaxations for the optimal power flow problem," *Operations Research*, vol. 64, no. 6, pp. 1177–1196, 2016.

[148] C. Bingane, M. F. Anjos, and S. L. Digabel, "CONICOPF: Conic relaxations for ac optimal power flow computations," in *2021 IEEE Power & Energy Society General Meeting (PESGM)*, pp. 1–5, 2021.

[149] C. Bingane, M. F. Anjos, and S. Le Digabel, "Tight-and-cheap conic relaxation for the ac optimal power flow problem," *IEEE Transactions on Power Systems*, vol. 33, no. 6, pp. 7181–7188, 2018.

[150] Gurobi Optimization, LLC, "Gurobi Optimizer Reference Manual," 2023.

[151] MOSEK ApS, *The MOSEK optimization toolbox for MATLAB manual. Version 10.0.*, 2022.

[152] R. Jabr, "Radial distribution load flow using conic programming," *IEEE Transactions on Power Systems*, vol. 21, no. 3, pp. 1458–1459, 2006.

[153] R. A. Jabr, "Optimal power flow using an extended conic quadratic formulation," *IEEE Transactions on Power Systems*, vol. 23, no. 3, pp. 1000–1008, 2008.

[154] G. P. McCormick, "Computability of global solutions to factorable nonconvex programs: Part I — convex underestimating problems," *Mathematical Programming*, vol. 10, pp. 147–175, Dec. 1976.

[155] J. Zhao, T. Zheng, and E. Litvinov, "Variable resource dispatch through do-not-exceed limit," *IEEE Transactions on Power Systems*, vol. 30, no. 2, pp. 820–828, 2015.

[156] A. S. Korad and K. W. Hedman, "Enhancement of do-not-exceed limits with robust corrective topology control," *IEEE Transactions on Power Systems*, vol. 31, no. 3, pp. 1889–1899, 2016.

[157] F. Qiu, Z. Li, and J. Wang, "A data-driven approach to improve wind dispatchability," *IEEE Transactions on Power Systems*, vol. 32, no. 1, pp. 421–429, 2017.

[158] W. Wei, F. Liu, and S. Mei, "Dispatchable region of the variable wind generation," *IEEE Transactions on Power Systems*, vol. 30, no. 5, pp. 2755–2765, 2015.

[159] Y. Liu, Z. Li, Q. H. Wu, and H. Zhang, "Real-time dispatchable region of renewable generation constrained by reactive power and voltage profiles in ac power networks," *CSEE Journal of Power and Energy Systems*, vol. 6, no. 3, pp. 528–536, 2020.

[160] W. Wei, J. Wang, and S. Mei, "Dispatchability maximization for co-optimized energy and reserve dispatch with explicit reliability guarantee," *IEEE Transactions on Power Systems*, vol. 31, no. 4, pp. 3276–3288, 2016.

[161] M. A. Bucher, S. Chatzivasileiadis, and G. Andersson, "Managing flexibility in multi-area power systems," *IEEE Transactions on Power Systems*, vol. 31, no. 2, pp. 1218–1226, 2016.

[162] N. Yorino, M. Abdillah, Y. Sasaki, and Y. Zoka, "Robust power system security assessment under uncertainties using bi-level optimization," *IEEE Transactions on Power Systems*, vol. 33, no. 1, pp. 352–362, 2018.

[163] J. Zhao, T. Zheng, and E. Litvinov, "A unified framework for defining and measuring flexibility in power system," *IEEE Transactions on Power Systems*, vol. 31, no. 1, pp. 339–347, 2016.

[164] Z. Qin, Y. Hou, S. Lei, and F. Liu, "Quantification of intra-hour security-constrained flexibility region," *IEEE Transactions on Sustainable Energy*, vol. 8, no. 2, pp. 671–684, 2017.

[165] C. Wang, F. Liu, J. Wang, W. Wei, and S. Mei, "Risk-based admissibility assessment of wind generation integrated into a bulk power system," *IEEE Transactions on Sustainable Energy*, vol. 7, no. 1, pp. 325–336, 2016.

[166] C. Wang, S. Wang, F. Liu, T. Bi, and T. Wang, "Risk-loss coordinated admissibility assessment of wind generation for integrated electric-gas systems," *IEEE Transactions on Smart Grid*, vol. 11, no. 5, pp. 4454–4465, 2020.

[167] C. Wang, Z. Gong, Y. Liang, W. Wei, and T. Bi, "Data-driven wind generation admissibility assessment of integrated electric-heat systems: A dynamic convex hull-based approach," *IEEE Transactions on Smart Grid*, vol. 11, no. 5, pp. 4531–4543, 2020.

[168] W. Wei, F. Liu, and S. Mei, "Real-time dispatchability of bulk power systems with volatile renewable generations," *IEEE Transactions on Sustainable Energy*, vol. 6, no. 3, pp. 738–747, 2015.

[169] A. Kalantari, J. F. Restrepo, and F. D. Galiana, "Security-constrained unit commitment with uncertain wind generation: The loadability set approach," *IEEE Transactions on Power Systems*, vol. 28, no. 2, pp. 1787–1796, 2013.

[170] T. C. Y. Chan, T. Lee, and D. Terekhov, "Inverse optimization: Closed-form solutions, geometry, and goodness of fit," *Management Science*, vol. 65, no. 3, pp. 1115–1135, 2019.

[171] K. Ghobadi, T. Lee, H. Mahmoudzadeh, and D. Terekhov, "Robust inverse optimization," *Operations Research Letters*, vol. 46, no. 3, pp. 339–344, 2018.

[172] A. Babier, T. C. Y. Chan, T. Lee, R. Mahmood, and D. Terekhov, "An ensemble learning framework for model fitting and evaluation in inverse linear optimization," *INFORMS Journal on Optimization*, vol. 3, no. 2, pp. 119–138, 2021.

[173] R. K. Ahuja and J. B. Orlin, "Inverse optimization," *Operations Research*, vol. 49, no. 5, pp. 771–783, 2001.

[174] M. D. Troutt, W.-K. Pang, and S.-H. Hou, "Behavioral estimation of mathematical programming objective function coefficients," *Management Science*, vol. 52, no. 3, pp. 422–434, 2006.

[175] Z. Liang and Y. Dvorkin, "Data-driven inverse optimization for marginal offer price recovery in electricity markets," in *Proceedings of the 14th ACM International Conference on Future Energy Systems*, e-Energy '23, p. 497–509, Association for Computing Machinery (ACM), June 2023.

[176] S. Boyd and L. Vandenberghe, *Convex optimization*. Cambridge university press, 2004.

[177] J. Lawrence, "Polytope volume computation," *Mathematics of Computation*, vol. 57, no. 195, pp. 259–271, 1991.